

**Using Image-based Multi-Scale Finite Element Model to Predict  
Rutting Behavior of Asphalt Mixtures**

by  
Cheng Ling

A dissertation submitted in partial fulfillment of the  
requirements for the degree of

Doctor of Philosophy

(Civil and Environmental Engineering)

at the  
University of Wisconsin-Madison  
2016

Date of final oral examination: 12/1/2016

The dissertation is approved by the following members of the Final Oral Committee:

Hussain U. Bahia, Professor, Civil and Environmental Engineering

William J. Likos, Professor, Civil and Environmental Engineering

James M. Tinjum, Associate Professor, Civil and Environmental Engineering

Brock D. Hedegaard, Assistant Professor, Civil and Environmental Engineering

Robert E. Rowlands, Professor, Mechanical Engineering

© Copyright by Cheng Ling, 2016  
All rights reserved

## **Dedication**

To my wife Zoe, and our daughter Claire, for their support, encouragement and love.

## **Acknowledgements**

First of all, I would like to acknowledge my advisor, Professor Hussain Bahia, for the lasting direction and encouragement on my study and research. I have gained an innumerable amount of knowledge from Professor Bahia and been exposed to the areas that I would not have had opportunity to explore otherwise. Also, I would express my sincere gratitude to my committee members Professor Rowlands, Professor Likos, Professor Tinjum and Professor Hedegaard for offering their guidance and suggestions on completing this dissertation. I would like to extend my gratitude to Dr. Andrew Hanz, Dr. Amir Arshadi and Mr. Dan Swiertz for their academic advice on my research.

Sincere thanks to all my friends who are working or have worked at Modified Asphalt Research Center for offering me help to accomplish this goal. I will cherish every moment to work with Dr. Pouya Teymourpour, Dr. Preeda Chaturabong, Dr. Tirupan Mandal, Mr. Erik Lyngdal, Mr. Ying Li, Miss Remya Varma and all undergraduate researchers during the research projects. I would also like to acknowledge the Asphalt Research Consortium and Wisconsin Highway Research Program for funding this research.

Finally I would like to thank my loved family. This work would not be possible without the lasting support and love from my family.

## Abstract

Rutting resistance is one of the essential needs in design of asphalt mixtures. Volumetric properties, binder modification, aggregates properties, and wheel tracking tests are used today to qualify the rutting resistance in practice. However, these tools are used on a trial and error basis and are mostly based on experience to achieve better resistance. With all the experience available today it is still not clear what is the contribution of aggregate structure, what air-voids content should be used, and if plastomeric or elastomeric modifiers are preferred for better resistance. While compiling larger databases and expanding the types of aggregates and binders used in testing could help, a more fundamental understanding of how aggregate contacts are formed and how binders can contribute to actual mechanics of rutting resistance is a better path for designing of mixtures. In the last decade significant improvement in imaging and multi-scale modeling has been achieved, which allows looking closer at how binders and aggregates could affect rutting resistance. One of the most challenging aspects of this modeling effort is dealing with aggregates proximity zones and how response of mixture changes when aggregates come into contact. This dissertation includes a modification of an Image-based Finite Element model for addressing this challenge and provide a solution that is simple yet effective in better simulating of rutting resistance of asphalt mixtures. The dissertation also includes validation of the model to simulate measured performance of mixtures produced with plastomeric and elastomeric modifiers with different viscoelastic properties, as well as different aggregate gradations. Results indicate that predefined contact points are necessary for reliable prediction of rutting resistance of mixtures. The results also show that the non-recoverable creep compliance of binders plays a significant role, while elasticity of modified binder is not important. Further application of the model shows that it can be successfully used to simulate effects of mixture confining pressure to simulate

pavement depth, and also to simulate effects of varying voids content. The dissertation also provides a method to simulate the effects of moisture damage and the weakening of the interface bond between aggregates and binder. It is expected that the improved modeling of contact zones will allow a more rational selection of aggregates and modification techniques to enhance the rutting resistance of asphalt pavements.

## Table of Contents

<b>Dedication</b> .....	i
<b>Acknowledgements</b> .....	ii
<b>Abstract</b> .....	iii
<b>Table of Contents</b> .....	v
<b>List of Figures</b> .....	viii
<b>List of Tables</b> .....	xi
<b>List of Equations</b> .....	xii
<b>I. Introduction</b> .....	1
1. Background.....	1
2. Problem Statement.....	2
3. Hypotheses.....	4
4. Research Objectives.....	4
5. Research Methodology.....	5
<b>II. Literature Review</b> .....	6
1. Modification of Asphalt Binder.....	6
2. Characterization of Asphalt Binder Rutting Resistance.....	7
2.1 Superpave Rutting Parameter.....	7
2.2 Repeated Creep and Recovery Test.....	8
2.3 Multiple Stress Creep Recovery Test.....	9
3. Rheological Models for Asphalt Binder.....	10
4. Characterization of Asphalt Mixture Rutting Resistance.....	13
5. Digital Image Processing and Analysis of Asphalt Mixtures.....	14
6. Effect of Aggregate Internal Structure on Asphalt Mixture Performance.....	16
7. Finite Element Analysis Method.....	18
8. Multi-scale Modeling of Asphalt Mixtures.....	20
9. Overview of the Image-based Multi-scale Model.....	23
9.1 Multi-scale Analysis Approach.....	23
9.2 Modeling of Aggregate Particle-to-Particle Contact.....	28
<b>III. Materials and Methods</b> .....	30
1. Materials.....	30

1.1	Asphalt Binders .....	30
1.2	Aggregate Gradations.....	31
2.	Asphalt Binder Tests.....	32
2.1	Frequency Sweep .....	32
2.2	Multiple Stress Creep Recovery Test.....	34
3.	Asphalt Mixture Tests.....	34
4.	Image-based Multi-scale Modeling Technique .....	36
<b>IV.</b>	<b>Prediction of Permanent Deformation of Asphalt Mixtures Using Image-based Multi-scale Model.....</b>	<b>40</b>
1.	Improvements of the Image-based Multi-scale Model .....	40
1.1	Needs for Improvement.....	40
1.2	Determination of Contact Function and Critical Contact Strain.....	42
1.3	Validation of the Contact Model.....	46
1.4	Summary of Image-based Multi-Scale Modeling Procedure.....	54
2.	Model Validation.....	56
3.	Development of MSCR-based Multi-scale Model .....	61
3.1	Binder Test and Rheological Model Fitting .....	62
3.2	Mixture Validation.....	64
<b>V.</b>	<b>Investigation of the Effects of Binder Modification Type and Aggregate Structure on Permanent Deformation of Asphalt Mixtures .....</b>	<b>67</b>
1.	Experimental Matrix.....	67
2.	Micro-Structure Analysis for Different Asphalt Mixtures .....	68
3.	Permanent Strain Analysis .....	73
4.	Stress and Strain Analysis .....	76
4.1	Stress/Strain Analysis Protocol.....	76
4.2	Stress Analysis.....	77
4.3	Strain Analysis.....	90
<b>VI.</b>	<b>Importance of Binder Non-recoverable Creep Compliance and Elasticity on Asphalt Mixture Rutting Resistance .....</b>	<b>99</b>
1.	Experimental Matrix.....	99
2.	Permanent Strain Analysis .....	101
3.	Effects of Jnr and %R in Mixes with Different Aggregate Structures.....	103
<b>VII.</b>	<b>Prediction of Permanent Deformation for Asphalt Mixtures under Different Conditions .....</b>	<b>107</b>

1. Application of the Model to Asphalt Mixtures with/without Confining Pressure.....	107
2. Investigate the Effect of Air Voids Content in Permanent Deformation of Asphalt Mixtures.....	111
3. Simulate Asphalt Mixtures under Moisture Damage.....	114
4. Effect of Loading Frequency on the Prediction of Permanent Deformation Using the Model .....	119
<b>VIII. Summary of Findings and Conclusions .....</b>	<b>122</b>
1. Summary of Findings .....	122
2. Conclusions .....	124
3. Future Work .....	124
<b>IX. References .....</b>	<b>126</b>

## List of Figures

Figure II-1: Passing curve in AASHTO M332 .....	10
Figure II-2: Illustration of simple rheological models .....	11
Figure II-3: Rheological models with multiple Maxwell/Voigt units .....	12
Figure II-4: Permanent deformation curve from Flow Number test .....	14
Figure II-5: Multiple length scales defined in multi-scale modeling [43] .....	21
Figure II-6: Flowchart of the multi-scale analysis procedure [9].....	24
Figure II-7: Mastic images with different RVE sizes: (a) $750\ \mu\text{m} \times 750\ \mu\text{m}$ (b) $450\ \mu\text{m} \times 450\ \mu\text{m}$ (c) $225\ \mu\text{m} \times 225\ \mu\text{m}$ (d) $150\ \mu\text{m} \times 150\ \mu\text{m}$ [9] .....	26
Figure II-8: Convergence of the mastic creep compliance curves [9].....	27
Figure II-9: Distribution of air voids based on the “bathtub” shape [9].....	28
Figure II-10: Contact law defined based on binder film elements .....	29
Figure III-1: Gradations used in this study [27].....	31
Figure III-2: Example of dynamic modulus curves of asphalt binder at $4^\circ\text{C}$ , $20^\circ\text{C}$ , $40^\circ\text{C}$ and $50^\circ\text{C}$ (from top to bottom).....	33
Figure III-3: Constructed master curve at $20^\circ\text{C}$ .....	33
Figure III-4: Schematic of Flow Number test setup [7] .....	35
Figure III-5: (a) Typical permanent strain curve and (b) permanent strain rate curve from Flow Number test [27] .....	36
Figure III-6: Multi-scale analysis scheme: (a) Mixture-scale (b) Mortar-scale (c) Mastic-scale [9] .....	38
Figure III-7: Loading and boundary conditions in FE analysis .....	39
Figure IV-1: Creep simulation of mastic with and without contact .....	43
Figure IV-2: Illustration of contact function and critical contact strain .....	44
Figure IV-3: Contact law defined at mastic scale .....	45
Figure IV-4: Contact function determined at mortar scale .....	45
Figure IV-5: Contact function determined at mixture scale .....	46
Figure IV-6: Simulation and test results for SBS modified asphalt binder .....	47
Figure IV-7: Simulation and test results for asphalt mastic.....	47
Figure IV-8: Comparison of simulation and test data for coarse mix .....	48
Figure IV-9: Description of linear contact law .....	49
Figure IV-10: Compressive strains proposed at which contacts initiated.....	50
Figure IV-11: Simulated permanent strain curves using three contact laws at mastic scale .....	51
Figure IV-12: Concept of pre-defined contact points.....	52
Figure IV-13: Simulation results after adding pre-defined contact points in mortar and mixture .	54
Figure IV-14: Master curves of the three binders used .....	57
Figure IV-15: Permanent strain curves from Flow Number test.....	59
Figure IV-16: Comparison of permanent strain curves using multi-scale model and FN test.....	60
Figure IV-17: Comparison of permanent strains after 70 cycles for simulation and test .....	61
Figure IV-18: MSCR test data fitting for SBS modified binder using two different methods .....	63
Figure IV-19: Validation of a fine mixture with SBS modified asphalt binder .....	65
Figure IV-20: Validation of a coarse mixture with SBS modified asphalt binder .....	66
Figure V-1: Different internal structures for two gradations included .....	68
Figure V-2: Correlation between Total Proximity Length and Flow Number [5] .....	69
Figure V-3: Total Proximity Length for different asphalt mixtures used in this study .....	70
Figure V-4: Correlation between TPL and FN at different stress levels .....	70

Figure V-5: Correlation between TPL with speculated FN at stress level of 600kPa .....	72
Figure V-6: Permanent strains after 70 cycles for different asphalt binders and aggregate internal structures .....	74
Figure V-7: Average of maximum compressive stress at 0.1s for mortar in (a) fine mix (b) coarse mix .....	79
Figure V-8: Average of maximum compressive stress at 69.1s for mortar in (a) fine mix (b) coarse mix.....	80
Figure V-9: Average of maximum compressive stress at 0.1s for mastic in (a) fine mix (b) coarse mix .....	83
Figure V-10: Average of maximum compressive stress at 0.1s for asphalt binder in (a) fine mix (b) coarse mix .....	84
Figure V-11: Average of shear stress at 0.1s for asphalt binder in (a) fine mix (b) coarse mix ....	85
Figure V-12: Distributions of maximum compressive stresses in mortar for (a) different binders (b) different structures (c) different gradations .....	87
Figure V-13: Distributions of maximum compressive stresses in binder for (a) different binders (b) different structures (c) different gradations .....	89
Figure V-14: Average of maximum compressive strain at 70s for mortar in (a) fine mix (b) coarse mix .....	91
Figure V-15: Average of maximum compressive strain at 0.1s for mortar in (a) fine mix (b) coarse mix.....	92
Figure V-16: Average of maximum compressive strain at 69.1s for mortar in (a) fine mix (b) coarse mix.....	93
Figure V-17: Average of maximum compressive strain at 0.1s for mastic in (a) fine mix (b) coarse mix.....	94
Figure V-18: Average of maximum compressive strain at 0.1s for binder in (a) fine mix (b) coarse mix .....	95
Figure V-19: Average of shear strain at 0.1s for binder in (a) fine mix (b) coarse mix .....	96
Figure V-20: Distributions of maximum compressive strains in binder for (a) different binders (b) different structures (c) different gradations .....	98
Figure VI-1: Creep and recovery curves of the four binders with different Jnr and %R .....	100
Figure VI-2: Permanent strain curves for the mixtures with different binders .....	102
Figure VI-3: Permanent strains after 70 cycles for all mixtures .....	103
Figure VI-4: Permanent strains after 70 cycles of repeated loading for (a) Neat structure and (b) CBE structure.....	104
Figure VII-1: Aggregate Gradation Used in This Study .....	108
Figure VII-2: Master curves for asphalt binders used in this study .....	109
Figure VII-3: Simulation and FN test results for Waukesha-MT-S-28 mixtures with and without confining pressure .....	110
Figure VII-4: Simulation and FN test results for Waukesha-MT-V-28 mixtures with and without confining pressure.....	110
Figure VII-5: Simulation results for Waukesha-MT-S-28 mixtures with air voids content of 4% and 7% .....	112
Figure VII-6: Simulation results for Waukesha-MT-V-28 mixtures with air voids content of 4% and 7% .....	113
Figure VII-7: Searching strategy for binder elements with reduced stiffness around aggregate element .....	115

Figure VII-8: Asphalt mastic image in ABAQUS with aggregate particle, asphalt binder and asphalt binder film elements .....	116
Figure VII-9: Permanent strain curves for two types of mixtures simulated under dry and wet conditions .....	117
Figure VII-10: Correlation between simulated slopes and test slopes .....	119
Figure VII-11: Simulations of permanent deformation under different loading frequencies .....	121

## List of Tables

Table III-1: Percent modifier used and the true grade of the modified asphalts .....	30
Table IV-1: Volume fractions of component materials at each scale.....	56
Table IV-2: Prony series parameters for all three asphalt binders .....	57
Table IV-3: Burger’s model fitted parameters for two methods .....	63
Table V-1: Recommended Flow Number limits from NCHRP 9-33 [] .....	71
Table V-2: Recommended minimum FN and TPL requirements .....	73
Table V-3: ANOVA for all mixtures analyzed.....	75
Table V-4: ANOVA for mixtures under three different aggregate structures .....	76
Table V-5: Average of maximum compressive stress at 0.1s.....	78
Table V-6: Average of maximum compressive stress at 69.1s.....	78
Table VI-1: Four binders with different levels of Jnr and %R included in this study.....	100
Table VI-2: ANOVA for all the mixtures analyzed using SBS structure.....	103
Table VI-3: ANOVA of permanent strains for (a) Neat structure and (b) CBE structure.....	105
Table VI-4: ANOVA for permanent strains of all mixtures with different structures .....	106
Table VII-1: Binder Test Results .....	108
Table VII-2: Comparison of permanent strain curve slope for mixtures with different air voids content .....	114
Table VII-3: Comparison of permanent strain after 70 cycles for mixtures with different air voids content .....	114
Table VII-4: Comparison of creep slope, stripping slope and creep/stripping slope ratio between simulation and HWTT test results for two mixtures .....	118

## List of Equations

Equation II-1 .....	29
Equation IV-1 .....	42
Equation IV-2 .....	43
Equation IV-3 .....	62
Equation IV-4 .....	63
Equation V-1.....	71
Equation V-2.....	71

## **I. Introduction**

### **1. Background**

Rutting, namely permanent deformation, refers to the surface depression in the wheel path as a result of repeated traffic loading, is one of the most critical distresses observed for asphalt pavements, especially during the warm seasons. Severe rutting is a significant cause of pavement failure, which affects the vehicle ride quality and causes the safety issue.

Two major mechanisms are associated with the rutting of asphalt pavement layers: consolidation (densification) and lateral movement (shearing). Consolidation occurs in pavements with insufficient compaction, while the shearing deformation occurs due to excessive asphalt binder and its adverse lubricating effect on aggregate interlock. Researchers [1, 2, 3, 4] found that rutting is dominated by distortion or shearing deformation, which is usually the result of a mix design problem, rather than the densification or volume change of the asphalt mixtures. To prevent rutting, the design and construction of asphalt mixtures needs to be conducted carefully to ensure the pavement created is capable of resisting ruts.

An asphalt pavement layer is constructed with asphalt mixtures containing mineral aggregate, asphalt binder and air voids. To characterize the rutting resistance of asphalt mixtures after being designed, a number of laboratory testing procedures have been proposed to measure the mechanical response of asphalt mixtures under loading to simulate what occurs in the field. Among the most common tests are the uniaxial stress test, tri-axial stress test, indirect tension test and loaded wheel track test [5]. A recent study from the

National Cooperative Highway Research Program (NCHRP) was performed to investigate the possibility of using simple performance tests to characterize asphalt mixtures under different temperatures [6]. A uniaxial repeated loading test procedure was also proposed in that study to characterize the rutting resistance of asphalt mixtures, which is relative easy and practical to use.

In addition to the traditional laboratory tests, imaging techniques have been developed recently to characterize the mechanical responses of asphalt mixtures and predict the material behaviors under different conditions. For the visualization of the asphalt mixture components, images are obtained through either destructive or non-destructive methods. Roohi et al. [7] adopted the destructive method to cut the asphalt mixture samples horizontally or vertically to provide a surface for scanning. They quantified and analyzed the internal structure of the mixtures from the images through proposed parameters such as contact points and contact length, aggregate segregation, and aggregate orientation. Other researchers used X-ray computed tomography (XRT) as a non-destructive imaging method to capture 2D or 3D images of asphalt mixture internal structure [8]. With the internal structure images of asphalt mixture available, researchers [9] have also started to simulate the material behaviors using Finite Element Method (FEM) by importing the image into the analysis program to run the “virtual” experiments.

## **2. Problem Statement**

Polymer modification has been widely used to improve asphalt binder performance. Plastomeric and elastomeric modifiers are the two most common types of polymer modifiers used in asphalt modification. Plastomer modified asphalt deforms much more slowly under loading and exhibits less flexibility, while elastomer modified asphalt shows

the ability to recover the deformation after the load is removed, namely elasticity. Both of the two types of modifiers are considered beneficial in improving the high temperature performance of asphalt binder, however it is not clear which modification technique is more preferred in enhancing the rutting resistance of asphalt binder and mixtures, and what mechanisms are behind this.

The Multiple Stress Creep and Recovery (MSCR) test, which is both performance-based and blind to modification type [10], was developed by FHWA as a replacement for the existing AASHTO M320 high-temperature asphalt binder test. The MSCR test has proven to be able to distinguish the difference in rutting potential between various binders including both modified and unmodified binders through numerous studies [10]. The non-recoverable strain and recoverable strain can be separated and represented by non-recoverable creep compliance ( $J_{nr}$ ) and elastic recovery (%R), respectively, through the MSCR test. However, the contributions of the  $J_{nr}$  and %R of asphalt binder to the rutting resistance of the asphalt mixture are not clear.

In addition, the effects of the asphalt properties and aggregate structure during the loading are always confounded with each other during the compaction. Since it is very difficult to distinguish the effect of asphalt binder properties and aggregate structures on the rutting resistance of asphalt mixtures through time-consuming and costly laboratory tests, there is a need to investigate the use of modeling as an alternative tool to predict the rutting behavior of asphalt mixtures and study the fundamental role of asphalt binders and aggregate structures during repeated creep loading.

### **3. Hypotheses**

Three hypotheses are proposed in this dissertation:

1. Image-based multi-scale model developed based on the volume fractions and properties of constituents can be successfully applied to predict the rutting behavior of asphalt mixtures composed of different asphalt binders and aggregate structures.
2. The multi-scale modeling cannot be applied reliably without considering the point-to-point contacts of aggregates created after compaction and prior to repeated loading simulation.
3. Although modification of asphalt binder and aggregate structure have important effects on the rutting behavior of asphalt mixtures, asphalt binder properties affect the rutting resistance of asphalt mixture more significantly in mixtures with a ‘poorly-packed’ aggregate structure relative to the mixtures with a ‘well-packed’ structure.

### **4. Research Objectives**

The primary objectives of this dissertation are listed as follows:

1. Further develop and improve the image-based multi-scale model through better aggregate contact model, and validate the model with different types of mixtures.
2. Compare the effect of binder viscoelastic properties and aggregate structure on the permanent deformation and stress/strain information within typical asphalt mixtures.
3. Investigate the effect of binder non-recoverable creep compliance and elasticity on permanent deformation of asphalt mixtures during repeated loading conditions.

## 5. Research Methodology

A comprehensive literature review is performed to evaluate the current state of knowledge on characterization methods of asphalt binder and mixtures. Digital imaging and multi-scale modeling techniques are also introduced to provide the basis of the research tool used in this dissertation.

The further development and improvement of the multi-scale model are conducted and detailed. To address the existing problem in the model, the model is improved to include the pre-defined contact points in both mixture and mortar images. The model is validated using the performance test data of mixtures with different binders and aggregate gradations. In addition, the model is further extended to utilize the asphalt binder data from MSCR test and also validated using the mixture performance test.

The improved model is applied as a tool to investigate the effect of binders with different viscoelastic properties on permanent deformation of asphalt mixtures and stress/strain within the asphalt mixtures, and study the effect of aggregate structure on the permanent deformation of asphalt mixtures. This analysis will lead to a better understanding of the effect of asphalt binder and aggregate structure in permanent deformation of asphalt mixtures and aid in more rational selection of modification techniques to enhance the rutting resistance of asphalt pavements.

Further applications of the model to predict the permanent deformations of asphalt mixtures under different conditions are also explored and discussed, including the simulations of asphalt mixtures with and without confining pressure, asphalt mixtures with different air voids contents and asphalt mixtures under moisture effect.

## **II. Literature Review**

### **1. Modification of Asphalt Binder**

A number of polymer modifiers have been added to asphalt binder and mixtures to address the problems of moisture damage, rutting, fatigue and thermal cracking existing in the asphalt pavements since 1950s. In general, two major types of polymers are commonly used in industry: plastomeric modifiers and elastomeric modifiers. Plastomeric modifiers such as polyethylene (PE) and Ethylene Vinyl Acetate (EVA) can help increase the stiffness of asphalt binder thus improving the resistance to permanent deformation of asphalt materials at high temperatures. Elastomeric modifiers such as Styrene-Butadiene-Styrene (SBS) and Styrene-Butadiene-Rubber (SBR) can be added to increase the elasticity of the asphalt binder which benefits the cracking resistance of asphalt binder.

Numerous studies have found that polymer modified asphalts (PMA) show better performances compared with unmodified binders. Collins et al. [11] compared the rheological properties of thermoplastic block copolymers modified asphalt binder and unmodified binder, and their corresponding mixture performances through the dynamic creep test and loaded wheel track test. They found that the polymer network in the modified asphalt binders resulted in a significant improvement of asphalt mixture performances at both high and low temperatures. Khattak et al. [12] studied the effect of SBS and SEBS triblock copolymers on the engineering properties of modified asphalt mixtures and found that the fatigue life and tensile strength were increased at intermediate temperature without affecting the elastic properties at low temperature. An increase in resilient modulus and resistance to permanent deformation were also observed at high temperatures. Kanitpong et al. [13] also evaluated the effects of modification on performances of asphalt mixtures

through indirect tensile strength test, uniaxial compression test and Hamburg Wheel Track test. They concluded that the polymer modified asphalt mixtures demonstrated overall better performance relative to unmodified and other types of modified asphalt mixtures.

## **2. Characterization of Asphalt Binder Rutting Resistance**

### **2.1 Superpave Rutting Parameter**

The Federal Highway Administration (FHWA) initiated a nationwide research program called the Strategic Highway Research Program (SHRP) in 1987 to address the limitations of the traditional characterization methods for asphalt binder [14]. The final outcome of this research was Superpave, of which Performance Grading (PG) of asphalt binder was one of the most important products. The Dynamic Shear Rheometer was introduced by Superpave as a tool to characterize the asphalt binder rheological properties, and the rutting parameter  $G^*/\sin \delta$  was proposed on the basis of energy dissipation calculated from the stress-strain curve [14].

Although the rutting parameter was specified in Superpave specification as the indicator of rutting resistance of asphalt binder, researchers found a very poor relationship between the rutting parameter and the permanent deformation observed in the field [15,16]. This parameter was considered inadequate in describing the rutting resistance of some binders, particular polymer modified binders. One of the major issue for the rutting parameter is that it is effective only in the linear viscoelastic region of asphalt binder properties. Since asphalt pavements typically experience high stress and strain situations under the traffic loading, the non-linear region of asphalt binder properties is also critical. In addition, polymer modified asphalt binders demonstrate high non-linear properties relative to the

traditional unmodified binders at high temperature; therefore, new characterization methods are deemed necessary to capture these properties for both unmodified and modified asphalt binders.

## **2.2 Repeated Creep and Recovery Test**

The FHWA sponsored NCHRP Project 9-10 “Superpave Protocols for Modified Asphalt Binders” evaluated the feasibility of the current Superpave system for modified asphalt binders [16]. It was concluded in the final report that the existing Superpave protocol cannot be applied to modified asphalt binder because the simplified assumptions for the Superpave procedure, such as linear viscoelasticity, cannot be extended to modified asphalt binders. The repeated creep and recovery (RCR) test was developed and recommended as a method to characterize the resistance of asphalt binder to permanent deformation in this project [16]. The RCR test utilized the DSR and recommend a shear stress ranging from 30 Pa to 300 Pa for 100 cycles with period of 1s loading and 9s unloading. A new parameter,  $G_v$ , was introduced as the viscous component of the creep stiffness based on the four-element Burger’s model to characterize the rutting resistance of asphalt binder.

The new test and parameter demonstrate a significant improvement in characterizing the rutting resistance of asphalt binders especially for polymer modified asphalt binders. Repeated loading is a more representative loading pattern of the actual loading on the pavement relative to the dynamic loading in Superpave; the RCR test also provides more information such as delayed elasticity which cannot be captured through the rutting parameter  $G^*/\sin \delta$  [17]. The RCR test is also capable of identifying the temperature susceptibility of asphalt mixtures to rutting [18]. However, researchers also found that a single stress level could not demonstrate the stress dependency of modified asphalt binders

and multiple stress levels were needed to better characterize the rutting resistance of asphalt binders [19]. Conducting the RCR test at multiple stress levels would require a significant amount of time which is not practical.

### **2.3 Multiple Stress Creep Recovery Test**

To improve the efficiency of the RCR test at multiple stress levels, the Multiple Stress Creep Recovery (MSCR) test was introduced based on the further development of the RCR test. The MSCR test currently specified in standard test method AASHTO T350 and specification AASHTO M332, which is both performance-based and blind to modification type [20], was developed by the FHWA as a replacement for the existing AASHTO M320 high-temperature asphalt binder test. Initially the MSCR test included 11 stress levels: 25, 50, 100, 200, 400, 800, 1600, 3200, 6400, 12800 and 25600 Pa [19]. Being further improved, the current MSCR test uses the 1s creep loading followed by 9s recovery over two stress levels of 0.1 and 3.2 kPa at 10 cycles for each stress level. The average non-recoverable strain for the 10 creep and recovery cycles is then divided by the applied stress for those cycles yielding the non-recoverable compliance,  $J_{nr}$ . Percent recovery (%R) is another important parameter from the MSCR test to reflect the elastic property of the asphalt binder, which is a measure of how much the asphalt binder sample returns to its initial shape after being repeatedly sheared and relaxed.

The MSCR test has proven to be able to distinguish the difference in rutting potential between various binders including both modified and unmodified binders through numerous studies [19, 20]. These findings indicated that the non-recoverable compliance  $J_{nr}$  is a suitable replacement for the SHRP high-temperature binder criteria and correlates well to the rutting resistance of asphalt mixtures [20, 21]. Moreover, the AASHTO M332

specification proposes a performance grading protocol for asphalt binder based on MSCR test as a supplement of the original PG system. Four traffic levels including standard, high, very high and extremely high traffic loading are designated and incorporated into the specification as levels of “S”, “H”, “V”, and “E”. This specification also recommends curve correlating  $J_{nr}$  versus %R as the criterion to determine the presence of an elastomeric polymer as presented in Figure II-1. The significance of  $J_{nr}$  and %R in permanent deformation of asphalt mixtures are not well understood yet.

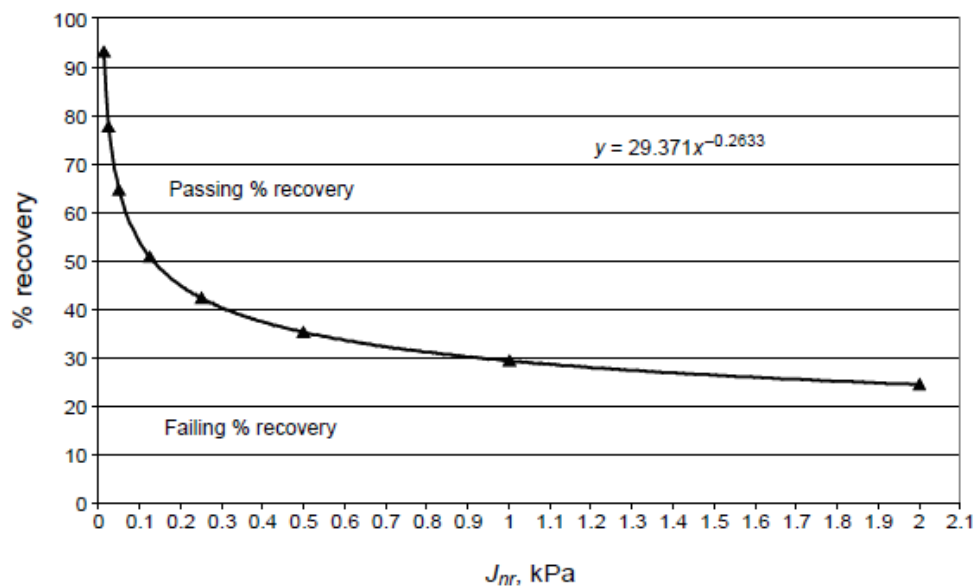
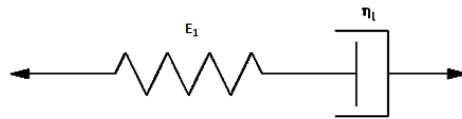


**Figure II-1: Passing curve in AASHTO M332**

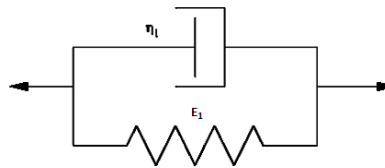
### 3. Rheological Models for Asphalt Binder

As a type of viscoelastic material, asphalt binder can be modeled in order to determine its stress-strain relationship and predict the mechanical response of the material under a specific loading condition. For the purpose of simplicity, linear viscoelasticity theory is usually applied for asphalt binder in constructing the rheological model. The viscoelastic behavior is described and modeled as linear combinations of springs and dashpots,

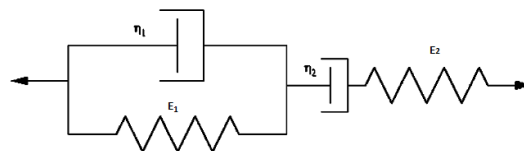
representing the elastic and viscous components, respectively. By arranging the elements differently, various viscoelastic models are constructed such as Maxwell model, Voigt model and Burger's model. The Maxwell model is a combination of spring and dashpot in series; the Voigt model is a combination of spring and dashpot in parallel; and the Burger's model is a combination of Maxwell unit and Voigt unit in series (Figure II-2). Researchers have applied these models to describe the rheological behavior of asphalt binders since early 1940s [22, 23].



(a) Maxwell model



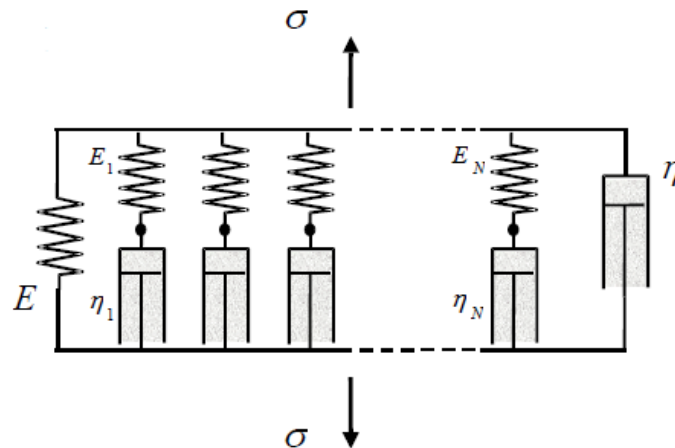
(b) Voigt model



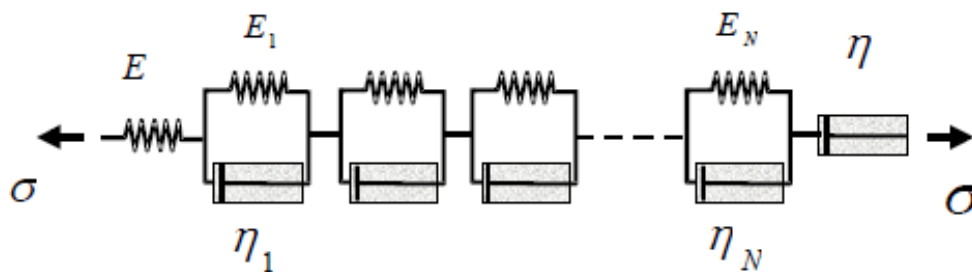
(c) Burger's model

**Figure II-2: Illustration of simple rheological models**

Although the Maxwell, Voigt and Burger's models seem straightforward and easy to understand, they also exhibit significant limitations in describing the asphalt rheological behavior as the model curves are not completely compatible with the results of laboratory tests [24]. Therefore more complex models constructed with more and more elements such as the generalized Maxwell model which consists of  $N$  Maxwell units in parallel and the generalized Voigt model which consists of  $N$  Voigt units in series are developed for adequate curve fitting (Figure II-3).



(a) Generalized Maxwell model



(b) Generalized Voigt model

**Figure II-3: Rheological models with multiple Maxwell/Voigt units**

The form of a Prony Series has been widely adopted in fitting the asphalt rheological test data following the generalized Maxwell model due to its good precision and efficient mathematical operations. A generalized Maxwell model with three Maxwell units in the form of a Prony Series was used by Papagiannakis et al. [25] to describe the asphalt binder viscoelastic behavior and further implemented into the finite element analysis software, demonstrating its effectiveness in simulating the dynamic modulus of asphalt mixtures under the Superpave Shear Test. Dai et al. [26] also used a generalized Maxwell model with one spring and four Maxwell units in form of Prony Series to represent the viscoelastic behavior of asphalt mastic and successfully predicted the complex modulus of asphalt mixtures.

#### **4. Characterization of Asphalt Mixture Rutting Resistance**

Four types of mixture rutting tests are widely used to characterize the permanent deformation of asphalt mixtures, including the uniaxial stress test, tri-axial stress test, indirect tensile loading test and loaded wheel track test. Among these tests, the Flow Number (FN) test, or repeated creep loading test, is one of the most commonly used.

The Flow Number test procedure was developed using the simple performance tester in NCHRP Report 465 [6] and is currently specified in AASHTO TP 79 to measure the rutting resistance of asphalt mixtures. The typical outcome from the Flow Number test is presented as Figure II-4. As observed, an asphalt mixture subjected to a repeated load shows three different creep response stages: primary, secondary, and tertiary. In the primary zone, the strain increases sharply and strain rate decreases rapidly to a constant rate; in the secondary zone, the strain increases linearly and the strain rate is constant up to tertiary zone; and in the tertiary zone, the strain rate increases rapidly, leading to complete failure of the asphalt

mixture structure. The flow number is defined as the number of cycles at which the sample starts the tertiary creep, or unstable flow. It can also be more clearly defined as the number of cycles at the minimum permanent strain rate of the sample under creep loading.

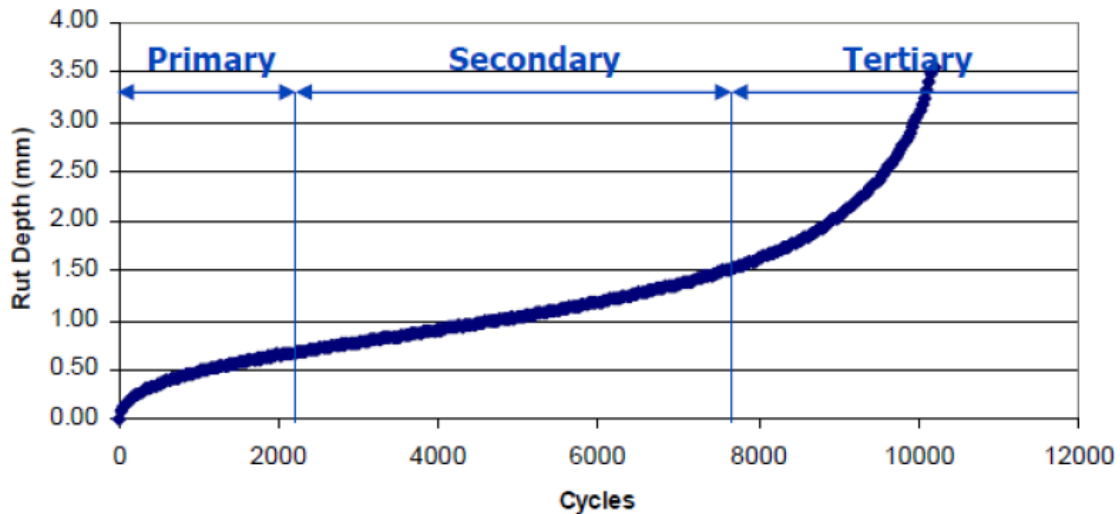


**Figure II-4: Permanent deformation curve from Flow Number test**

The NCHRP Report 465 [6] demonstrated a strong correlation between the field performance and the flow number tested in laboratory, indicating the effectiveness of Flow Number test in characterizing the rutting resistance of asphalt mixtures. In addition, the simplicity and practicality of uniaxial tests have made the uniaxial Flow Number test (without confined pressure) a widespread test for determining the rutting response of the material relative to the tri-axial Flow Number test (with confined pressure).

## **5. Digital Image Processing and Analysis of Asphalt Mixtures**

Digital Image Processing and Analysis techniques have recently been developed as researchers found that the change of internal structures of the asphalt mixtures dominates the variation of mechanical responses for the asphalt mixtures [27, 5]. In order to

characterize the internal structure properties and distribution of the air voids, an internal mix image is acquired, processed and analyzed. Both destructive and non-destructive methods exist for acquiring the mixture image. Destructive methods require cutting of the asphalt mixture sample horizontally or vertically to provide a surface for scanning. Non-destructive methods, such as X-ray computed tomography (XRT), can capture 2D and 3D images of asphalt mixture without damaging the sample. Once the mixture internal structure image is obtained, image processing is needed to enhance the quality and reduce the noise of the image. The processed image of the mixture internal structure is analyzed and the desired parameters related to the microstructure are proposed and quantified.

The XRT was used to study the air void distribution in asphalt mixtures by Masad et al. [28] and it was found that a 'bathtub' shape distribution exists in the air voids of gyratory compacted asphalt mixture samples. Adhikari et al. [29] also utilized the XCR technique to study the aggregate orientation, aggregate gradation, mastic distribution and air voids in asphalt mixtures. Although the XRT provides more precise images and is capable of capturing images for 3D re-construction of the asphalt mixture sample, the cost of the XRT equipment make it difficult be widely used in the research.

Many researchers have been working on improving the precision of the 2D images in representing the asphalt mixture internal structures to make 2D visualization a more effective tool [27, 5]. The Image Processing & Analysis System (iPas) is a 2D image processing software developed at the University of Wisconsin-Madison to quantify the internal features of compacted asphalt mixture [27, 5]. To obtain the image of asphalt mixtures, the compacted mixture sample is cut into three sections and each section is scanned by a standard office scanner. The scanned digital image is converted to a binary

image for microstructure analysis by selecting a threshold value. Once a representative binary image is determined, microstructure analysis is performed based on the image. The microstructure properties such as contact points and contact lengths, aggregate orientation and aggregate segregation can be quantified to provide the information related to the internal structure of asphalt mixtures [27, 5].

With the internal structure images of asphalt mixture available, researchers have also begun using Finite Element Methods (FEM) by mapping the pixels from the processed image to the elements in FEM to simulate the mechanical behavior of asphalt mixtures. Arshadi [9] introduced an image-based multi-scale procedure for simulating the fatigue behavior of asphalt mixtures using finite element software. The asphalt mixture sample was cut and a flatbed scanner was used to capture color images of sample cross sections. A 2D digital image processing technique was used to convert the color images to binary images and the binary images were imported into the finite element software ABAQUS through mapping the image pixels to elements in ABAQUS using MATLAB codes. With this image-based model, the fatigue behavior of the asphalt mixtures was successfully predicted and validated using asphalt mixture performance test [9].

## **6. Effect of Aggregate Internal Structure on Asphalt Mixture Performance**

It has been widely recognized that the modification of asphalt can improve the overall performance of asphalt mixtures. The improved rheological properties of modified asphalt binder were usually considered as the major contributor to this improvement in the past decades. However since the aggregate internal structure is the portion that provides the skeleton of the mixtures and the load bearing capacity, the effect of the modification on the

formation of the aggregate structure is not well investigated. Due to the difficulty in evaluating aggregate structure independently through laboratory tests, very few research studies exist on studying effect of aggregate structure on the performances of asphalt mixtures. Recently with the development of image processing and analysis techniques, the aggregate structure can be represented effectively, thus making it possible to study the characteristics of the internal structures in asphalt mixtures.

Yue et al. [30] adopted the digital image processing and analysis technique to evaluate the effect of compaction methods on the aggregate internal structure properties by quantifying the aggregate gradation, aggregate shape and particle orientation. They also validated the existence of correlation between aggregate structure properties and asphalt mixture performance. Masad et al. [31] used the XRT technique to study the effect of different compaction effort levels on aggregate internal structure. Parameters such as aggregate segregation, aggregate proximities and air voids distribution were developed to quantify the internal structure features. It was found that aggregates followed a certain orientation during the initial compaction effort and tended to be randomly distributed after reaching a certain compaction level. The utilization of the image processing and analysis technique sheds light on the capability of imaging technique in studying the internal structure of asphalt mixtures and its correlation with mixture performances.

A 2D image analysis software named as Image Processing and Analysis System (iPas) was introduced and developed in the University of Wisconsin-Madison [27, 5] to investigate the microstructure properties of asphalt mixtures. A typical digital image processing method was used in the software to convert the scanned image to binary image. Different parameters were proposed to characterize the internal structure of asphalt mixtures

including contact length and contact points, aggregate orientation and aggregate segregation. A strong correlation between the internal structure parameter of contact length and the rutting resistance of asphalt mixture obtained from performance test was found [5]. Researchers also extended the use of the imaging technique to investigate the correlation between the aggregate structure and low temperature properties, and found that both thermo-volumetric property and tensile strength at low temperatures were directly related to the internal structure of asphalt mixtures [32, 33].

## **7. Finite Element Analysis Method**

Due to the significant amount of time and cost needed for running laboratory mechanical tests for the evaluation of asphalt mixture performance, the incapability of separating the confounded effects in the materials on the performances, and describing the microstructure characteristics of the asphalt mixtures, the Finite Element Method (FEM) has been used as an effective research tool to predict and evaluate the mechanical responses of asphalt mixtures [34, 35].

The Finite Element Method was first introduced systematically by Turner et al. [36] in Aerospace Engineering. The concept of the FEM is based on the discretization of the domain of the problem into subdomains (i.e. elements). The displacements, stresses and strains of an element are calculated through the nodal displacements of the element. The element stiffness matrices are calculated and assembled to form the global stiffness matrix in order to calculate all the unknown displacements or forces.

Researchers have successfully applied the FEM in simulating and investigating the mechanical behavior of asphalt mixtures during the past twenty years. Chen et al. [37]

investigated the effect of axial load on asphalt mixture performance through the FE software ABAQUS, and found that asphalt pavement layers experienced higher tensile stress under uniform pressure relative to irregular pressure. Kose et al. [34] studied the distribution of strain in asphalt binder using the 2D FEM. Papagiannakis et al. [25] also developed a 2D FE model to predict the shear modulus of the compacted asphalt mixtures. Helwany et al. [38] used a 3D FE model and applied it to study the sensitivity of the strains at the top and bottom of asphalt concrete layer to the tire pressure. The 3D FE analysis seems to be more representative in describing the material behaviors, however a study conducted by Hua et al. [39] indicated that the difference between 2D and 3D FE analysis for the pavement rutting is not significant and the maximum difference of the rut depth between the two methods is less than 2%. Considering the amount of time and resources needed for running the 3D FE model, 2D analysis is a more practical option in most cases. Due to the complexity of the asphalt material properties, more advanced constitutive models are used to describe the behavior of asphalt materials. Therefore it is necessary to incorporate this type of user-defined material behavior through the user material subroutine (UMAT) of the FE analysis software ABAQUS to improve the precision of simulation results. Dai et al. [40] adopted Schapery's non-linear viscoelastic model and defined a rate-independent damage behavior for the asphalt materials, and incorporated this behavior into ABAQUS through the UMAT subroutine to study its effect on the mechanical response of asphalt mixtures. In another study, a thermodynamic-based constitutive relationship coupling the non-linear thermo-viscoelasticity, thermos-viscoplasticity and damage behavior of asphalt materials was proposed by Darabi et al. [41] and further implemented into the FE software through UMAT.

## 8. Multi-scale Modeling of Asphalt Mixtures

Asphalt mixtures consist of asphalt binder, air voids and aggregate particles with different sizes and shapes. Simulating such a complex composite material including all elements of asphalt binder and aggregate through the numerical methods such as FEM requires tremendous computational cost [42]. This has led researchers to seek more advanced analysis methods for the microstructure mechanics of asphalt mixtures at a reasonable cost. Multi-scale modeling technique have been one of the popular methods for studying the mechanical response of asphalt mixtures.

Multi-scale modeling refers to the modeling technique performed at different length scales of asphalt mixtures, typically including asphalt binder scale, mastic scale, and mortar scale [43]. The macro-scale material properties can be predicted from the lower-scale material properties through the multi-scale modeling technique [42, 43]. The material properties at the lower-scale is determined and homogenized, then transferred to the next higher scale through upscaling [43]. Different length scales are linked with each other through homogenization as presented in Figure II-5. Due to the homogenization process at each scale, the computational cost can be significantly reduced in simulating the macro-scale material behaviors without adversely affecting the accuracy of results as all properties of constituents are still taken into account in the analysis.

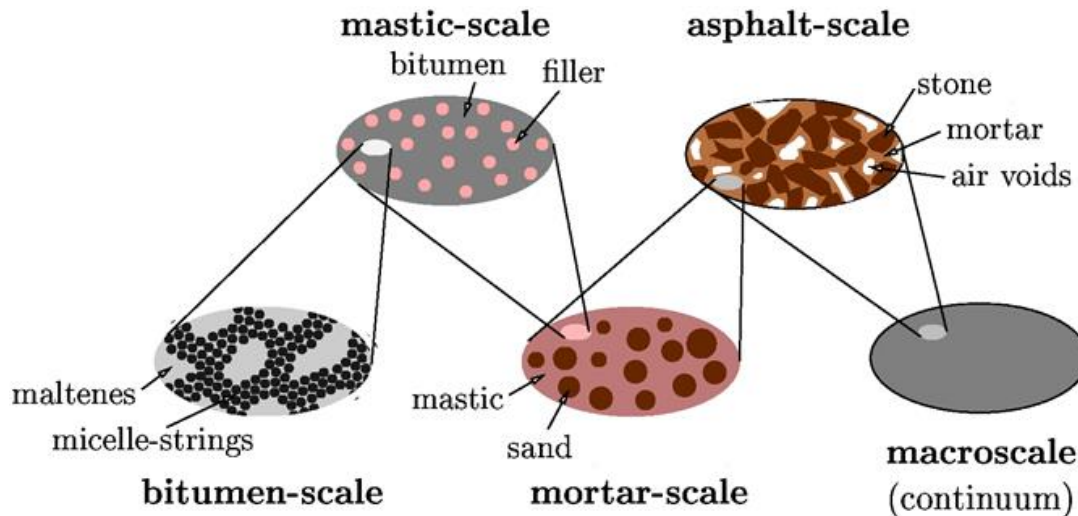


**Figure II-5: Multiple length scales defined in multi-scale modeling [43]**

Multi-scale modeling of asphalt mixtures is becoming a popular technique as it gains improved insight into the microstructure mechanisms that affects the macro-scale material behavior and eventually its performance. A number of research efforts have been paid to investigate the use of this modeling tool to evaluate and predict the asphalt mixture properties [42, 43, 44, 45, 46]. Aigner et al. [43] proposed a concept of using multi-scale models to predict the mechanical behavior of asphalt mixtures. The rheological properties of asphalt binder was measured and employed as input to determine the property of asphalt mastic through the “Elastic-Viscoelastic Correspondence Principle”. The mortar property was determined from the asphalt mastic, and similarly for the asphalt mixture. Agreement was found between the predicted creep properties of asphalt mixtures from the multi-scale model and the laboratory test results. Lutif et al. [42] performed a study to investigate the effect of material properties such as heterogeneity, inelasticity and anisotropic damage accumulation at micro-scale on the macro-scale behavior of asphalt mixtures. They concluded that this effect can be effectively captured through the multi-scale modeling and finite element simulation. It was also shown that by using the multi-scale modeling

technique, the computational cost was significantly reduced compared with a single scale analysis including all of the materials properties. Yin et al. [45] simulated the three-point bending fracture test by combining the macro-scale and meso-scale analysis through a multi-scale model to account for the heterogeneity of asphalt mixtures. They claimed that comparable modeling results were obtained relative to the experiment results using the multi-scale model, which reduced a significant amount of elements to be analyzed in the model. Underwood [46] also utilized the concept of multi-scaling to develop a constitutive multi-scale model linking the different length scales into a model capable of predicting the effects of microstructure changes on the macro-scale behavior of asphalt mixtures.

Recently an image-based multi-scale modeling approach has been developed based on the Finite Element (FE) Method to investigate the fatigue behavior of asphalt mixtures by Arshadi [9]. In this approach four different scales were modeled including asphalt binder, mastic, mortar and mixture scale. Homogenization and up-scaling techniques were used to transfer the material properties from lower scale to higher scale. The mastic scale contains fillers ranging from  $1\mu\text{m}$  up to  $75\mu\text{m}$  in a binder matrix; the mortar scale contains fine aggregates ranging from  $75\mu\text{m}$  to  $1.18\text{mm}$  in a mastic matrix, and the mixture scale contains all larger aggregates (those detected using 2D scanners and imaging filters) in a continuous mortar matrix. The data from binder Frequency Sweep tests were used to derive the binder master curve and fitted in the form of Prony Series. The binder properties were implemented into ABAQUS via the user material subroutine (UMAT). The 2D artificial images of mastic and mortar were generated based on the real aggregate particle shapes, and the aggregate distributions and volume fractions characterized through FE simulations. The 2D scanned images of asphalt mixtures were then used by elimination of the fine

particles and addition of the artificial air voids to study the asphalt mixture mechanical behavior. This multi-scale model was used by Arshadi [9] to predict the fatigue damage in asphalt mixtures through coupling the viscoelastic continuum damage (VECD) mechanics from binder scale to mixture scale. The simulation results of the asphalt mixture matched well with indirect tensile fatigue test results, indicating the capability of this model in predicting the fatigue behavior of asphalt mixtures under loading. Arshadi also explored the possibility of using this model to predict the permanent deformation of asphalt mixture under repeated loading by applying a simple particle-to-particle contact model and a non-linear superposition method to transfer the effect of the particle contact at lower scale to the next higher scale.

## **9. Overview of the Image-based Multi-scale Model**

### **9.1 Multi-scale Analysis Approach**

The image-based multi-scale analysis procedure developed in a previous research study to predict the fatigue behavior of asphalt mixtures using the Finite Element Analysis was similarly used in this study [9]. Different steps of the multi-scale analysis are summarized and shown in Figure II-6. The material properties are modeled heterogeneously at each scale and homogenized as the inputs of the matrix for the next higher scale. The detailed homogenization and up-scaling procedure is described as follows.

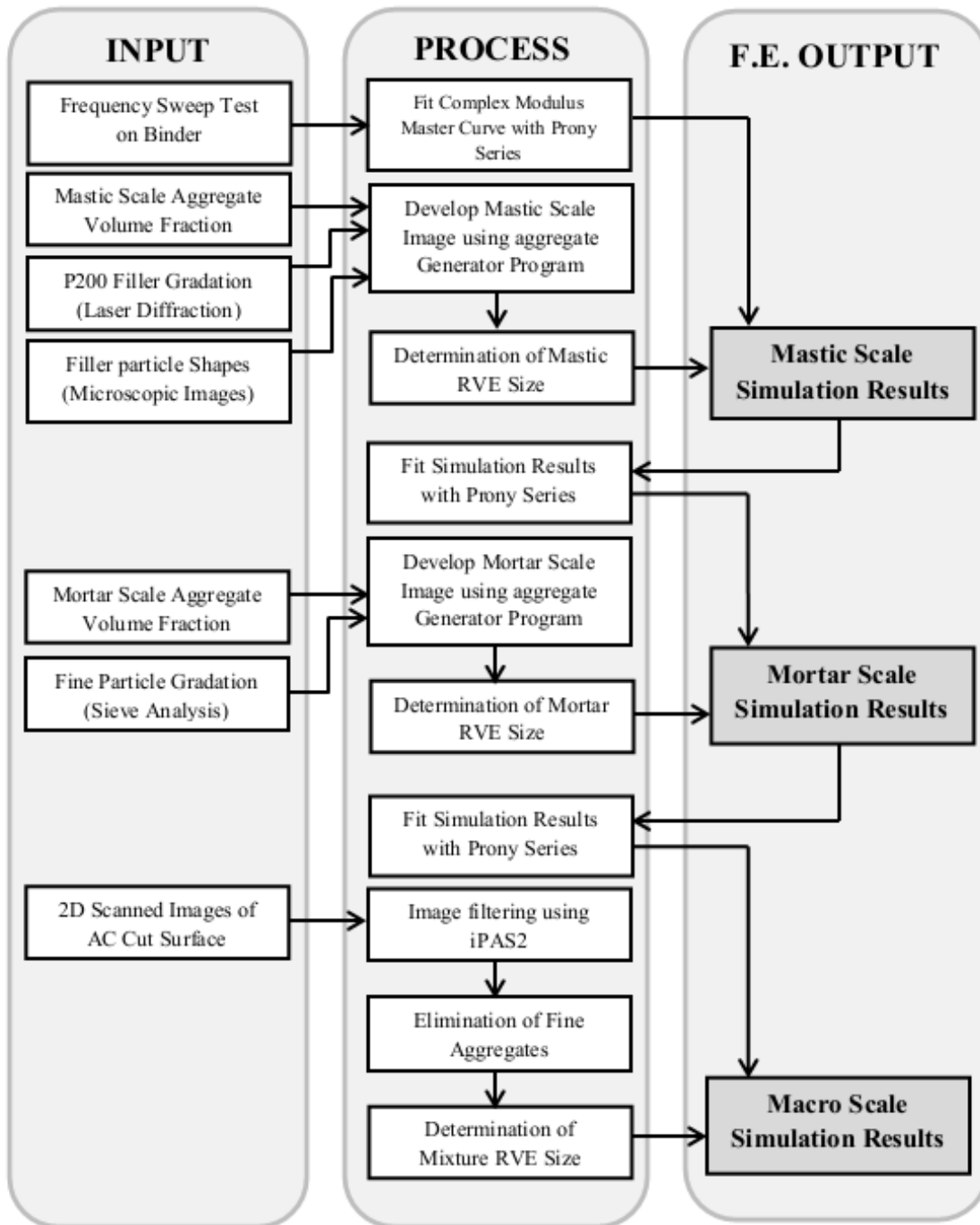


**Figure II-6: Flowchart of the multi-scale analysis procedure [9]**

The linear viscoelasticity assumption is followed so that the Boltzmann Integral can be used as the constitutive relationship for asphalt binder. The shear Frequency Sweep test is performed on the asphalt binder using DSR and the relaxation moduli out of the test is

fitted using the Generalized Maxwell model in the form of a Prony Series, which is a commonly used phenomenological model to describe the rheological behavior of asphalt binder. The shear relaxation moduli are converted to elastic relaxation moduli using Poisson's ratio of 0.49 for asphalt binders, and further entered into ABAQUS as the binder inputs. The numerical implementation is also performed on the one-dimensional linear constitutive model for asphalt binder based on the incremental finite-element modeling scheme with constant strain rate over each time increment proposed by Zocher et al. [47] to formulate the three-dimensional behavior of asphalt binder through the user material subroutine UMAT of ABAQUS.

The volume fractions for the components at each scale are critical in creating the mastic and mortar images using the MATLAB generated program, and can be calculated from the mix design information. The mastic binary image is created by a MATLAB based program using the realistic shapes of the filler particles, the particle gradation and the volume fraction of the fillers to randomly distribute the filler particles into the asphalt binder matrix. The "Laser Diffraction" technique is used to experimentally determine the gradation of fillers and the realistic geometries of the filler particles are captured through microscopic imaging. Frequency sweep simulation was applied on mastic scale by applying a uniaxial sinusoidal strain controlled loads with loading frequencies ranging from 0.01 to 100 Hz to determine the complex modulus master curve at a low strain amplitude level. The contact law and contact function were also proposed by Arshadi to explore the possibility of using the model to predict the permanent deformation of asphalt mixtures other than fatigue behavior. The information regarding contact law and contact function are further introduced in the following sections.

The representative volume element (RVE) is the smallest volume/area that can be used to representatively determine the bulk properties of the composite material. Determination of RVE is important in modeling as it significantly reduces the amount of computations needed by decreasing the number of elements. To determine the RVE, mastic image with different sizes as shown in Figure II-7 are modeled to determine the convergence of the creep compliance curves of the mastic. In the example of the mastic shown in Figure II-7 and Figure II-8, the RVE is determined as  $225 \mu\text{m} \times 225 \mu\text{m}$ .

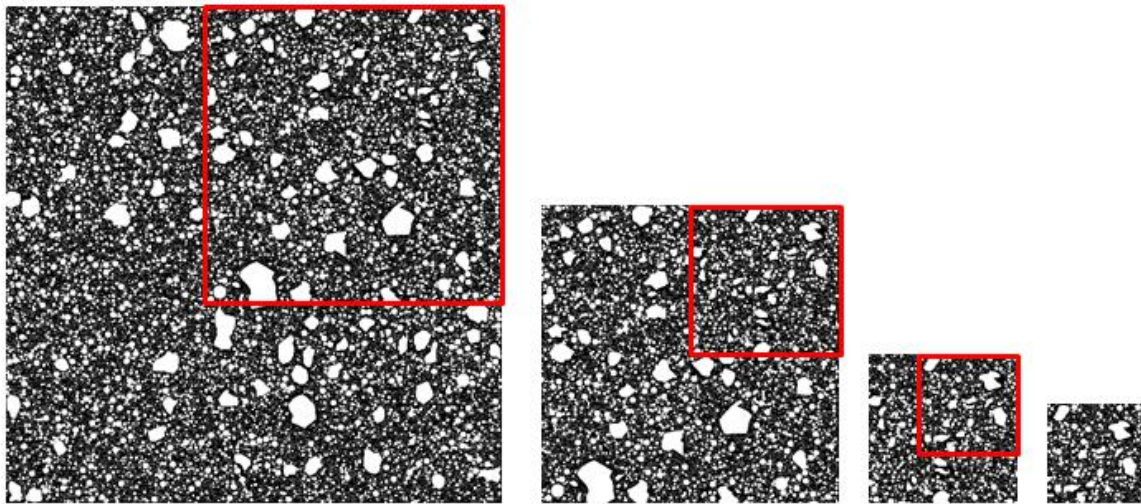


**Figure II-7: Mastic images with different RVE sizes: (a)  $750 \mu\text{m} \times 750 \mu\text{m}$  (b)  $450 \mu\text{m} \times 450 \mu\text{m}$  (c)  $225 \mu\text{m} \times 225 \mu\text{m}$  (d)  $150 \mu\text{m} \times 150 \mu\text{m}$  [9]**

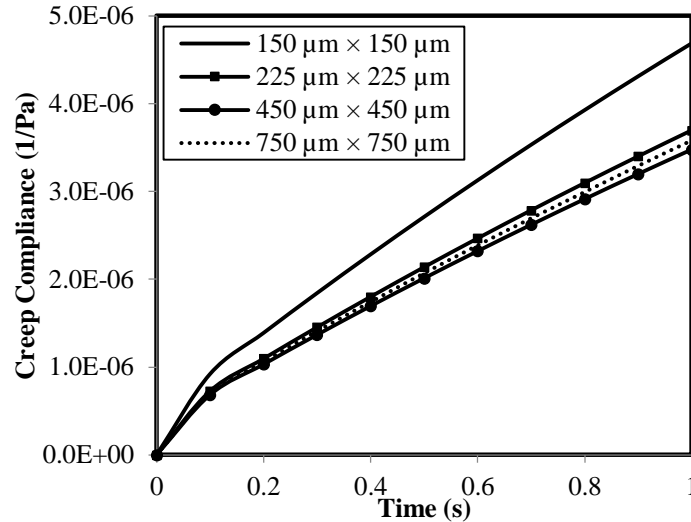


**Figure II-8: Convergence of the mastic creep compliance curves [9]**

Similar to the mastic scale, the mortar image is generated based on the real aggregate shapes, gradation and volume fraction. The RVE of mortar is determined and the simulations to obtain the master curve of mortar and particle contact function at mortar scale are also performed. To obtain the mixture image for simulation, the mixture sample is compacted and cut vertically, and the cross section of the mixture is scanned using a flatbed office scanner. A 2D image processing technique using iPas software is used to convert the colored images to binary images. Due to the limitations of the resolution of the scanner, the aggregate with size smaller than 1.18mm cannot be captured accurately. Therefore those aggregates are eliminated from the mixture image using a MATLAB program and considered at the lower scales. In addition, due to the lack of contrast between air voids and the asphalt in the mixture images, the artificially generated air voids are embedded into the mix image (Figure II-9) based on the ‘bathtub’ shape distribution found by Masad et al. [28]. The air voids are considered as empty spaces in ABAQUS simulation without any material properties assigned. Once the mixture image is prepared and imported

into ABAQUS, the loading and boundary conditions are added and the mechanical response of the asphalt mixtures can be simulated.

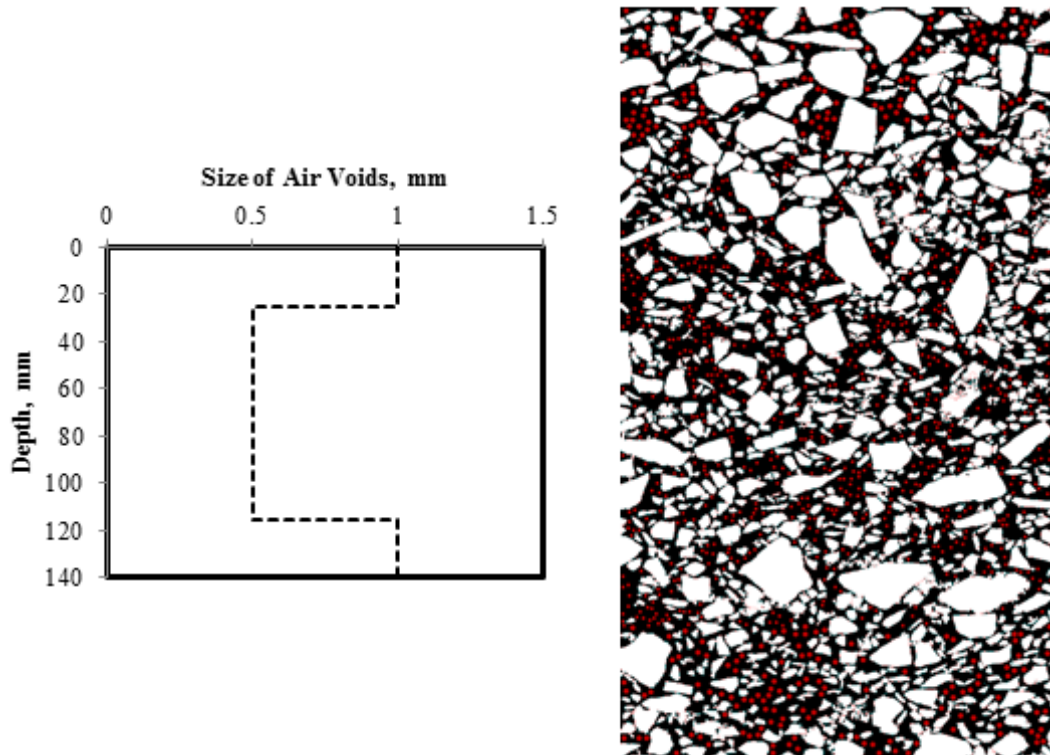


**Figure II-9: Distribution of air voids based on the “bathtub” shape [9]**

### **9.2 Modeling of Aggregate Particle-to-Particle Contact**

A simple aggregate particle-to-particle contact law was proposed by Arshadi [9] to simulate the permanent deformation of asphalt mixtures based on the distance between the particles (binder film thickness) as shown in Figure II-10. As the aggregate particles approach each and come in contact (with binder film thickness equal to zero), the binder elements in between are stiffened with the stiffness being replaced as aggregate stiffness. This contact law is implemented into ABAQUS through the user material subroutine UMAT for simulation of mastics.

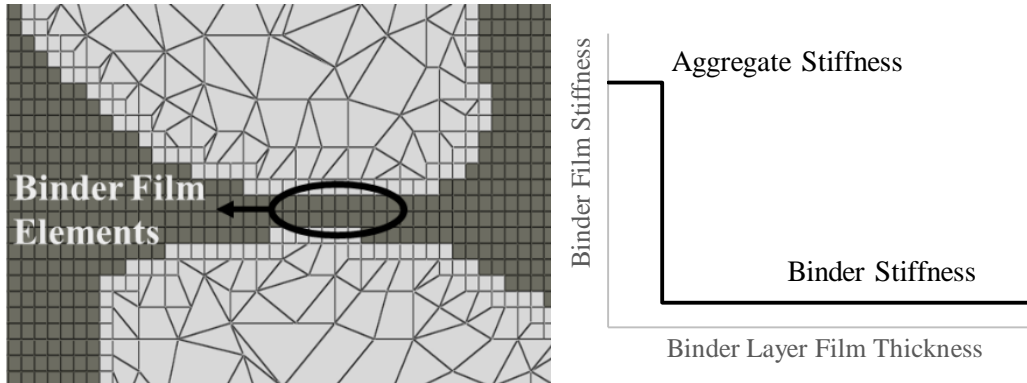


**Figure II-10: Contact law defined based on binder film elements**

In order to upscale the effect of the contact law at mastic scale on the material behaviors at the next higher scale, namely mortar scale, a quasi-linear superposition is used for the relaxation modulus in the constitutive equation to allow the dependency of relaxation modulus to strain level (Equation II-1).

$$\sigma(t) = \int_0^t E(t - \tau, \epsilon(\tau)) \frac{d\epsilon(\tau)}{d\tau} d\tau.$$

**Equation II-1**

Where  $E(t, \epsilon) = E(t) \cdot \Omega(\epsilon)$ .

A creep loading simulation at mortar scale with contact law included for mastic phase is performed to determine the creep compliance of mortar which was further converted to the time and strain dependent relaxation modulus through Laplace Transforms. The strain-dependent part  $\Omega(\epsilon)$  of the relaxation modulus, namely contact function, was calculated with the already known  $E(t)$  from the frequency sweep simulation. A similar procedure is followed to determine the contact function at the mixture scale based on the simulations at the mortar scale.

### III. Materials and Methods

#### 1. Materials

In order to validate the improved image-based multi-scale model in this study and investigate the effects of modification of asphalt binders and aggregate internal structure on the permanent deformation of asphalt mixtures, mixtures with three different binders and two aggregate gradations were designed and produced.

##### 1.1 Asphalt Binders

A single asphalt binder source was used in this study with asphalt PG 64-22. Two types of polymers, namely elastomeric modifier (linear styrene-butadiene-styrene block copolymer, denoted as SBS) and plastomeric modifier (polyethylene, denoted as CBE throughout this dissertation) were added targeting two high temperature grade bumps for the neat binder. The modifiers were blended with the neat binder at the percent presented in Table III-1. Note that the percent is based on the weight of the asphalt binder. The neat binder was also included in this study as the control binder. To simulate the short-term aging condition in the asphalt mixtures and asphalt pavement in the field, all the asphalt binders studied were aged using Rolling Thin Film Oven (RTFO) before the binder properties were characterized.

**Table III-1: Percent modifier used and the true grade of the modified asphalts**

<b>Modifier Type</b>	<b>Percent (%)</b>	<b>True Grade (°C)</b>
Elastomeric Modifier (SBS)	3.2	77.88
Plastomeric Modifier (CBE)	4.7	78.08

## 1.2 Aggregate Gradations

Two significantly different gradations of the limestone aggregates used in a previous study on internal aggregate structure [27] were also used in this study, categorized as coarse and fine gradations as shown in Figure III-1. The two gradations were designed as the extreme conditions according to the current Superpave mix design limits in order to maximize the difference between the two gradations and better present the influence of the aggregate gradations.

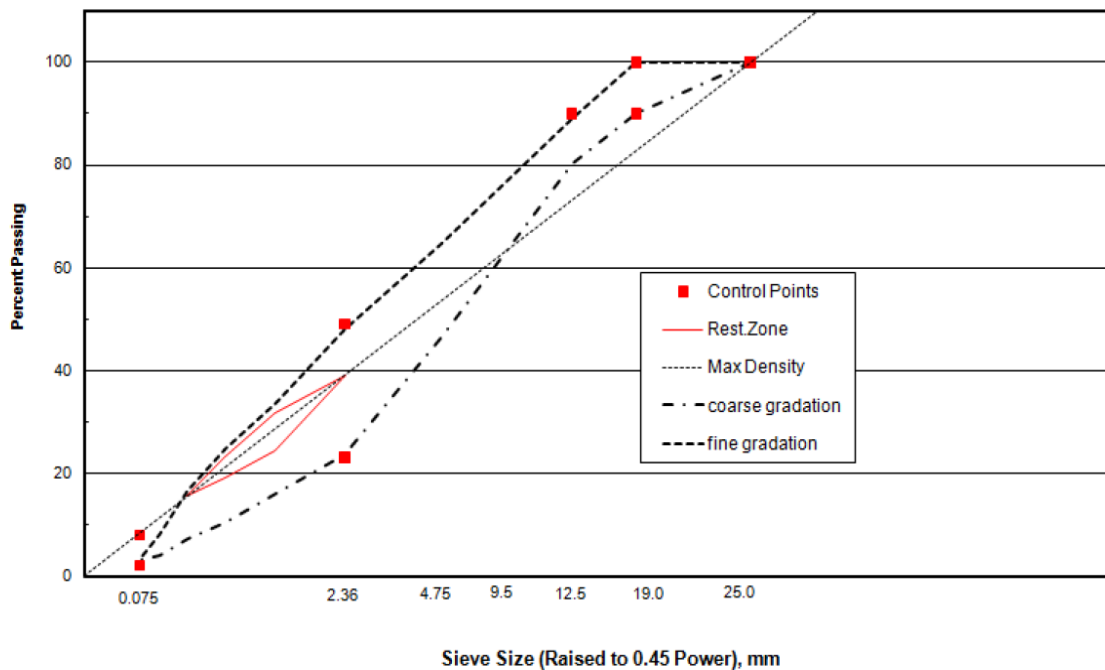


**Figure III-1: Gradations used in this study [27]**

Fine and coarse graded mixtures with unmodified and modified binders were designed and compacted for performance tests. The optimum asphalt contents were determined to be 4.62% and 5.55% for the fine and coarse mixtures of neat binder, respectively, based on the Superpave mix design targeting the air voids of 4%, and maintained for the other two

modified asphalt mixtures. Then the performance samples were prepared targeting the air voids of 7% based the mix design information obtained.

## **2. Asphalt Binder Tests**

Two types of asphalt binder tests were used to determine the rheological properties of asphalt binder in this study: Frequency Sweep (FS) test and Multiple Stress Creep Recovery (MSCR) test.

### **2.1 Frequency Sweep**

Frequency Sweep (FS) test is a common test used to characterize the rheological properties of asphalt materials. The FS test was performed at selected temperatures (i.e. 5°C, 25°C, 45°C and 58°C in this study) in the Dynamic Shear Rheometer (DSR). An oscillatory shear loading at a constant amplitude was applied on the specimen over a range of loading frequencies. In this study the strain amplitude of 0.1% was used over a range of frequencies listed as follows (in Hz): 0.2, 0.4, 0.6, 0.8, 1.0, 2.0, 4.0, 6.0, 8.0, 10, 20, 30. The complex shear modulus and phase angle were recorded at each frequency.

Since asphalt is a thermo-rheologically simple material, meaning that the effect of temperature is equivalent to a time shift on material properties, the time-temperature superposition principle can be applied [48]. The Arrhenius relation and WLF equation are commonly used to determine the shift factor [49, 50]. The master curve which describes the asphalt rheological property over a wide range of frequencies can be derived after shifting the curves at different temperature to the reference temperature. An example of the construction of the master curve for asphalt binder is presented in Figure III-2 and Figure

III-3. In this study, the reference temperature was selected as 46°C to be consistent with the mixture performance tests.

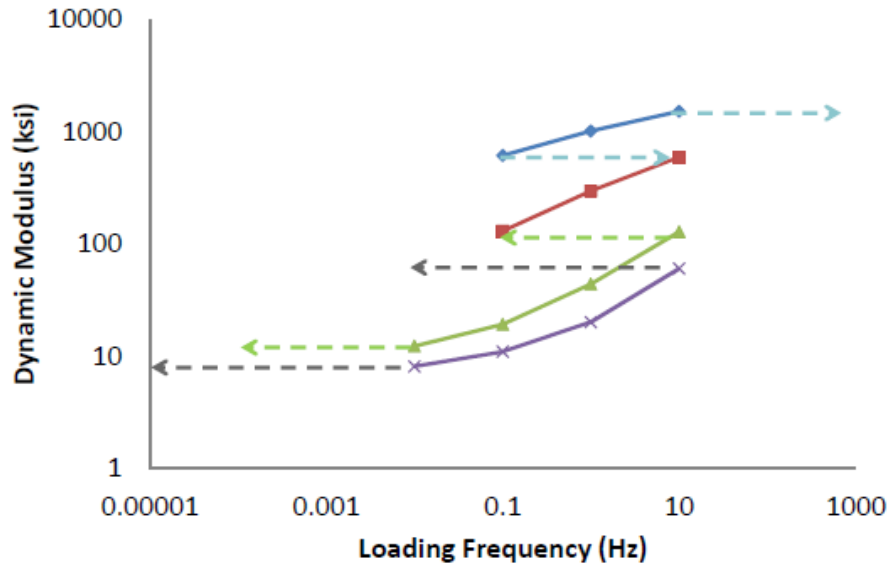


Figure III-2: Example of dynamic modulus curves of asphalt binder at 4°C, 20°C, 40°C and 50°C (from top to bottom)

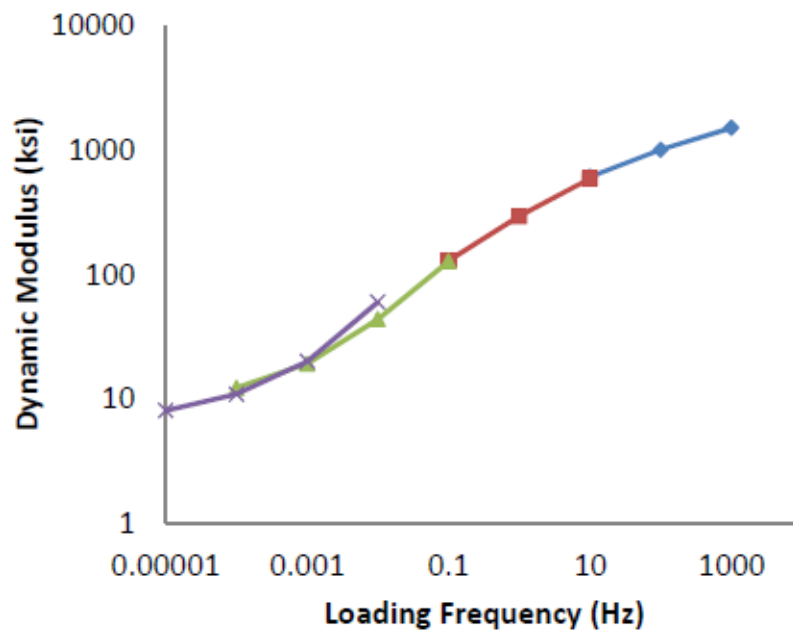


Figure III-3: Constructed master curve at 20°C

## **2.2 Multiple Stress Creep Recovery Test**

The Multiple Stress Creep Recovery (MSCR) test procedure specified in standard test method AASHTO T350 was followed in this study. The test temperature was selected as 46°C in this study to maintain the consistency with other binder and mixture tests.

## **3. Asphalt Mixture Tests**

The repeated creep loading test (commonly known as the Flow Number test) specified in AASHTO TP79 was used in this study to evaluate the rutting performance of different mixtures and validate the modeling results with the experimental data. The schematic of the test setup is presented in Figure III-4. The linear variable differential transformers (LVDT) are used to measure the accumulated axial deformation of the asphalt mixture sample. The Flow Number test consists of 0.1s pulse loading and 0.9s rest period. In this study the test was conducted at 46°C on the sample with diameter of 100mm and height of 150 mm compacted to the target air voids of  $6.5\pm 0.5\%$ . Two replicates were tested for each type of mixture. The flow number was defined as the number of cycles required for the asphalt mixtures to exhibit the tertiary flow as shown in Figure III-5 (a). It can also be more clearly defined as the number of cycles at the minimum permanent strain rate of the mixture sample under creep loading as shown in Figure III-5 (b). The unconfined condition and the stress level of 345 kPa were used in this study.

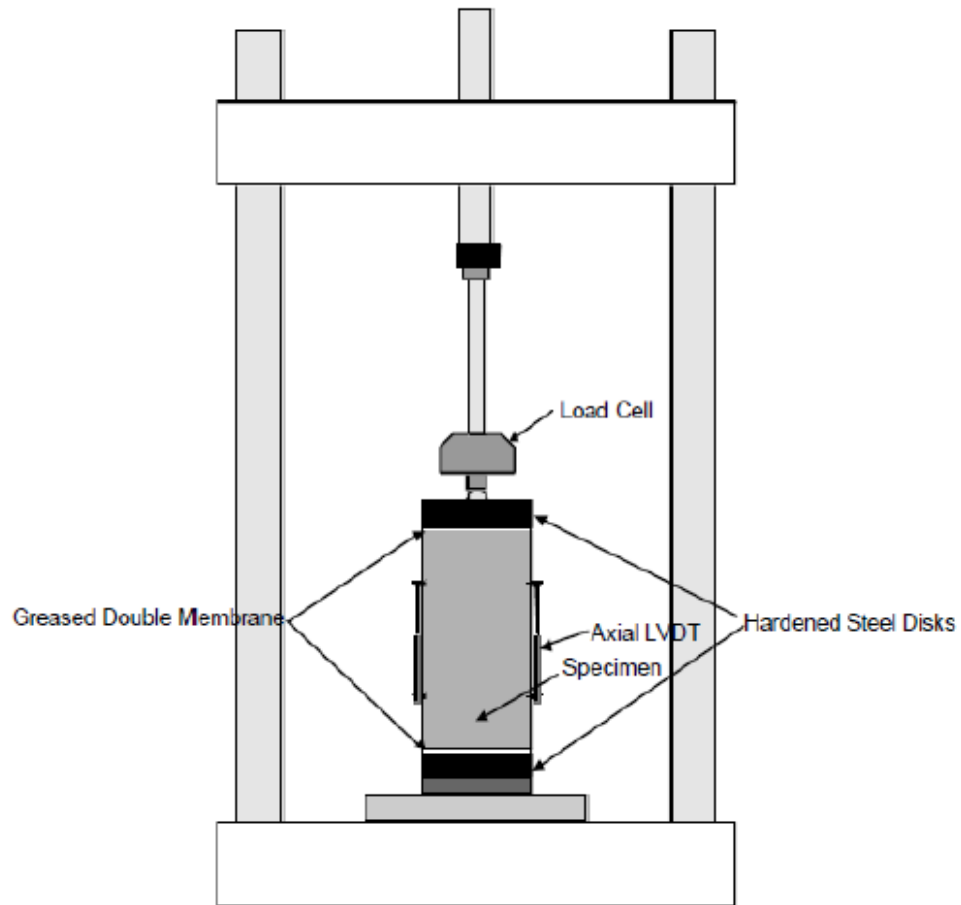
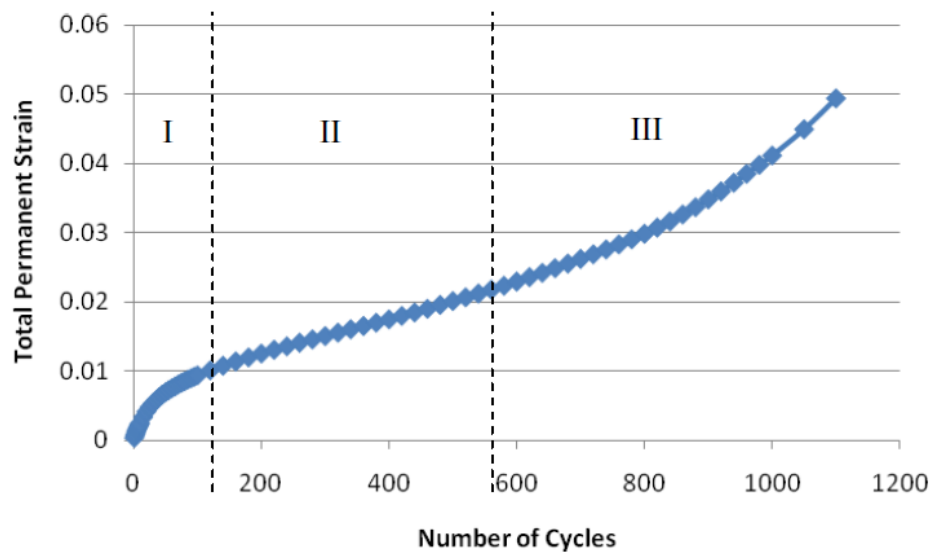
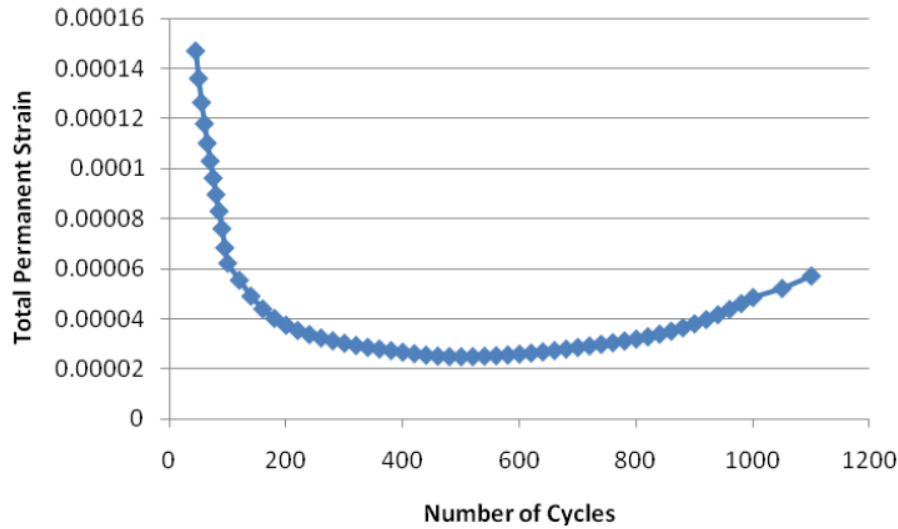


Figure III-4: Schematic of Flow Number test setup [7]



(a)



(b)

**Figure III-5: (a) Typical permanent strain curve and (b) permanent strain rate curve from Flow Number test [27]**

#### **4. Image-based Multi-scale Modeling Technique**

An image-based multi-scale modeling approach developed based on the Finite Element (FE) Method recently in University of Wisconsin-Madison [9] was followed with improvements in this study. In this approach four different length scales were modeled including asphalt binder, mastic, mortar and mixture scale (as shown in Figure III-6). Homogenization and up-scaling techniques were used to transfer the material properties from lower scale to higher scale. It should be noted that the asphalt binder property was assumed as linear in this study therefore no stress/strain dependency on the material behavior was considered. The experimental data from binder Frequency Sweep test were used to derive the binder master curve in the form of Prony Series. The binder properties were incorporated into ABAQUS via the user material subroutine (UMAT). The 2D artificial images of mastic and mortar were generated based on the real aggregate particle

shapes, the aggregate distributions, and volume fractions and characterized through FE simulations. The 2D scanned images of asphalt mixtures were then used by elimination of the fine particles, addition of the artificial air voids and mapping of each image pixel into a quadrilateral element in FE software to simulate the asphalt mixture behavior under loading. Although this multi-scale model was proved to be capable of predicting fatigue behavior of asphalt mixtures under certain loading conditions in the previous study [9], modifications and improvements of the model may be necessary to characterize the permanent deformation of asphalt mixtures as the damage mechanisms of fatigue and rutting are much different. The fatigue cracking generally takes place in the binder phase therefore is mainly controlled by binder properties; however permanent deformation is significantly affected by the aggregate packing other than binder properties therefore the contacts between aggregate particles are extremely important in the rutting simulations. Arshadi [9] also explored to apply a simple contact law between aggregate particles to the model and validated the model using limited asphalt mixture test data however more mixture validation especially for coarse mixes is needed to determine the effectiveness of the model or if possible improvements are needed. The details about the further development of the model is presented in the following chapter.

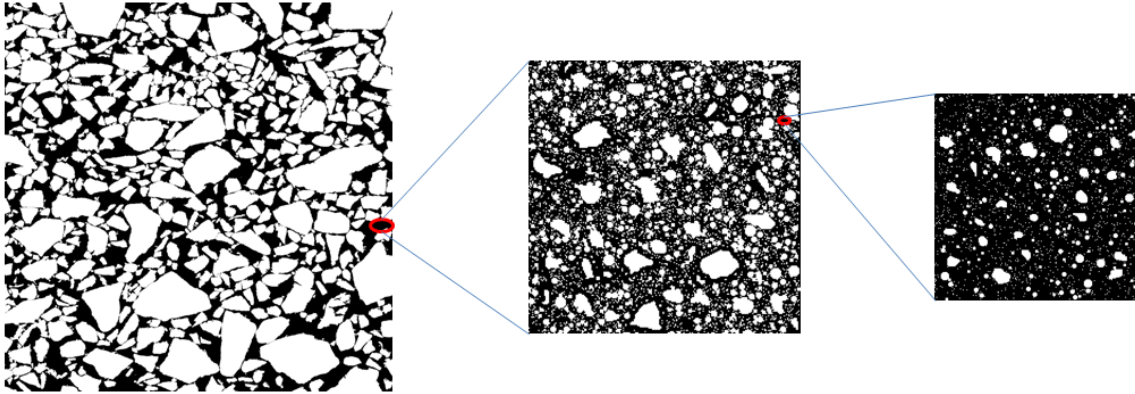


**Figure III-6: Multi-scale analysis scheme: (a) Mixture-scale (b) Mortar-scale (c) Mastic-scale [9]**

In this study, the simulations of permanent deformation for all asphalt mixtures were performed under the load of 345 kPa for 70 cycles, with each cycle consisting of 0.1s loading and 0.9s recovery period. Each mixture image pixel was mapped to a 4-node bilinear quadrilateral plane strain element (CPE4) in ABAQUS. The loading and the boundary conditions defined in FE analysis are shown in Figure III-7. The Poisson's ratio of asphalt binder was assumed as 0.49 while the Young's modulus and Poisson's ratio of aggregate were set as 25 GPa and 0.25 respectively following a previous study [9]. The RVE sizes for asphalt mastic, mortar and mixture were determined as 0.225mm x 0.225mm, 3.5mm x 3.5mm and 65mm x 65mm, respectively. Due to the large amount of simulations needed and limitation of computational resources and storage space available, 70-cycles was selected from the practical point of view; a single simulation for the permanent deformation of an asphalt mixture under repeated creep and recovery loading takes 14 hours using a computer with processor of Intel (R) Core (TM) i5-2410M CPU @ 2.30GHz and generates a 64GB output file. Temperature was not considered as a factor in simulation as all the binder and mixture tests were all performed at 46°C.

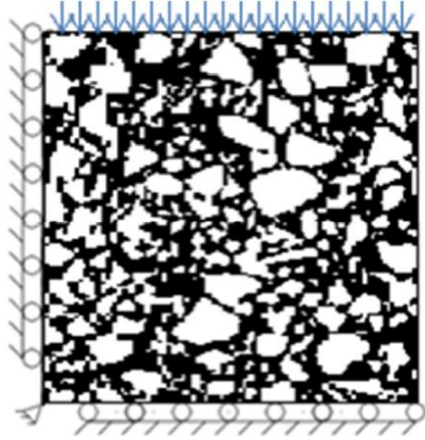


**Figure III-7: Loading and boundary conditions in FE analysis**

## **IV. Prediction of Permanent Deformation of Asphalt Mixtures Using Image-based Multi-scale Model**

### **1. Improvements of the Image-based Multi-scale Model**

#### **1.1 Needs for Improvement**

Although the previously introduced image-based multi-scale model was proved to be capable of predicting the fatigue behavior of asphalt materials under cyclic loading [9], the effectiveness of this model in simulating other performances of asphalt mixtures such as rutting resistance has not been thoroughly evaluated. Arshadi proposed a simple contact law and explored the possibility of using the model to predict the permanent deformation of asphalt mixtures [9]. However there are several problems associated with the proposed model to be addressed which can be summarized as follows:

- Determination of the contact function is redundant and time-consuming. Arshadi defined a simple contact law at the mastic scale and transferred the contact to the mortar scale through a quasi-linear superposition method to determine the contact function at the mortar scale (as seen in Equation II-1). Creep loading simulation on the mastic model with the contact law was performed to determine the strain-dependent part of the relaxation modulus (contact function) using Equation II-1, while the time-dependent part was known from the previous frequency sweep simulation. However since the creep loading was applied, the creep compliance was first obtained and then converted to relaxation modulus through several Laplace Transforms. The contact function was then derived based on ratio of relaxation modulus of mastic derived from simulations with and without contact law. This

procedure involves a lot of data manipulation and numerical analysis therefore it is considered redundant and time-consuming.

- The form of the contact function was determined arbitrarily using a polynomial function and no uniform shape of the contact function was designated. In Arshadi's work the form of the contact function was not specified nor the criteria of the determination of contact function was described. Therefore the contact function could be selected by the user arbitrarily resulting in variability of the simulation results with the contact function applied.
- Critical contact strain for the mortar and mixture levels were not clearly defined. Arshadi didn't define any critical contact strain at which the contact law or contact function starts being effective and left it to be user defined. This strain is important as it determines the initiation of the contact at each length scale. The arbitrary selection by the user of the point may lead to variation of the results and/or deviation from the real test curve.
- The proposed model by Arshadi with contact law and contact function has only been validated with very limited number of asphalt mixtures. Further validations are necessary especially on coarse mixtures where contacts play a more significant role in the permanent deformation of asphalt mixtures.

Therefore further improvement of the model and validation of the use of the multi-scale model in predicting the permanent deformation of asphalt mixtures is deemed necessary, especially considering the fact that aggregate particle-to-particle contact plays a much more important role in resisting permanent deformation than fatigue cracking.

### 1.2 Determination of Contact Function and Critical Contact Strain

In the previous research by Arshadi [9] a simple contact law was defined at the mastic scale (Figure II-10) and transferred to the mortar scale through a quasi-linear superposition method. As described in the previous section the calculation process of this procedure is redundant and time-consuming, and the form of the contact function was not specified.

To improve the efficiency of calculation for the contact function, and also reduce the variability of the simulation results, the following modifications to the contact function were conducted. Instead of calculating the contact function based on the relaxation modulus from creep loading and frequency sweep simulation, creep strain or creep compliance data from the creep simulations with and without the contact law are used to simplify this process (Figure IV-1). The form of the contact function was proposed as a six-degree polynomial or a power law equation, whichever fits the data better. The critical contact strain (CCS) was defined as the strain at which the strain ratio curve for the mastic or mortar starts increasing. The procedure for determining the contact function at mortar scale can be described as follows:

1. Run a creep simulation of 100 seconds for mastic with contact law to obtain the creep strain  $\varepsilon_1$  and the increment of creep strain for each time increment (0.2s)  $\Delta\varepsilon_1$ ;
2. Run creep simulation of 100 seconds for mastic without contact law to obtain the creep strain  $\varepsilon_2$  and the increment of creep strain for each time increment  $\Delta\varepsilon_2$ ;
3. Calculate the ratio (R) of  $\Delta\varepsilon_2$  to  $\Delta\varepsilon_1$  for each time increment, therefore:

$$R = \frac{\Delta\varepsilon_2}{\Delta\varepsilon_1} = \frac{J_2}{J_1} \approx \frac{E_1}{E_2}$$

**Equation IV-1**

- Where  $J_1$  and  $E_1$  refer to the creep compliance and relaxation modulus of mastic considering contact, and  $J_2$  and  $E_2$  refer to the creep compliance and relaxation modulus of mastic without contact. Note that  $E_1$  is both time and stress dependent based on Equation IV-1 while  $E_2$  is only time dependent.
4. Fit the ratio curve using mathematical equation (such as the polynomial, power law or other forms of equations, whichever fits the best) (with  $y=R$  and  $x=\epsilon_1$ );
  5. The following equation is determined as contact function:

$$\Omega(x) = \begin{cases} 1 & (\text{when } x \leq CCS) \\ Ax^6 + Bx^5 + Cx^4 + Dx^3 + Ex^2 + Fx + G \text{ or} \\ Ax^B, \text{ etc.} & (\text{when } x > CCS) \end{cases}$$

Equation IV-2

6. Implement the contact function into UMAT for upscaling.

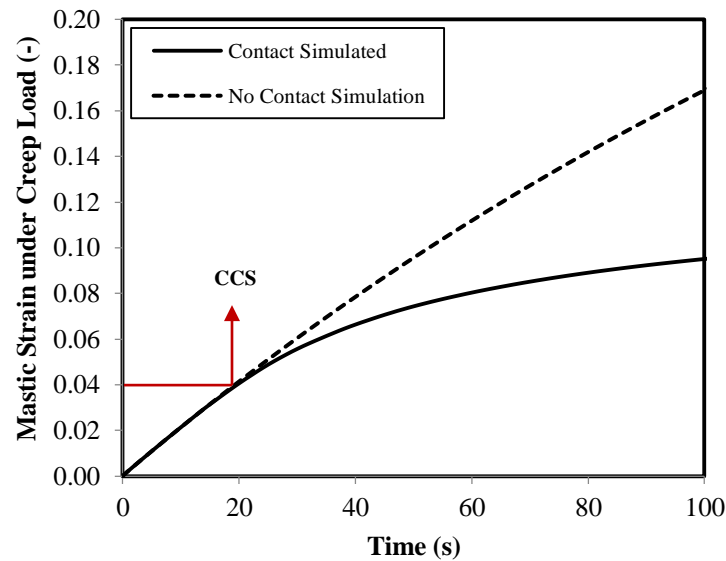
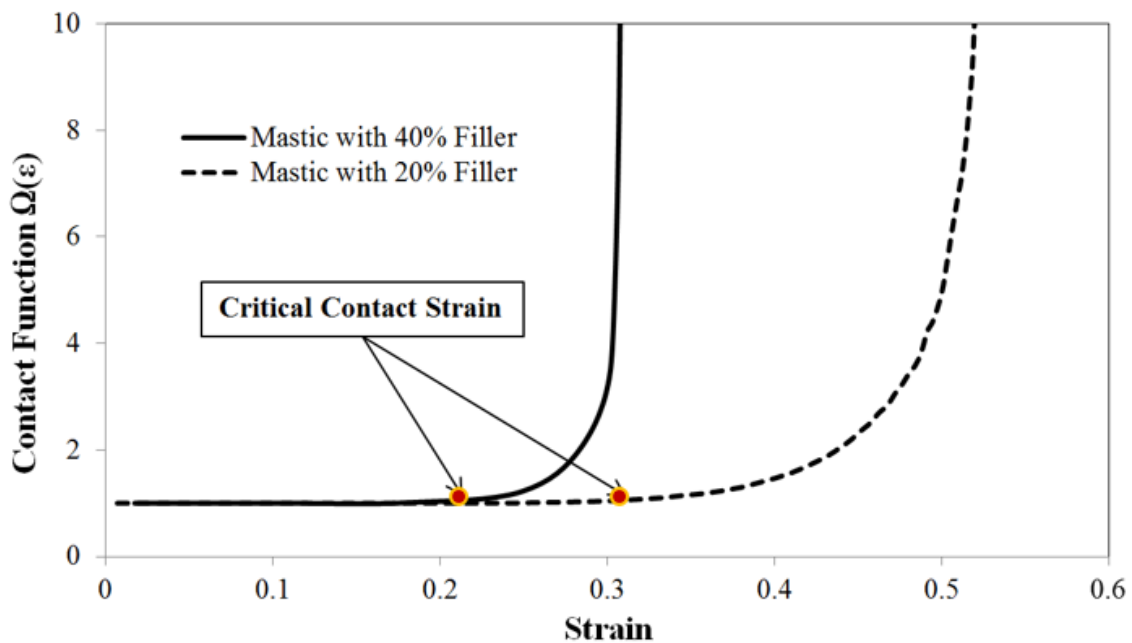


Figure IV-1: Creep simulation of mastic with and without contact

In this study, the critical contact strain is defined as the strain at which the ratio ( $R$ ) reaches the value of 1.02, meaning that the contact function starts being effective after the creep

strain ratio increased by 2% from unity. An illustration of the contact function and critical contact strain for mastics with different filler content is presented in Figure IV-2. As shown the critical contact strain for the mastic with higher amount of filler is much lower than the one for the mastic with lower filler content due to the increased contacts involved in the mastic with higher filler content. The same procedure for determining the contact function at mixture scale was performed by running creep simulation with and without contact function on mortar. The creep loading stresses applied were selected as 10kPa for mastic and 100kPa for mortar, which were based on the average compressive stress values in the continuous phase elements obtained from several trial analyses.



**Figure IV-2: Illustration of contact function and critical contact strain**

It should also be noted that the implementation of contact law and contact function into ABAQUS User Materials Subroutine (UMAT) program was realized through controlling the compressive strain of the continuous phase elements instead of the distance between the aggregate elements as it was found much easier to be coded. Therefore the contact law

illustrated in Figure II-10 is in fact demonstrated as in Figure IV-3 where the critical contact strain equals to -1. This represents the situation that the aggregate elements come into contact and the binder element thickness decreases to zero. Similar concepts of the contact functions at mortar and mixture scales derived from the simulations at lower scales are also presented in Figure IV-4 and Figure IV-5. Before the strain in mastic (or mortar) elements reach the critical contact strain (CCS), the mastic (or mortar) stiffness which is derived from the frequency sweep simulations at the mastic (or mortar) scale is maintained. Once the CCS is achieved the contact function is activated and applied to the mastic (or mortar) stiffness and stiffen the mastic (or mortar). Eventually the contact effect is transferred from lower scale to the higher scale until the mixture scale.

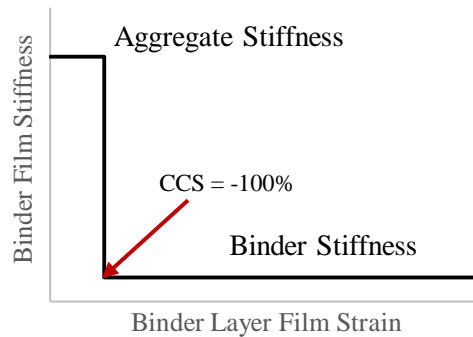


**Figure IV-3: Contact law defined at mastic scale**

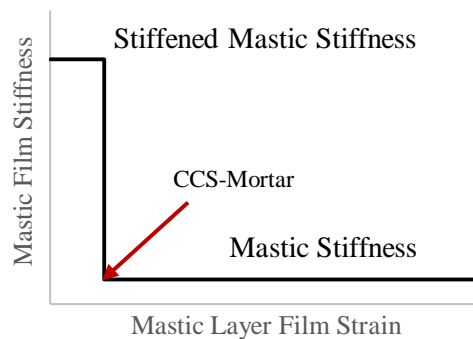


**Figure IV-4: Contact function determined at mortar scale**

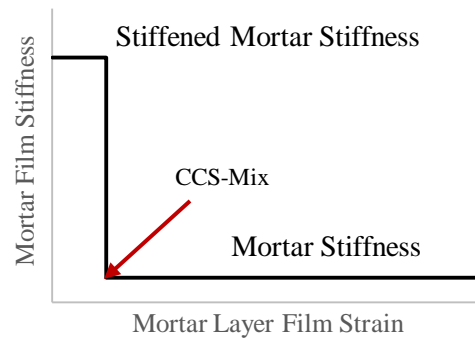


**Figure IV-5: Contact function determined at mixture scale**

### 1.3 Validation of the Contact Model

An asphalt mixture with SBS modified asphalt binder was designed and used to study the effectiveness of applying the model (with clearly defined critical contact strain and contact function as introduced in the previous section) on predicting the permanent deformation of asphalt mixtures. The coarse gradation presented in Figure III-1 was used as the coarse mix is more critical in the rutting simulation due to the higher number of coarse aggregate particle contacts involved. The asphalt content was determined as 5.55% and the performance samples were compacted to 6.5% air voids. Based on the calculation of the volume fraction, 68.0%, 41.2% and 16.2% of aggregates were included at the mixture, mortar and mastic scale respectively. A frequency sweep test was performed on the asphalt binder and the test data was fitted using a Prony Series as the model inputs. The frequency sweep test was also performed on the mastic to validate the frequency sweep data from modeling. The simulations of mastic and mortar were conducted following the multi-scale analysis procedure presented above. The comparison between the simulated data and tested master curves for binder and mastic are presented in Figure IV-6 and Figure IV-7. Results show that the master curves of binder and mastic can be effectively modeled using the frequency sweep simulations.

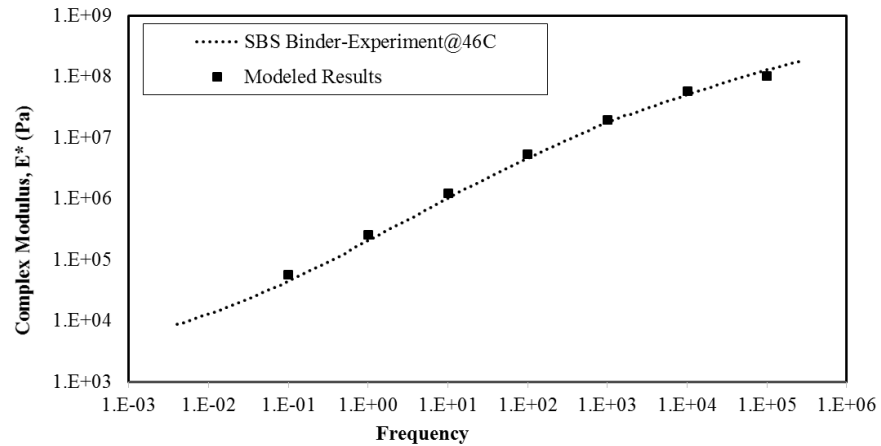


**Figure IV-6: Simulation and test results for SBS modified asphalt binder**

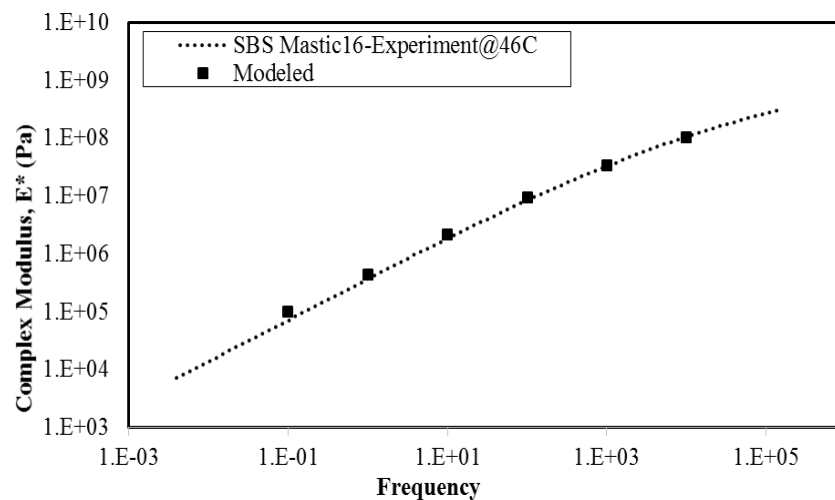


**Figure IV-7: Simulation and test results for asphalt mastic**

The repeated creep and recovery simulation was performed under the load of 345 kPa with 0.1s loading and 0.9s unloading period for 70 cycles at the mixture scale to mimic the loading conditions in the Flow Number test. The simulated results of the asphalt mixture were compared with the mixture test data from the Flow Number test performed at 46°C as shown in Figure IV-8. As seen from the figure, by applying the contact function the permanent strain curve significantly deviates from the curve without considering the

contact. However it is also seen that a gap exists between the simulation curve and test curve, particularly for the first few cycles, resulting in a difference between the simulated and tested permanent strains after 70 cycles. This indicates that possible contacts may still be missing at the initial cycles; it's also possible that the contact law and contact function needs to be improved to better predict the permanent deformation of asphalt mixtures. The resolution efforts for this issue are presented as follows.

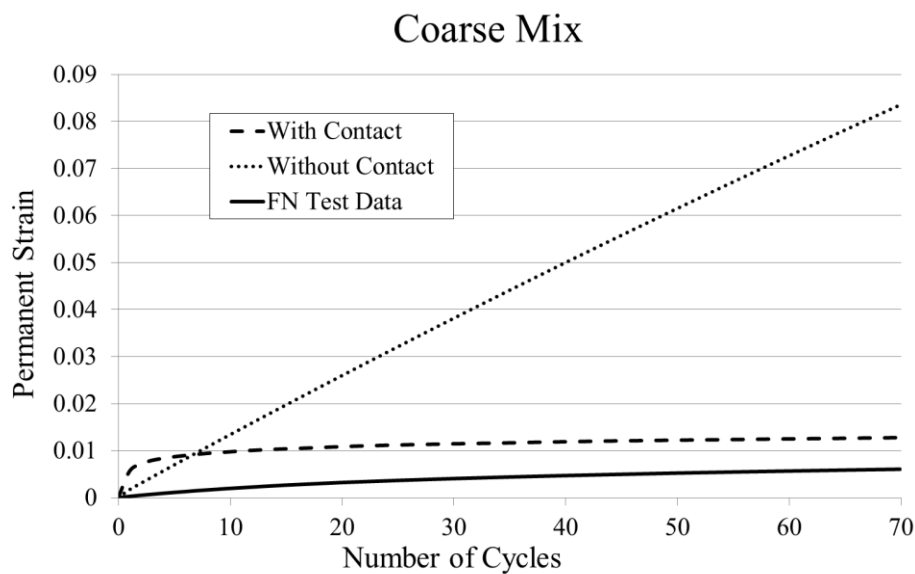


**Figure IV-8: Comparison of simulation and test data for coarse mix**

### *1.3.1 Application of Linear Contact Law*

A simple step function was defined as the contact law at mastic scale by Arshadi [9], however it is unknown if a linear function could improve the result which assumes that the contact occurs gradually. Therefore a linear contact law was proposed in the section to validate this assumption and the concept is described in Figure IV-9. The stiffness of asphalt binder film starts increasing linearly at a specified distance (strain) between the

aggregate particles until the particles are completely in contact; the stiffness of asphalt binder reaches the value of aggregate stiffness at the contact.

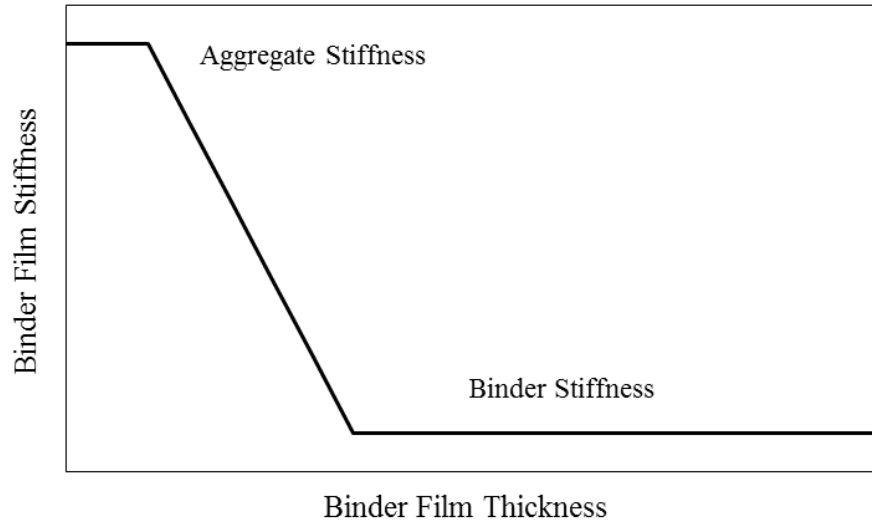


**Figure IV-9: Description of linear contact law**

The compressive strain was used in previous study to implement the contact law into UMAT instead of distance as it was found to be much more easily realized in coding. This study continued using the compressive strain to implement the contact law and three compressive strains including -0.2, -0.6 and -1.0 (unity) at which the contacts initiated were proposed (Figure IV-10) and the corresponding linear functions were obtained to study the effect of the implementation of linear contact law. Note that the compressive strain of -1.0 is the one that was proposed in previous study which is essentially the step function [9].

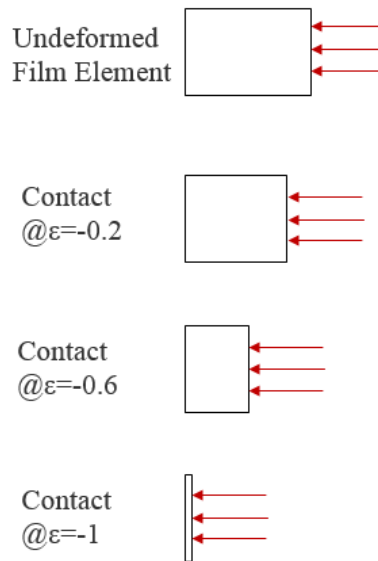


**Figure IV-10: Compressive strains proposed at which contacts initiated**

The contact functions at mortar and mixture scales were derived through simulations based on the proposed linear contact laws at the mastic scale, and the simulated permanent strains of the asphalt mixtures under creep and recovery loading using the three different linear contact laws are shown in Figure IV-11. It is seen that the issue at initial cycles is still unresolved and the permanent strain rates of the simulation curves are reduced after the first few cycles when the contacts are assumed to be occurring sooner (with contacts initiated at smaller compressive strains). Although the permanent strains after 70 cycles using the linear contact laws are closer to the experimental data, the rate of permanent strain doesn't seem to be comparable with the FN test data curve and the issue of initial cycles still exists. Therefore the application of linear contact function was not considered valid in improving the curve and it is not included in the later simulations.

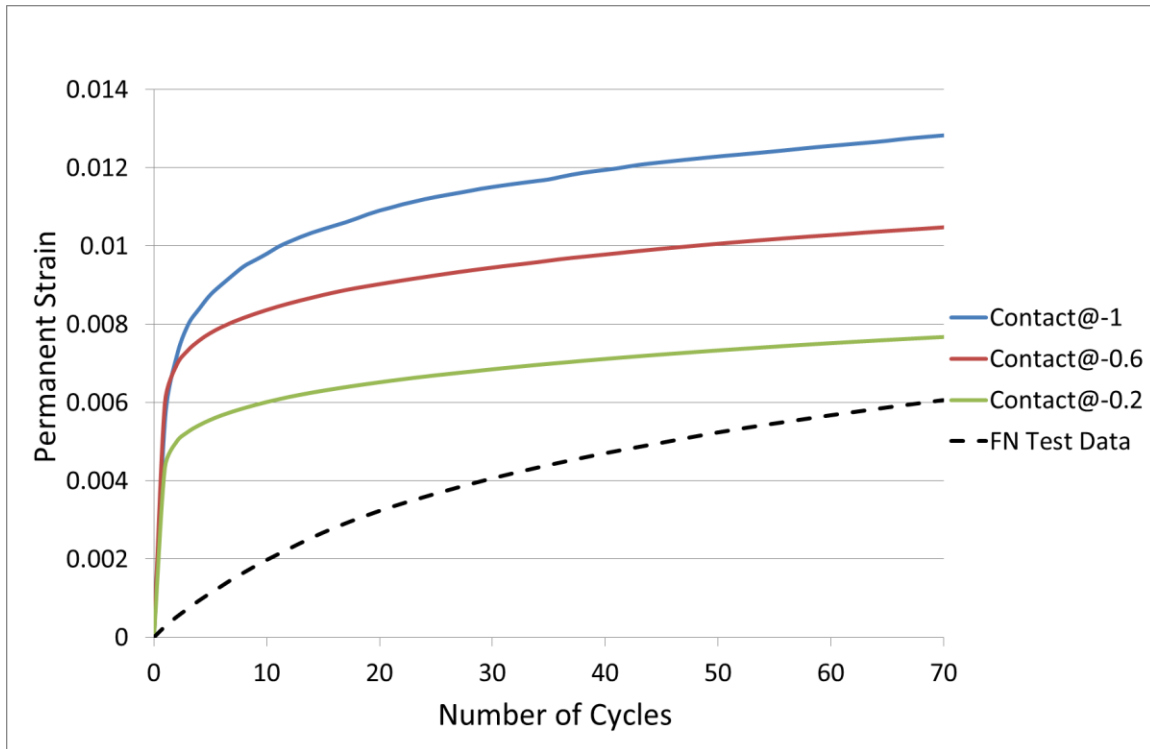


**Figure IV-11: Simulated permanent strain curves using three contact laws at mastic scale**

### 1.3.2 Pre-defined Contact Points in Mixture and Mortar Images

The image processing techniques such as filtering and erosion were used to prepare the mixture images for microstructure analysis [27, 5]. However due to the limitation of the resolution of the scanner and the median filtering, the fine particles with sizes less than 0.075mm (filler) cannot be captured and processed through imaging. Therefore in the contact analysis performed by Roohi [5] a proximity distance of 0.1 mm was proposed indicating that all particles with distances less than 0.1 mm were considered as being in contact. In this study a similar situation exists and the filler particles cannot be captured through imaging. Therefore there's a possibility that some contact points in the mixture image are missing during the filtering process, which may have already existed when the aggregate structure is formed after the mixture is compacted.

To account for the effect of these initial particle contacts, the initial contact points were defined based on the concept that if the distance between the two aggregate elements is equal to a specified distance, then the binder element in between is converted to an aggregate element to generate pre-defined contact points, as shown in Figure IV-12. The distance was selected as 0.1 mm at mixture scale in this study based on the filler particle size and maintained as the value used in previous contact analysis study [5]. Based on the resolution of the mixture image, the number of binder elements converted to aggregate elements as pre-defined contact points was determined as one. A MATLAB generated program was written to process the images (Appendix A).

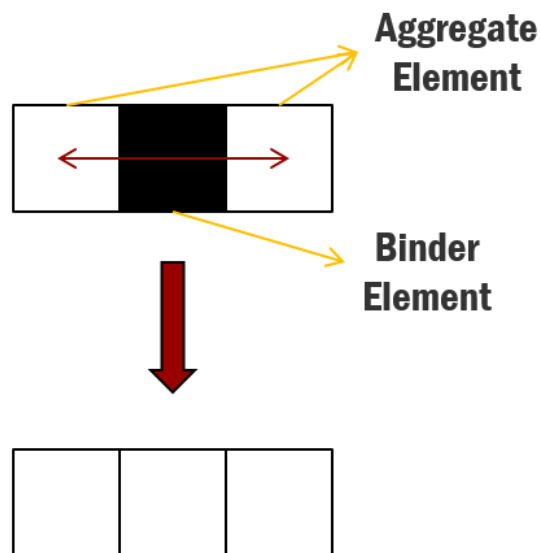


**Figure IV-12: Concept of pre-defined contact points**

The pre-defined contact points were added to the mixture image to determine their effect on the deformation curve. As presented in Figure IV-13, the permanent strain curve has been improved but still cannot match the experimental curve at initial cycles. The pre-defined contact points were then further added to the mortar image with three levels of

critical distance to determine the contact based on the resolution of mortar image: 0.05mm (1 pixel), 0.10mm (2 pixels) and 0.15mm (3 pixels) (Appendix B). For the mixture scale the distance of 0.1 mm (which represent 1pixel for the resolution of mixture image) was always used. As shown in Figure IV-13 the simulation result was significantly improved when pre-defined contact points with critical distance of 0.1mm were added into both mix (1 pixel) and mortar (2 pixels) images. Previous research indicates that the filler particles, which are smaller than 0.075mm, are considered as part of the mastic. Therefore the finest particle in mixture image analysis is logically equal to or larger than 0.075mm (5). This also applies to the mortar. Therefore the filler particles with sizes smaller than 0.1mm may potentially exist as “contact points” between the aggregate particles in the mortar and mixture images. The simulation results shown in Figure IV-13 validate this assumption since when using 1 pixel (0.05 mm) for the mortar scale as the predefined contact the deformation from simulation is still larger than the measured deformation. However, when 2 pixels in the mortar scale ( 0.1 mm) was selected the deformations from simulation and from measurements give very similar trends with time. Moreover, when 3 pixels of the mortar scale (0.15mm) was selected the simulated deformation is much smaller than the measured. These results are in agreement with the selection of 0.1mm as the critical contact distance that was initially proposed in the image analysis and correlation of proximity zones with measured rutting (5). The permanent strain curve shown in Figure IV-13 from the simulation matches well with the experimental curve, and the permanent strain simulated after 70 cycles is just slightly higher (less than 20%) than the result from FN test, indicating the effectiveness of the concept of pre-defined contact points applied in mortar and mixture images.

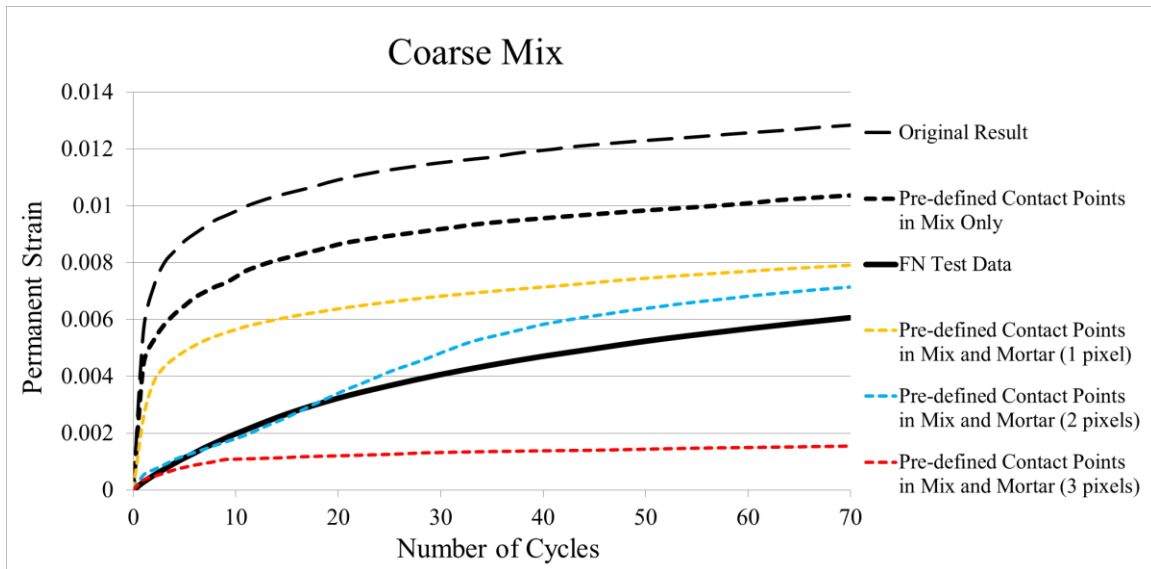


**Figure IV-13: Simulation results after adding pre-defined contact points in mortar and mixture**

#### 1.4 Summary of Image-based Multi-Scale Modeling Procedure

According to the improvements presented above, the image-based multi-scale modeling procedure can be summarized for each length scale as below:

##### Binder Scale

- Conduct the binder frequency sweep (FS) test.
- Fit the data in the constitutive model (Prony Series).

##### Mastic Scale

- Calculate the volume fractions of each components at different scales.
- Generate mastic image using MATLAB codes.
- Create input file for ABAQUS using MATLAB.
- Determine RVE of image size.
- Run FS simulation at mastic scale.

- Export simulation results and fit the data in the constitutive model (Prony Series).
- Run simulations of creep loading with and without the activation of contact law in UMAT to determine the contact function for mortar scale.

#### Mortar Scale

- Generate mortar image and add the pre-defined contact points using MATLAB codes.
- Create input file for ABAQUS using MATLAB codes.
- Determine RVE of image size.
- Run FS simulation at mortar scale.
- Export simulation results and fit the data in the constitutive model (Prony Series).
- Run simulations of creep loading with and without the activation of contact function in UMAT to determine the contact function for mixture scale.

#### Mixture Scale

- Cut and scan the mixture sample.
- Run image filtering using IPAS2 and eliminate the aggregate particles with size <1.18mm using MATLAB codes.
- Insert air voids into the mixture image and create input file for ABAQUS using MATLAB codes.
- Activate the contact function in UMAT.
- Run repeated loading and recovery simulation for 70 cycles at mixture scale.
- Export the simulation results.

## 2. Model Validation

To further validate the improvement of simulation using the predefined contacts with the selection of 0.1mm distance, six different types of asphalt mixtures with three binders (Neat, SBS modified and CBE modified) and two aggregate gradations (coarse and fine) described in CHAPTER III were used for simulation and testing. The volume fractions for the coarse and fine mixtures at each scale were calculated based on the mix design information and presented in Table IV-1. The mastic and mortar images were created based on the volume fractions and real aggregate particle shape database. It should be noted that the mixture FN test data was obtained directly from Report O of Asphalt Research Consortium project completed by previous researchers at the University of Wisconsin-Madison (51).

**Table IV-1: Volume fractions of component materials at each scale**

Mixture Type	Mixture Scale			Mortar Scale		Mastic Scale	
	Aggregate	Mortar	Air Voids	Fine Aggregates	Mastic	Fillers	Asphalt Binder
Coarse	0.680	0.255	0.065	0.412	0.588	0.162	0.838
Fine	0.551	0.384	0.065	0.658	0.342	0.189	0.811

The frequency sweep test was performed on all the three binders and the master curves of the binders at the reference temperature of 46°C were constructed as shown in Figure IV-14. The complex moduli of SBS modified binder is lower at high frequencies and higher at low frequencies relative to neat binder. The CBE modified binder has the highest moduli over all frequencies compared to the other two binders. The master curves of the three binders were fitted using the Prony series and the fitted parameters are presented in Table

## IV-2.

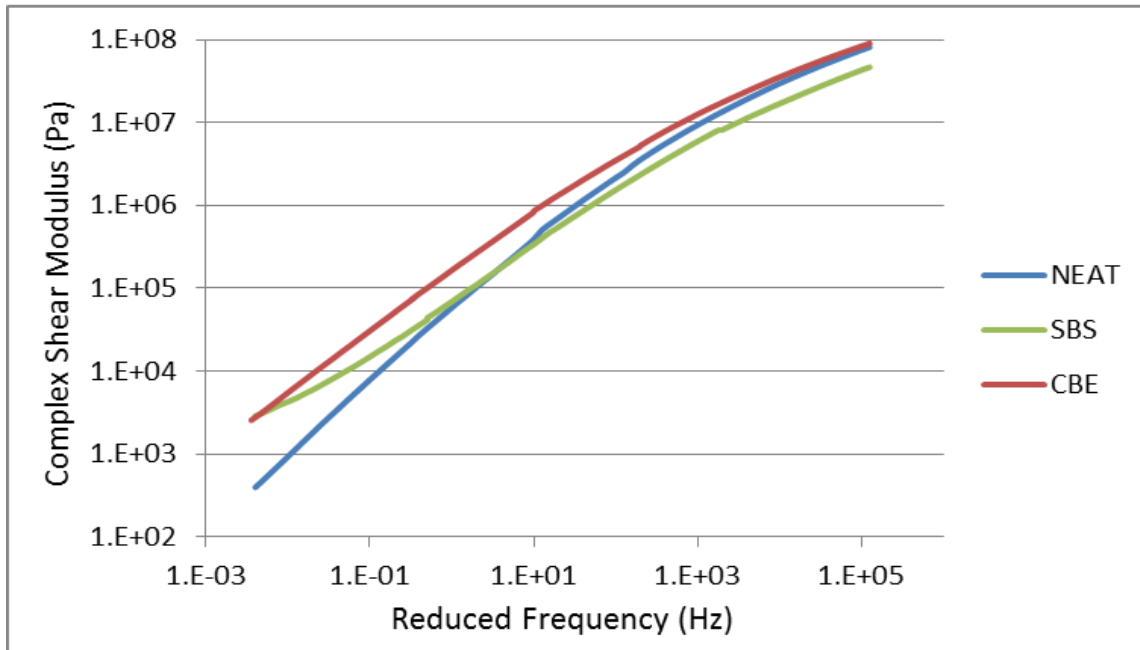


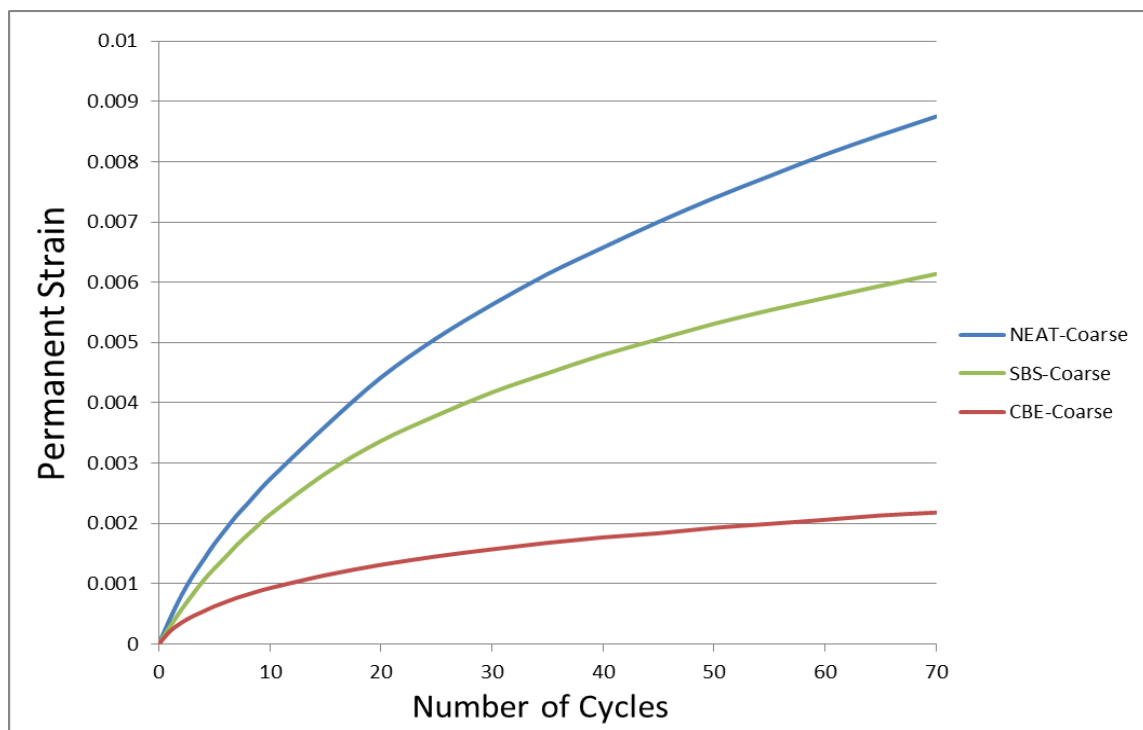
Figure IV-14: Master curves of the three binders used

Table IV-2: Prony series parameters for all three asphalt binders

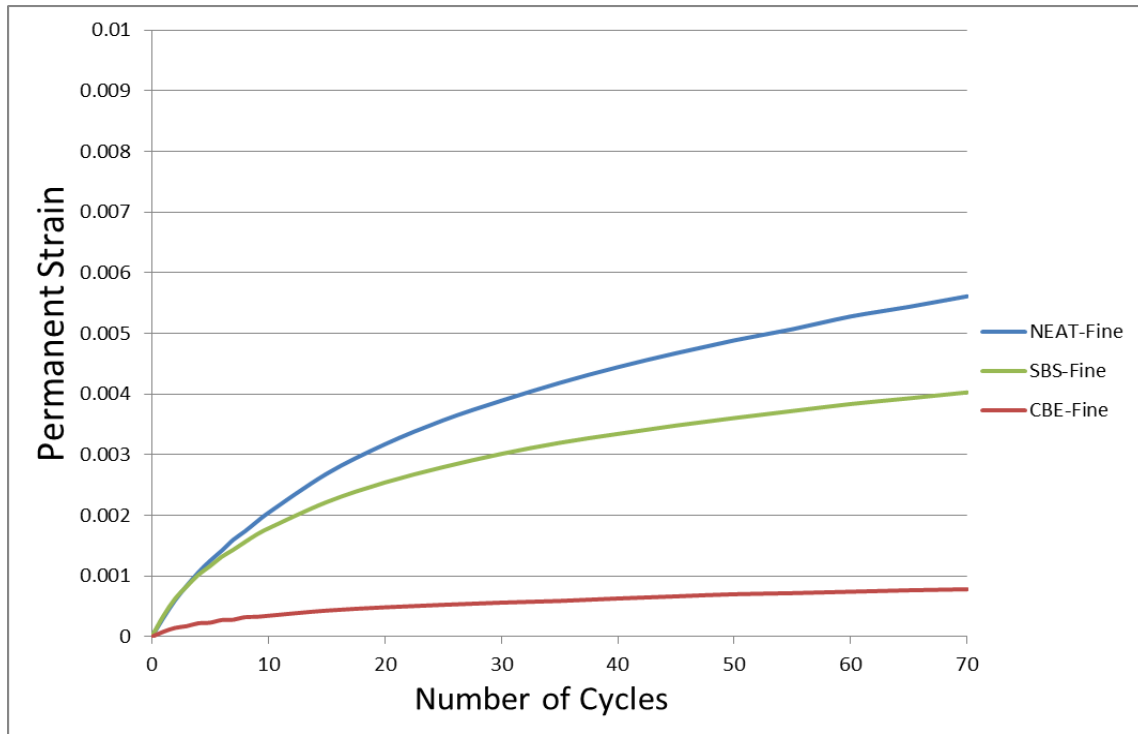
Relaxation Moduli (Pa)						Relaxation Times (s)	
NEAT		SBS		CBE			
$E_{\infty}$	0	$E_{\infty}$	0	$E_{\infty}$	0		
$E_1$	3.92E+01	$E_1$	4.17E+03	$E_{\infty}$	2.63E+03	$\tau_1$	1E+02
$E_2$	4.91E+02	$E_2$	7.21E+03	$E_1$	1.12E+04	$\tau_2$	1E+01
$E_3$	1.21E+04	$E_3$	3.71E+04	$E_2$	7.39E+04	$\tau_3$	1E+00
$E_4$	1.20E+05	$E_4$	1.48E+05	$E_3$	4.39E+05	$\tau_4$	1E-01
$E_5$	1.21E+06	$E_5$	8.97E+05	$E_4$	2.63E+06	$\tau_5$	1E-02
$E_6$	6.97E+06	$E_6$	4.46E+06	$E_5$	1.12E+07	$\tau_6$	1E-03
$E_7$	3.17E+07	$E_7$	1.51E+07	$E_6$	4.04E+07	$\tau_7$	1E-04
$E_8$	9.52E+07	$E_8$	6.04E+07	$E_7$	1.05E+08	$\tau_8$	1E-05
$E_9$	8.79E+07	$E_9$	5.64E+06	$E_8$	9.06E+07	$\tau_9$	1E-06

The artificially created mastic images were converted to input files for ABAQUS through a set of MATLAB generated codes. Simulations of frequency sweep and creep loading were performed to determine the complex moduli of mastic and contact function for

mortar. The complex moduli were fitted using the Prony Series again to generate the material property inputs of continuous phase at mortar scale. The improved mortar images with pre-defined contact points were used and converted to ABAQUS input files, and the simulations performed are similar as those done at the mastic scale. The mixture images were processed using the filtering and the air voids and pre-defined contact points were added. After the images were imported into ABAQUS, the contact function was activated and creep and recovery simulations were performed for 70 cycles. The FN test results were used for all six mixtures to verify the simulation results. The tested permanent strain curves are presented in Figure IV-15.



(a) Coarse mixtures



(b) Fine mixtures

**Figure IV-15: Permanent strain curves from Flow Number test**

The simulation results were compared to the test results for all six type of mixtures as shown in Figure IV-16. Results show that in general the simulated permanent strain curves are in good agreement with the tested curves. The permanent strains after 70 cycles using multi-scale model and FN test were also compared as shown in Figure IV-17. Figure IV-17 shows that the results between the simulation and physical test are comparable and the ranking of the materials remains the same. This indicates that the improved multi-scale model can be effectively used in prediction of rutting performance of asphalt mixtures.

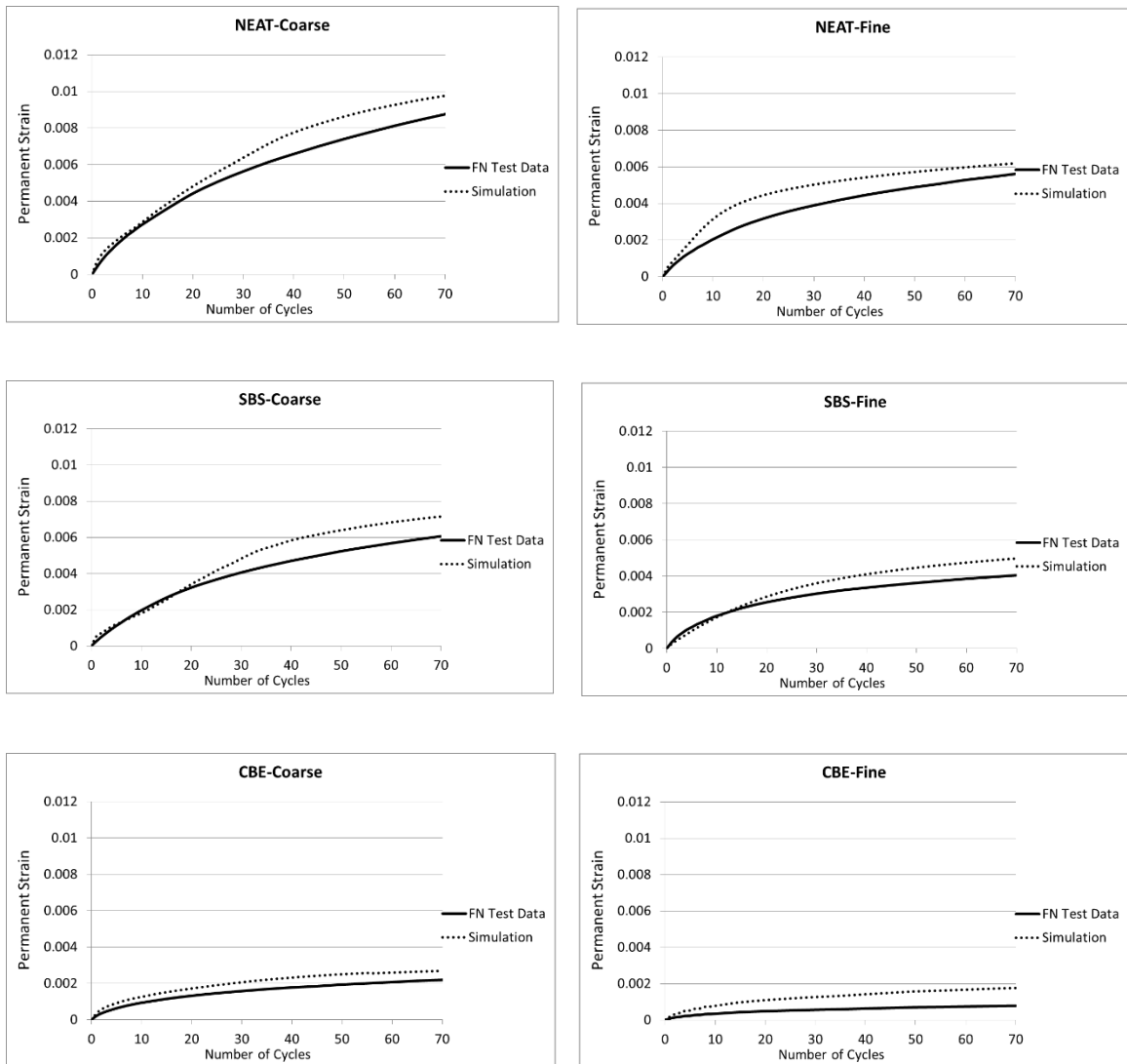
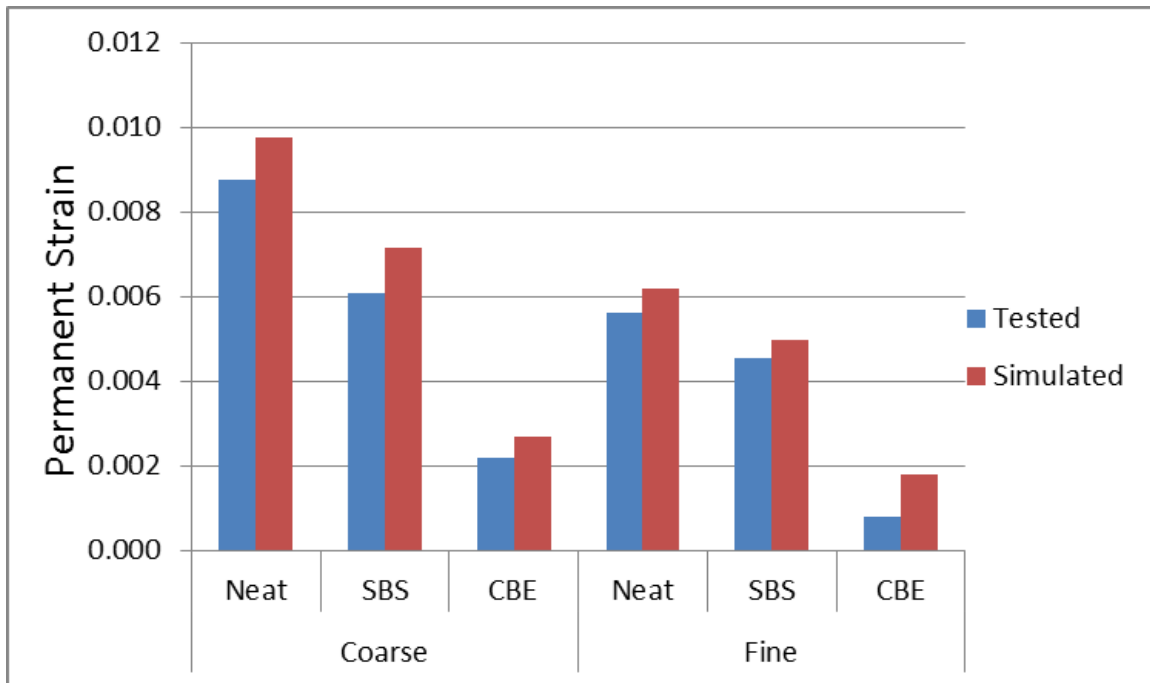


Figure IV-16: Comparison of permanent strain curves using multi-scale model and FN test



**Figure IV-17: Comparison of permanent strains after 70 cycles for simulation and test**

### **3. Development of MSCR-based Multi-scale Model**

As stated previously, the MSCR test is a performance-based test which is capable of distinguishing the difference in rutting potential between various binders including both modified and unmodified binders. Also, the non-recoverable creep compliance and elastic recovery of asphalt binder can be separated and represented by  $J_{nr}$  and %R, respectively, through the MSCR test. However, the contributions of  $J_{nr}$  and %R of asphalt binder to the rutting resistance of the asphalt mixture are not clear. Since it is very difficult to distinguish the effects of  $J_{nr}$  and %R on the rutting resistance of asphalt mixtures through laboratory tests, multi-scale modeling could be used as a surrogate method to predict the rutting behavior of asphalt mixtures and study the fundamental roles of asphalt binders and aggregate structures during repeated creep loading. For this purpose, the aforementioned

multi-scale model based on the frequency sweep test was modified by using the MSCR test. The modifications of the modeling procedure are introduced below.

### 3.1 Binder Test and Rheological Model Fitting

The MSCR test was used instead of frequency sweep test to obtain the binder properties as the inputs of the model. The linear viscoelasticity assumption was followed in this study so only the MSCR test results at 0.1 kPa were used. The MSCR test was performed at 46°C following the AASHTO T350 procedure and strain data of the first ten cycles at 0.1kPa were fitted using the Burger's model following Equation IV-3.

$$\varepsilon(t) = \sigma(t) \left( \frac{1}{G_m} + \frac{1}{\eta_m} + \frac{1}{G_k} \left( 1 - e^{-\frac{G_k t}{\eta_k}} \right) \right)$$

**Equation IV-3**

Two fitting methods were proposed and compared in the following validation: all-cycle-fitting and average-cycle-fitting. The previous option fits all the ten cycles obtained from MSCR test while the latter fits the average cycle of the ten cycles only. The fitted curves for SBS modified binder are presented in Figure IV-18 and fitted parameters are shown in Table IV-3. It is seen that both methods can fit the MSCR curve well, however the fitted parameters differ significantly. The selection of the fitting method was determined through the validation of mixture test data presented in the next section.

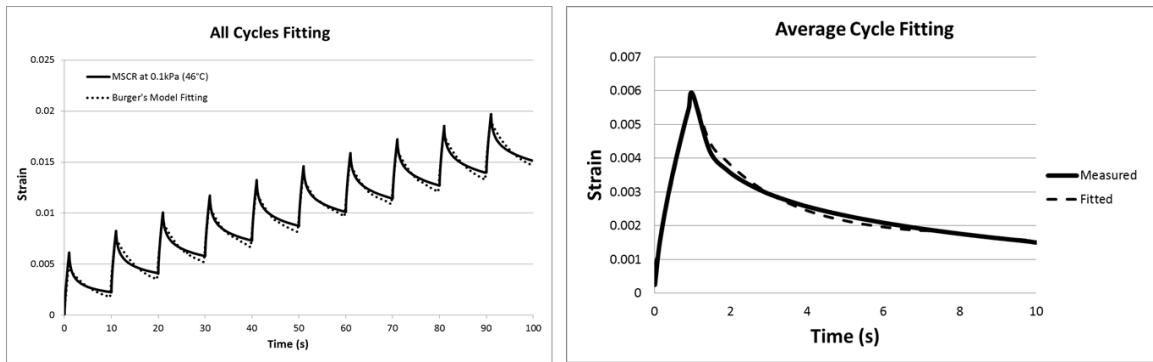


**Figure IV-18: MSCR test data fitting for SBS modified binder using two different methods**

**Table IV-3: Burger's model fitted parameters for two methods**

Parameters	Average-cycle-fitting	All-cycle-fitting
$G_m$ (Pa)	1.41E+05	2.10E+05
$\eta_m$ (Pa·s)	5.92E+04	8.95E+04
$G_k$ (Pa)	1.14E+04	4.49E+03
$\eta_k$ (Pa·s)	2.24E+04	2.47E+04

Since the FE software ABAQUS requires the material inputs to be entered in the form of Prony series, the Burger's model parameters need to be further converted to Prony series parameters. The method introduced by Kong et al. [52] was followed to convert the Burger's model parameters to Prony Series inputs for ABAQUS by applying Laplace transformation to Boltzmann Integrals, manipulating terms and applying another inverse Laplace transformation. The final converted shear modulus in the form of Prony series and the relevant parameters are presented in Equation IV-4 below. Note that the solutions are analytical, not numerical.

$$G(t) = G_{\infty} + G_1 e^{-\frac{t}{\tau_1}} + G_2 e^{-\frac{t}{\tau_2}}$$

**Equation IV-4**

Where:  $G_\infty = 0$ ,  $G_1 = \frac{G_m}{(\alpha-\beta)} \left( \frac{G_k}{\eta_k} - \beta \right)$ ,  $G_2 = \frac{G_m}{(\alpha-\beta)} \left( \alpha - \frac{G_k}{\eta_k} \right)$ ,  $\tau_1 = \frac{1}{\beta}$ ,  $\tau_2 = \frac{1}{\alpha}$ ;

$$\alpha, \beta = \frac{p_1 \mp \sqrt{p_1^2 - 4p_2}}{2p_2}, p_1 = \frac{\eta_m G_m + \eta_m G_k + \eta_k G_m}{G_m G_k}, p_2 = \frac{\eta_m \eta_k}{G_m G_k}.$$

Finally, the shear relaxation moduli in the Prony series were converted to elastic relaxation moduli for asphalt binders and entered into ABAQUS for simulating mastic behavior. The same mastic and mortar images for SBS modified binder as those used in above FS-based model validations were used, and the same simulation process for the mastic and mortar were also maintained.

### 3.2 Mixture Validation

The comparison of the two fitting methods was conducted using a dense-graded mixture with the fine gradation provided in Figure III-1. The fine mixture was selected as the volume fraction of the continuous phase in the fine mixture is higher than the coarse mixture, therefore the simulation results could be more sensitive to the change of binder properties in fine mixture. The FN test data was included to validate the simulation results as shown in Figure IV-19. It is seen that both of the fitting methods are close to each other and comparable to the test data curve, of which the all-cycle-fitting is best. Therefore the all-cycle-fitting method was used in the binder fitting for all the MSCR-based multi-scale modeling and analysis.

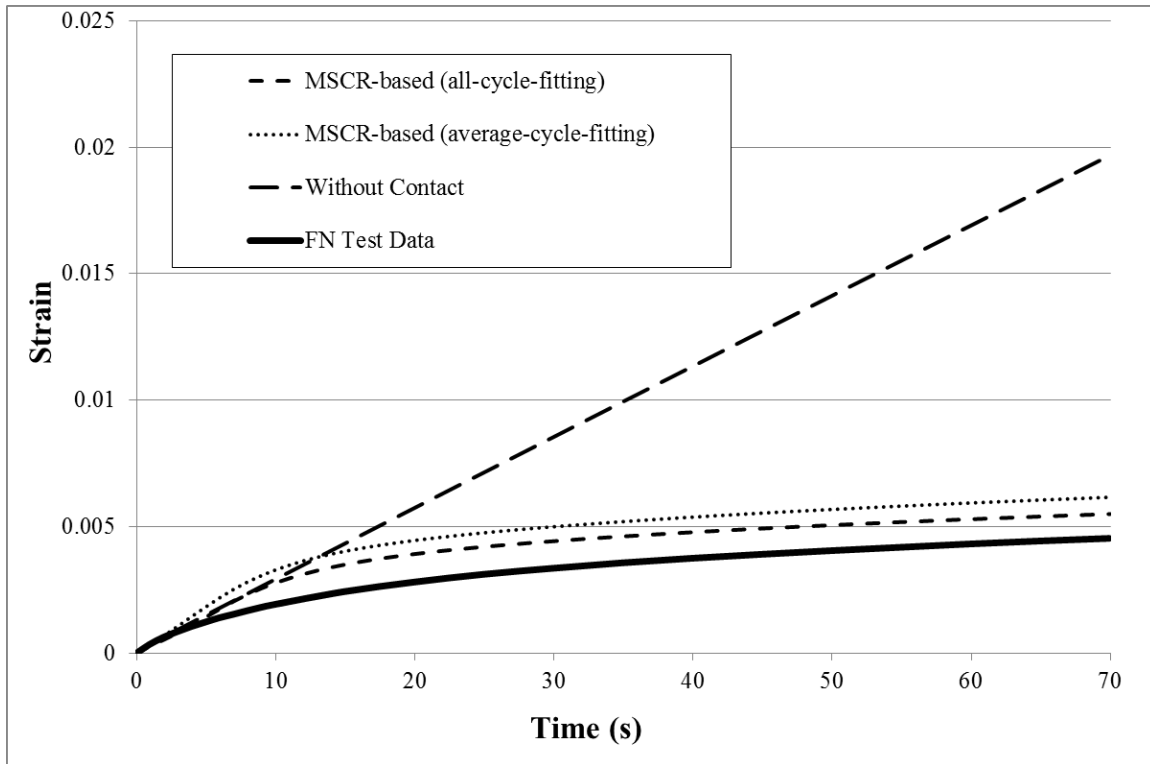


**Figure IV-19: Validation of a fine mixture with SBS modified asphalt binder**

The validation was also conducted using the coarse mix with the results provided in Figure IV-20. Results presented in Figure IV-19 and Figure IV-20 demonstrate the capability of the MSCR-based model in predicting the permanent deformation of asphalt mixtures under creep loading and recovery. The simulation results without considering the particle contacts were also included in both figures to demonstrate how the inclusion of the contacts affects the permanent strain curves.

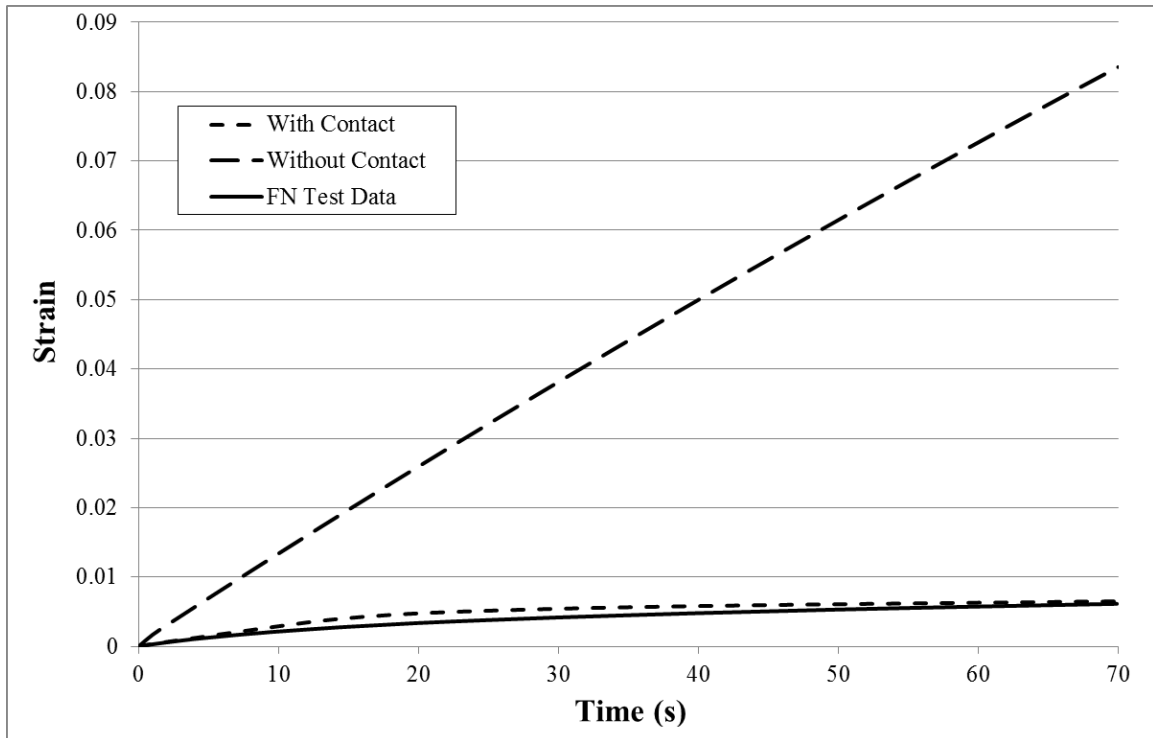


**Figure IV-20: Validation of a coarse mixture with SBS modified asphalt binder**

## **V. Investigation of the Effects of Binder Modification Type and Aggregate Structure on Permanent Deformation of Asphalt Mixtures**

It is accepted that the use of polymer modified asphalt binder can improve the rutting resistance of asphalt mixtures, however the mechanisms behind this behavior are not clear as the aggregate structures are also usually changed significantly when modified asphalt mixtures are compacted. Due to this confounded effect, it is difficult to study the effects of modified asphalt and aggregate structures independently on the rutting resistance of asphalt mixtures through experimentation. Use of the image-based multi-scale model can help solve this problem and provide a tool to study the fundamental role of modified asphalt binders and aggregate structures.

### **1. Experimental Matrix**

The FS-based multi-scale model was used to study the effects of modification of asphalt binder and aggregate structure. Binder modification, aggregate gradation and aggregate internal structures are the three factors considered in this study. Three binders listed in CHAPTER III namely neat, SBS modified and CBE modified binders and two aggregate gradations were also included. To study the effects of aggregate structure, three structure images from mixture samples for each of the two gradations which were used to validate the simulations results in CHAPTER IV, as shown in Figure V-1. It is anticipated that by maintaining the aggregate structure or asphalt binder properties in the simulations, the individual effects on the permanent deformation of asphalt mixtures can be better understood.

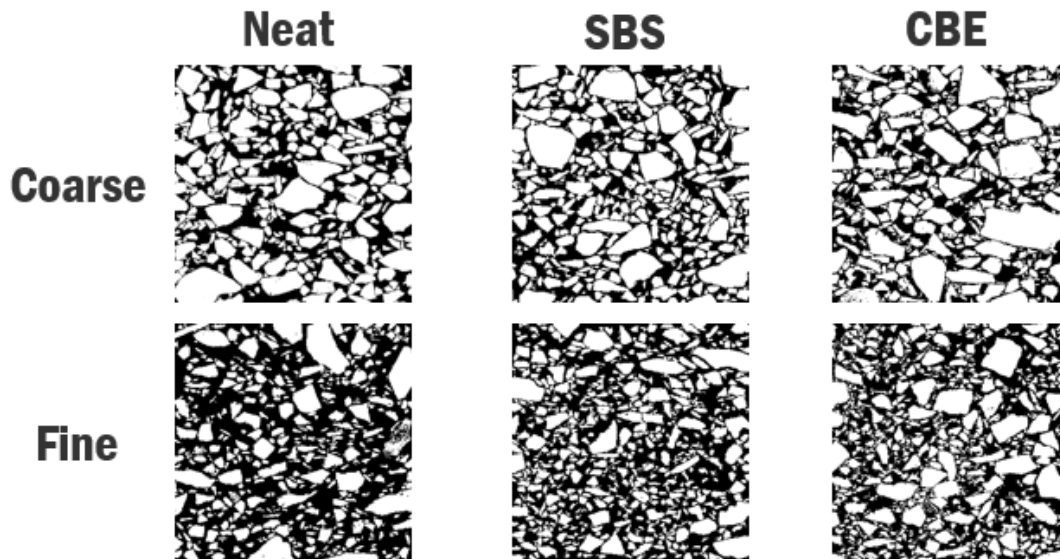


**Figure V-1: Different internal structures for two gradations included**

## **2. Micro-Structure Analysis for Different Asphalt Mixtures**

The Flow Number test is typically used to evaluate the asphalt mixture packing level and resistance to permanent deformation. To illustrate if the aggregate structure in asphalt mixture is well packed or not, image-based micro-structure analysis method was used in this study to eliminate the use of mixture FN test, which has been recently developed to evaluate the aggregate structure and correlate the micro-structure properties with mechanical properties of asphalt mixtures [5]. Research shows that the resistance to permanent deformation of asphalt mixture measured by Flow Number test can be well correlated to the property of internal aggregate structure (i.e. Total Proximity Length) as shown in Figure V-2. To prepare the samples for image analysis, six sections are cut from the compacted bulk mixture sample and scanned using a flatbed scanner. Aggregate structure was characterized using the image analysis software (iPas2) developed by University of Wisconsin-Madison. The details of the image analysis procedure can be found in other literature [5, 7, 27].

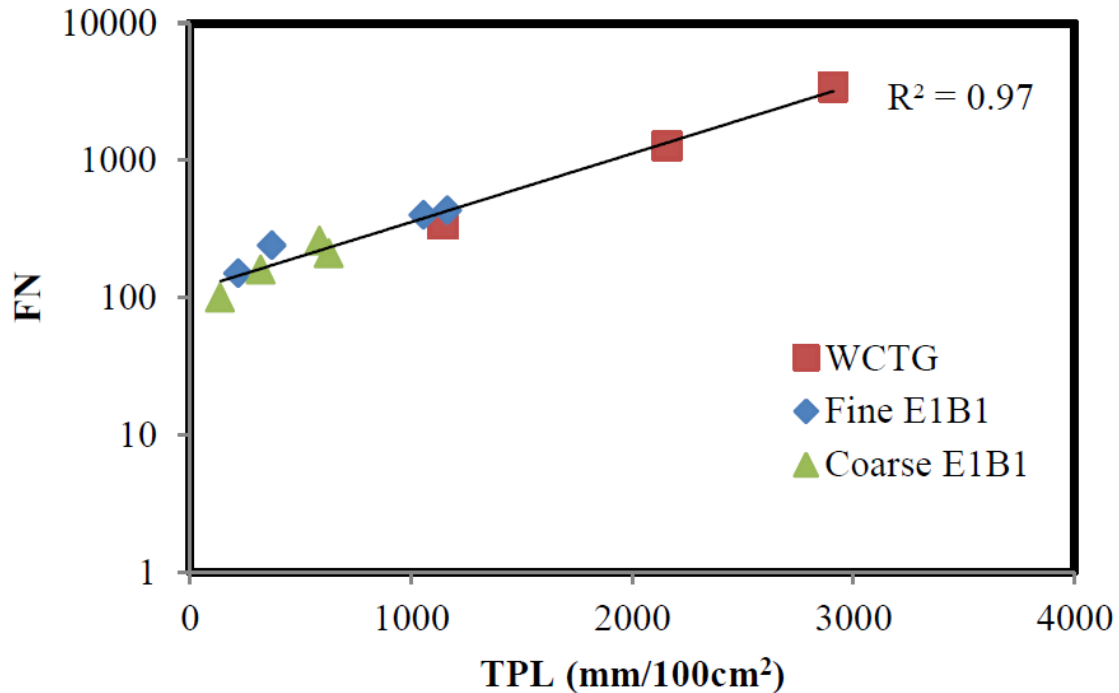


**Figure V-2: Correlation between Total Proximity Length and Flow Number [5]**

As mentioned in Chapter IV the FN test data was obtained from Asphalt Research Consortium project [51] for the six different mixtures used in this study. The same materials as used in that project were re-collected and compacted to fabricate another FN sample for each mix for the purpose of image analysis. The samples were then cut, scanned and analyzed to validate the correlation between total proximity lengths and flow number. The analyzed results of Total Proximity Length (TPL) after normalization through aggregate gradations [5] for the six different structures used in this study are shown in Figure V-3. As seen from the figure the fine mixes have higher TPL values than coarse mixes; TPL values for CBE modified mixes are significantly higher than neat mixes and SBS modified mixes. The flow number values at two stress levels (50psi/345kPa and 150psi/1034kPa) from mixture tests were obtained to validate the correlation between the TPL and FN. As presented in Figure V-4, the TPL correlates very well with FN values at

both stress levels indicating the effectiveness of this parameter in evaluating the rutting resistance of asphalt mixtures.

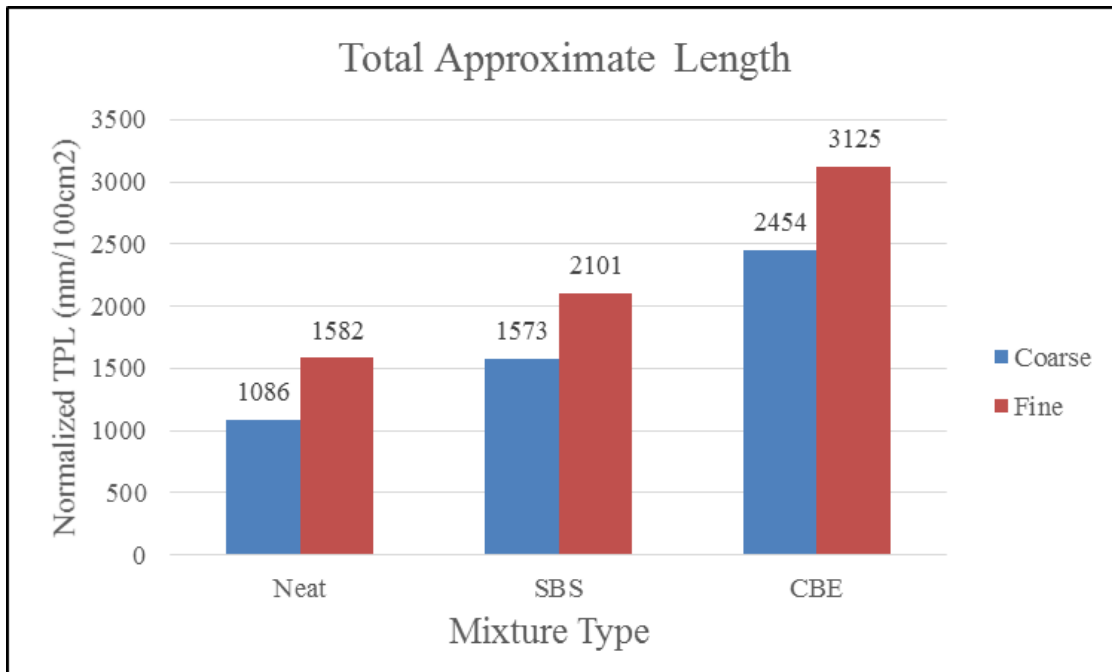


**Figure V-3: Total Proximity Length for different asphalt mixtures used in this study**

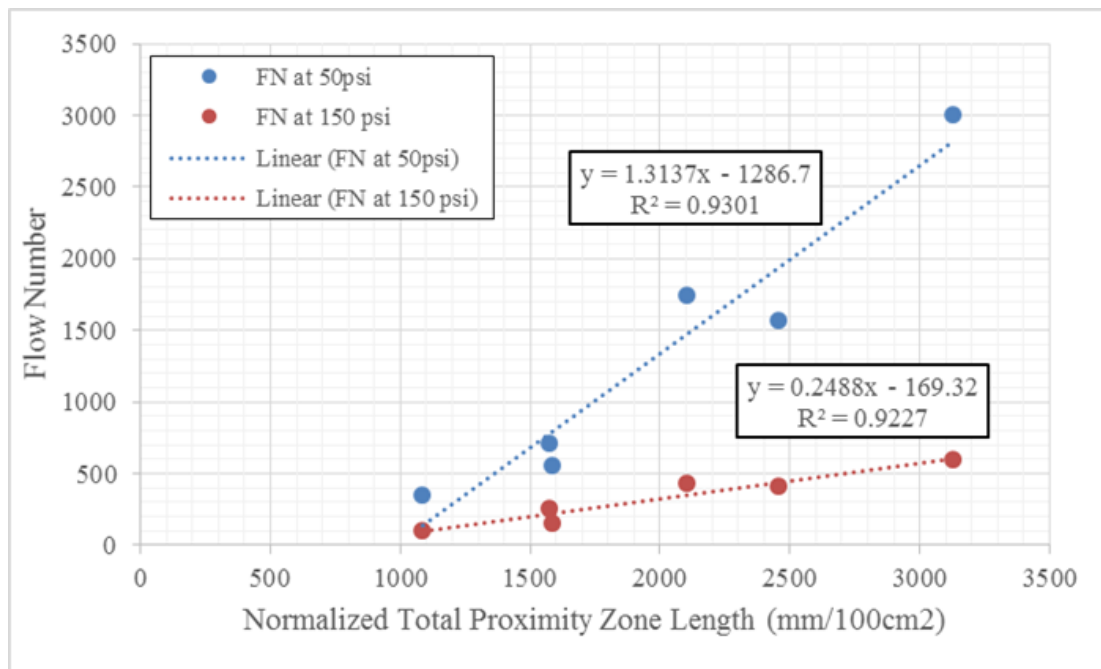


**Figure V-4: Correlation between TPL and FN at different stress levels**

The TPL was further adopted in this study as an indicator of aggregate structure packing level. Higher TPL value from image analysis indicates a better-packed aggregate structure. With the correlation between the TPL and FN as well as the FN limits recommended by NCHRP 9-33 project (Table V-1), it is also possible to derive the limits for the TPL values according to different design traffic levels to replace the FN.

**Table V-1: Recommended Flow Number limits from NCHRP 9-33 [53]**

<b>Traffic Level Million ESALs</b>	<b>Minimum Flow Number Cycles</b>
< 3	---
3 to < 10	53
10 to < 30	190
≥ 30	740

It should be noted that the FN limits recommended by NCHRP 9-33 are derived under stress level of 600kPa instead of either stress level used in Figure V-4. NCHRP 1-37 and AAPT 04-02 reports investigated the relationship between FN and stress levels and found the following relationship [54, 55]:

$$FN \propto \sigma^A$$

**Equation V-1**

Where: FN-Flow Number;  $\sigma$ -Deviatoric Stress Level; A-Constant

Therefore the following relationship can be derived:

$$\text{Log}(FN) = A * \text{Log}(\sigma) + B$$

**Equation V-2**

Where: FN-Flow Number;  $\sigma$ -Deviatoric Stress Level; A, B-Constants

According to Equation V-2, the FN at 600kPa can be speculated from FN at 345kPa and 1034kPa and the correlation between TPL and speculated FN at 600kPa is presented in Figure V-5. Based on the linear relationship the TPL limits corresponding to FN limits at different design traffic levels can also be found as shown in Figure V-5 and Table V-2. Table V-2 can be potentially implemented to any specification for asphalt mixtures where the FN limits are required or recommended.

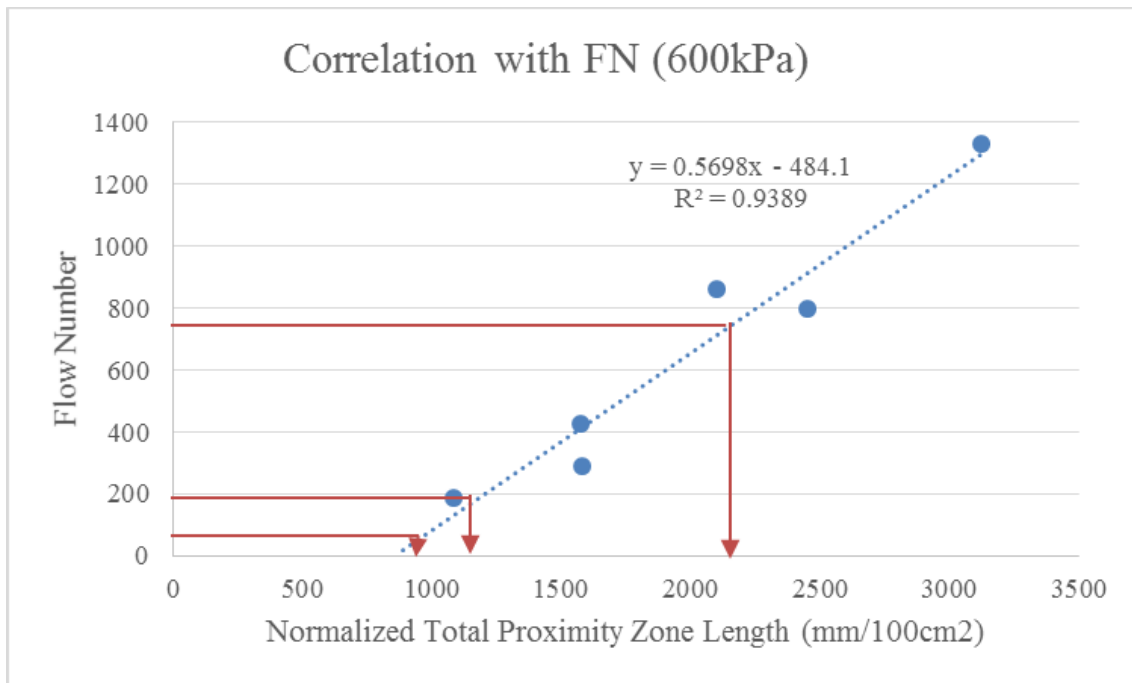


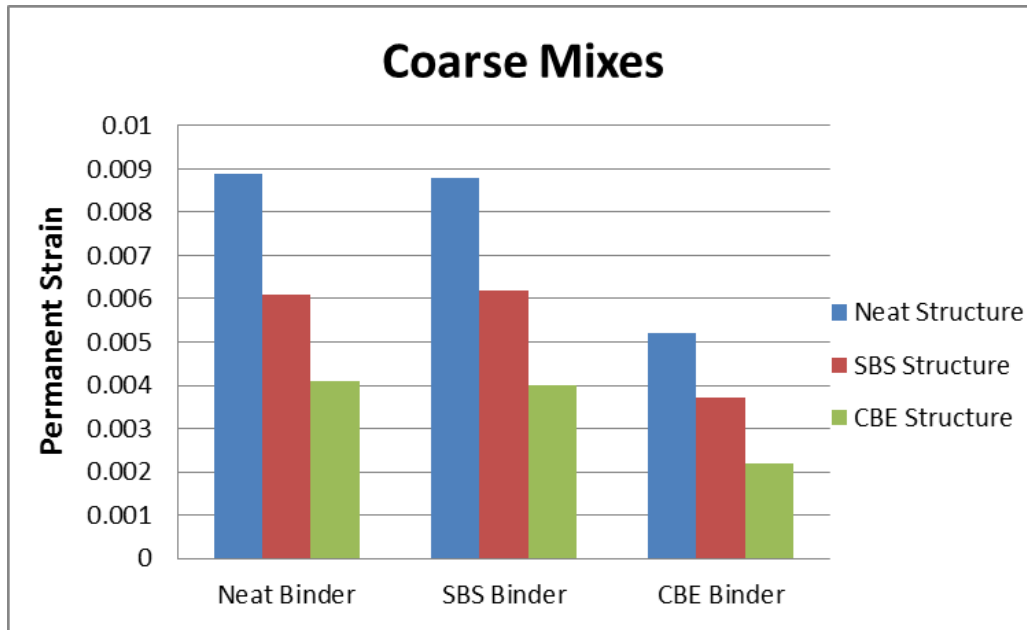
**Figure V-5: Correlation between TPL with speculated FN at stress level of 600kPa**

**Table V-2: Recommended minimum FN and TPL requirements**

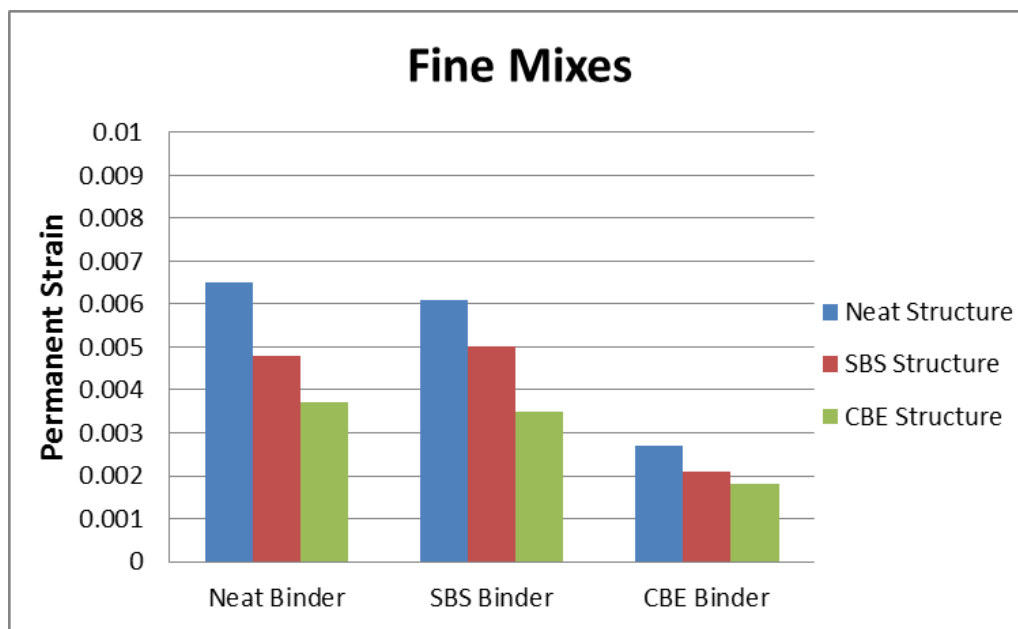
<b>Recommended Minimum TPL Requirements</b>		
Traffic Level Million ESALs	Minimum Flow Number	Minimum TPL mm/100cm <sup>2</sup>
< 3	-	-
3 to < 10	53	943
10 to < 30	190	1183
≥ 30	740	2148

### **3. Permanent Strain Analysis**

The simulated permanent strains after 70 cycles of repeated loading and recovery for different binders and structures are presented in Figure V-6 for coarse and fine mixtures, respectively. In general the fine mixtures performs better than the coarse mixtures in this study with lower permanent strains. Among the three types of binders, CBE modified binder shows the best rutting resistance due to the highest stiffness while the neat binder and SBS modified binder are relatively similar.. The internal structure of the CBE modified asphalt mixture (coded as “CBE structure”) similarly helps increase the rutting resistance of asphalt mixture relative to SBS structure and neat structure. Therefore it is concluded that packing of the aggregates is significantly affected by the binder modifiers as some additives can results in a better-packed aggregate internal structure that is much more effective in improving rutting resistance of mixtures.



(a) Coarse mixtures



(b) Fine mixtures

**Figure V-6: Permanent strains after 70 cycles for different asphalt binders and aggregate internal structures**

A statistical analysis was also performed to investigate the significance of each factor. The ANOVA table of the analysis for all mixtures is presented in Table V-3. All three factors are deemed significant, where asphalt binder type and aggregate structure are the two most significant. It should also be noted that the aggregate structure is more important than aggregate gradation with a higher F-value, indicating that obtaining a better structure is more critical than modifying the aggregate gradation in improving the rutting resistance of asphalt mixtures. However, changing aggregate gradation may also help to improve the aggregate structure.

**Table V-3: ANOVA for all mixtures analyzed**

ANOVA - All Mixtures				
	DF	F-Value	Pr (>F)	Significance
Gradation	1	19.95	7.70E-04	***
Binder	2	30.82	1.87E-05	***
Structure	2	31.72	1.62E-05	***
Residuals	12			
$R^2_{adj}=92.36\%$				

An ANOVA analysis were also conducted for each of the three structures individually to study the importance of asphalt binder in different structures. As shown in Table V-4, the binder type is significant in all three mixtures; however the relative importance is not the same between structures. In a highly packed mixture structure such as CBE, the binder type is the least significant with the lowest F-value compared with the binder type in other two structures. In a poorly packed structure (i.e. neat structure), the binder type has the highest significance with the largest F-value and smallest p-value relative to the factor of binder type in other structures. Therefore it is concluded that the asphalt binder properties affect

the rutting resistance of asphalt mixture more significantly in mixtures with a poor-packed aggregate structure relative to the mixtures with a well-packed structure.

**Table V-4: ANOVA for mixtures under three different aggregate structures**

(a) Neat structure

ANOVA - NEAT Structure				
	DF	F-Value	Pr (>F)	Significance
Gradation	1	825.14	0.0012	**
Binder	2	753.57	0.0013	**
Residuals	2			
$R^2_{adj}=99.79\%$				

(b) SBS structure

ANOVA - SBS Structure				
	DF	F-Value	Pr (>F)	Significance
Gradation	1	129.31	0.0076	**
Binder	2	212.54	0.0047	**
Residuals	2			
$R^2_{adj}=99.10\%$				

(c) CBE structure

ANOVA - CBE Structure				
	DF	F-Value	Pr (>F)	Significance
Gradation	1	169.00	0.0059	**
Binder	2	133.00	0.0075	**
Residuals	2			
$R^2_{adj}=99.82\%$				

## 4. Stress and Strain Analysis

### 4.1 Stress/Strain Analysis Protocol

One of the significant advantages for finite element modeling is that the stress/strain information regarding each element can be extracted for detailed analysis after simulation.

In the previous section the permanent deformation simulations for 18 different mixtures including 2 aggregate gradations, 3 aggregate structures and 3 types of asphalt binders generate the database files for further stress/strain analysis. However since the multi-scale models are involved in this study, it is deemed necessary to develop a protocol to back-calculate the stress/strain in continuous phase at each length scale.

Unlike the process of multi-scale modeling, the stress/strain analysis starts from the highest scale which is mixture scale, and then the information obtained from higher scale is utilized in the next lower scale for further analysis down to the mastic scale. Eventually the stress/strain information for continuous phase at different scales from mortar to binder is obtained. Once the simulation for asphalt mixture is complete, the minor principle stress/strain (maximum compressive stress/strain) for all the mortar elements are obtained and averaged. The averaged compressive stress of mortar is then applied to mortar model and after a creep simulation the compressive stress/strain for all mastic elements are extracted and averaged. The similar procedure is also applied to mastic model and finally the compressive stress/strain and shear stress/strain for all binder elements can be extracted. The detailed results of stress/strain in each continuous phase for all different mixtures following this procedure are introduced in the following sections.

#### **4.2 Stress Analysis**

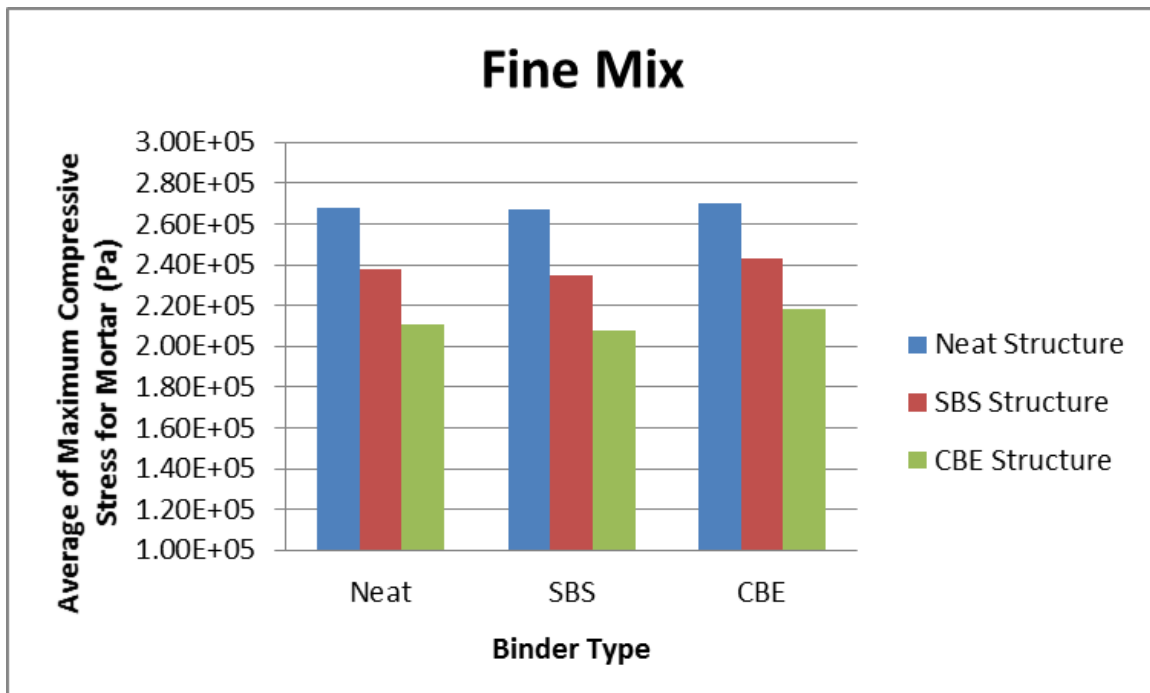
The average of maximum compressive stresses at the end of loading for both first (0.1s) and last cycle (69.1s) were extracted from the mixture simulation files and presented in Table V-5 and Table V-6. The compressive stresses of mortar for both coarse and fine mixtures are also presented in Figure V-7 and Figure V-8.

**Table V-5: Average of maximum compressive stress at 0.1s**

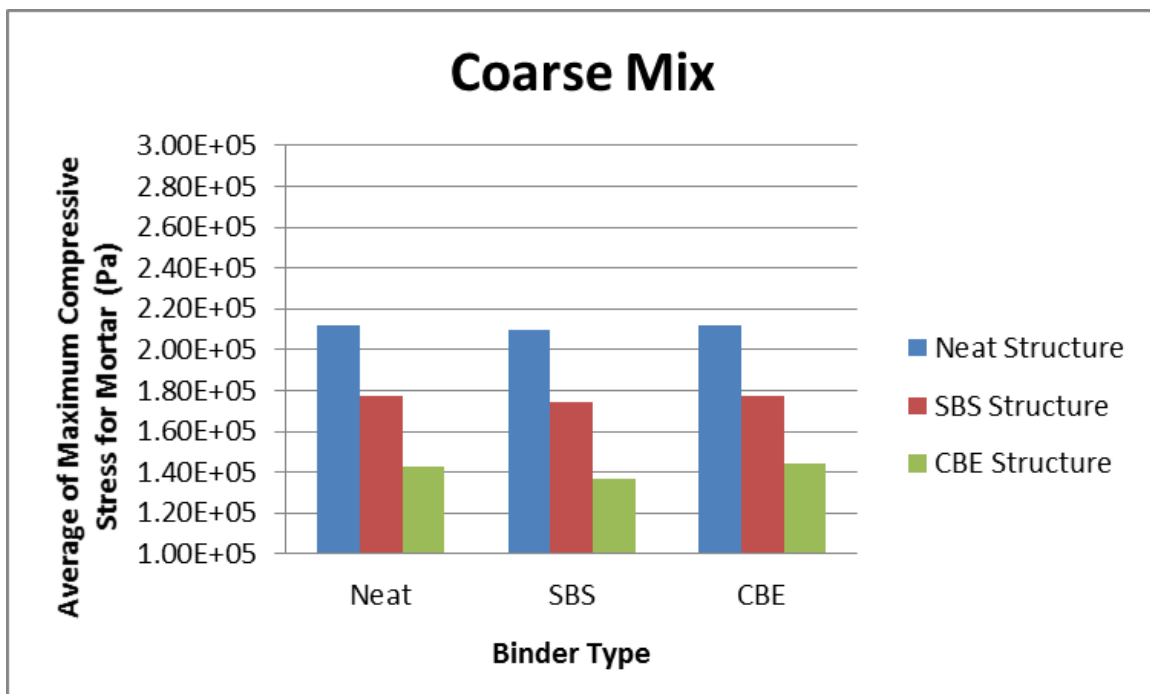
Average of Maximum Compressive Stress at 0.1s					
Gradation	Binder	Structure	Averaged Stress for Mortar	Averaged Stress for Aggregate	Ratio
Fine	Neat	Neat	2.68E+05	7.00E+05	38.3%
		SBS	2.38E+05	7.54E+05	31.6%
		CBE	2.11E+05	7.46E+05	28.3%
	SBS	Neat	2.67E+05	7.01E+05	38.1%
		SBS	2.35E+05	7.65E+05	30.7%
		CBE	2.08E+05	7.58E+05	27.4%
	CBE	Neat	2.70E+05	6.56E+05	41.2%
		SBS	2.43E+05	6.92E+05	35.1%
		CBE	2.18E+05	6.85E+05	31.8%
Coarse	Neat	Neat	2.12E+05	6.89E+05	30.8%
		SBS	1.77E+05	6.84E+05	25.9%
		CBE	1.43E+05	7.23E+05	19.8%
	SBS	Neat	2.10E+05	7.04E+05	29.8%
		SBS	1.74E+05	7.03E+05	24.8%
		CBE	1.37E+05	7.58E+05	18.1%
	CBE	Neat	2.12E+05	6.72E+05	31.5%
		SBS	1.77E+05	6.68E+05	26.5%
		CBE	1.44E+05	7.05E+05	20.4%

**Table V-6: Average of maximum compressive stress at 69.1s**

Average of Maximum Compressive Stress at 69.1s					
Gradation	Binder	Structure	Averaged Stress for Mortar	Averaged Stress for Aggregate	Ratio
Fine	Neat	Neat	2.52E+05	9.34E+05	27.0%
		SBS	2.22E+05	9.62E+05	23.1%
		CBE	1.92E+05	9.06E+05	21.2%
	SBS	Neat	2.46E+05	9.57E+05	25.7%
		SBS	2.15E+05	1.12E+06	19.2%
		CBE	1.84E+05	1.03E+06	17.9%
	CBE	Neat	2.62E+05	9.08E+05	28.9%
		SBS	2.38E+05	9.15E+05	26.0%
		CBE	2.12E+05	9.11E+05	23.3%
Coarse	Neat	Neat	1.90E+05	8.46E+05	22.5%
		SBS	1.50E+05	7.82E+05	19.2%
		CBE	1.23E+05	7.90E+05	15.6%
	SBS	Neat	2.08E+05	1.05E+06	19.8%
		SBS	1.50E+05	9.19E+05	16.3%
		CBE	1.26E+05	9.25E+05	13.6%
	CBE	Neat	1.96E+05	9.10E+05	21.5%
		SBS	1.60E+05	8.76E+05	18.3%
		CBE	1.32E+05	8.12E+05	16.3%

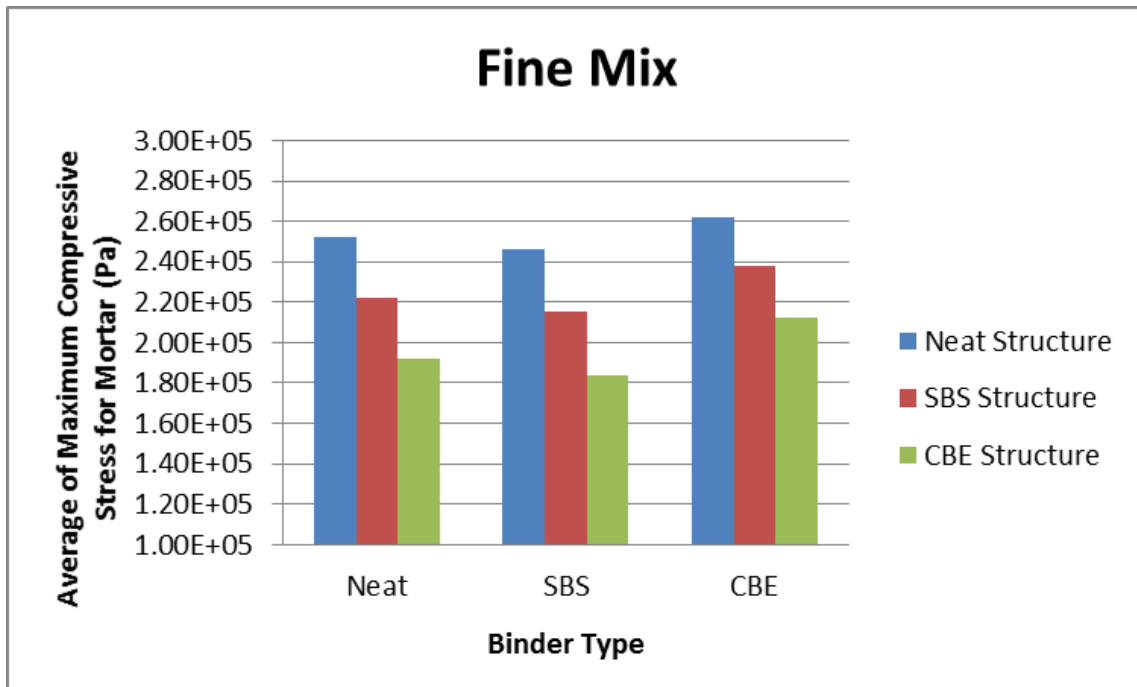


(a)

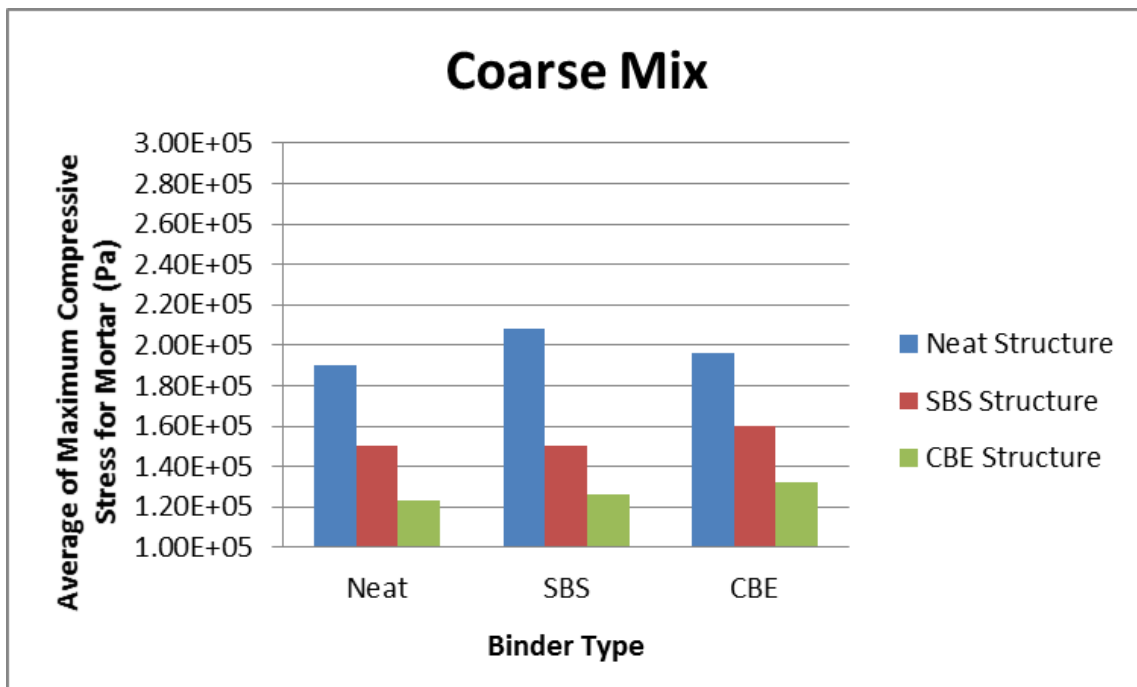


(b)

Figure V-7: Average of maximum compressive stress at 0.1s for mortar in (a) fine mix (b) coarse mix



(a)



(b)

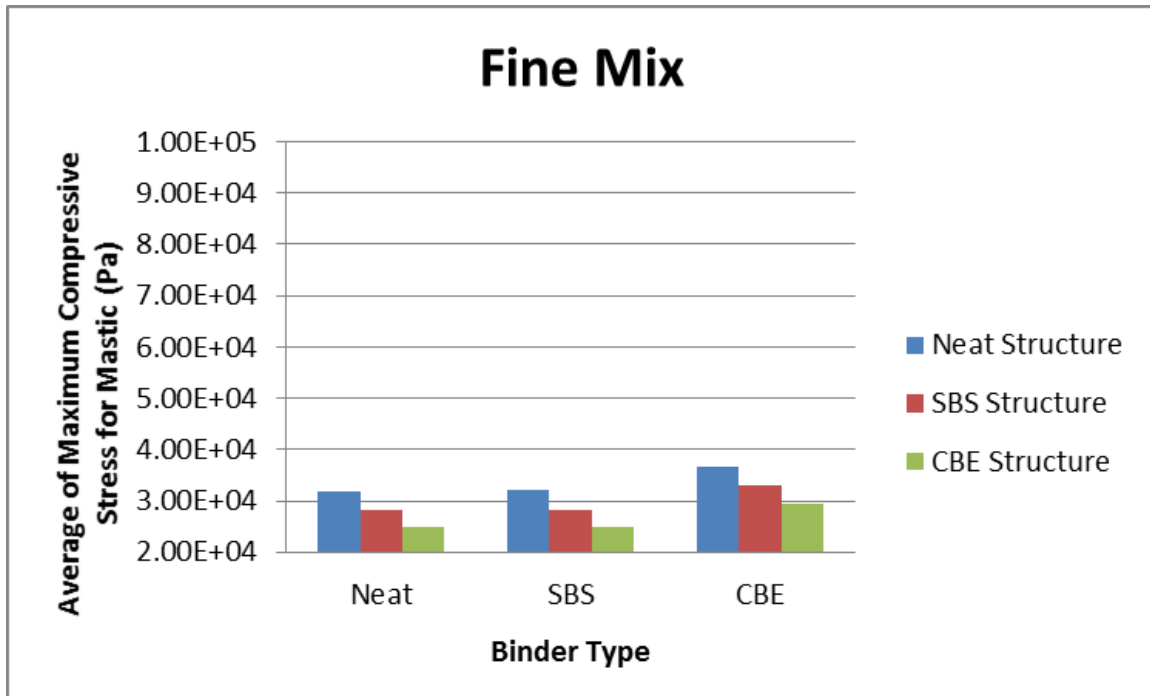
Figure V-8: Average of maximum compressive stress at 69.1s for mortar in (a) fine mix (b) coarse mix

From Table V-5 and Figure V-7 shown above, it is found that by the end of loading time for the first cycle (0.1s) the average stresses of mortar in mixtures with three different binders are very close to each other for both fine and coarse mixtures therefore the stresses are not sensitive to the binder modification in this case. However the stresses of mortar in mixtures with different aggregate structures are significantly different, where the mortar in mixtures with neat structure has much higher stress level than the mortar in mixtures with SBS structure; the mortar in mixtures with CBE structure has the lowest stress. As described in Section 2 of this chapter the mixtures with CBE structure have much better packing levels compared to mixtures with the other two structures which leads to a better stress distribution and much lower stresses in the continuous phases. In general the stresses in coarse mixes are much lower than the fine mixes due to the higher volume fraction at mixture scale; therefore more stresses are taken by the aggregate elements than the mortar elements. The trends of the ratios of stresses in mortar and stresses in aggregate are generally consistent with the trends seen in mortar as the stress levels in aggregate elements are in a relative narrow range.

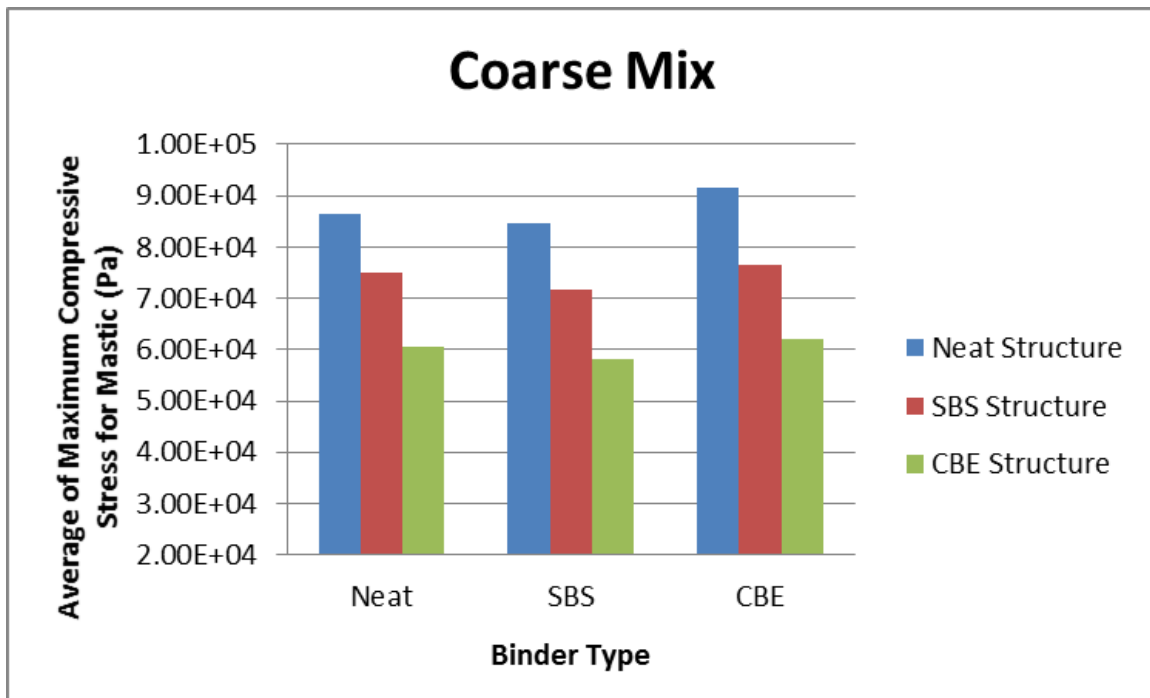
Similar trends are also found for the average maximum compressive stresses at 69.1s as shown in Table V-6 and Figure V-8. Therefore it was decided to adopt the compressive stresses at 0.1s for simulations at mortar scale. The results of the compressive stresses of mastic for both fine and coarse mixes are presented in Figure V-9. The trends for different asphalt binder and aggregate structure found for mortar are also seen for mastic. However the stresses of mastic in fine mixes are significantly lower than the coarse mixes. Considering at mortar scale the volume fraction of aggregate in fine mortar is about 25% higher of the total volume of mortar than the one in coarse mortar (Table IV-1), more

aggregate elements in fine mortar take the stresses than the ones in coarse mortar thus reducing the stresses in mastic.

Similar analysis procedure was followed to calculate the average maximum compressive stresses and shear stresses of asphalt binders in different asphalt mixtures at 0.1s of loading. The results are presented in Figure V-10 and Figure V-11. Both types of the stresses in asphalt binders also follow the similar trends as found in mastics. The stresses are not quite sensitive to binder modification; it seems that CBE binder has slightly higher stress levels than the other two binders. Stresses in mixtures with neat structure are higher than mixtures with the other two structures due to better packing. Binders in fine mixtures have much lower stresses than the binders in coarse mixtures due to the lower compressive stresses applied on the mastic models.

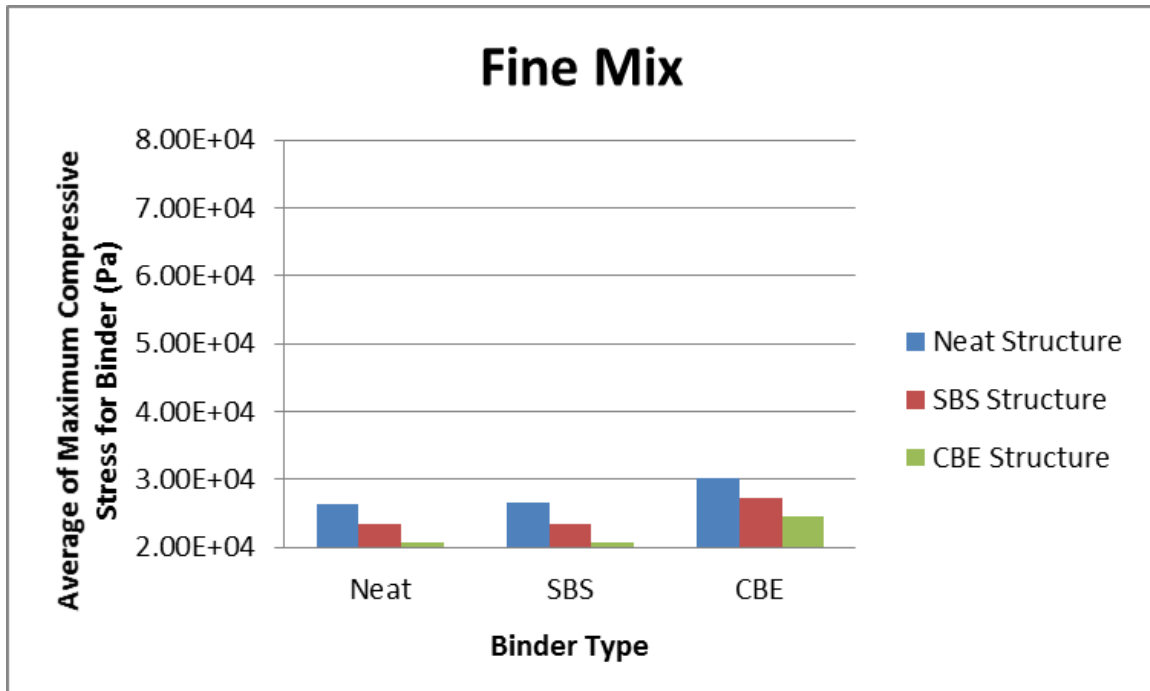


(a)

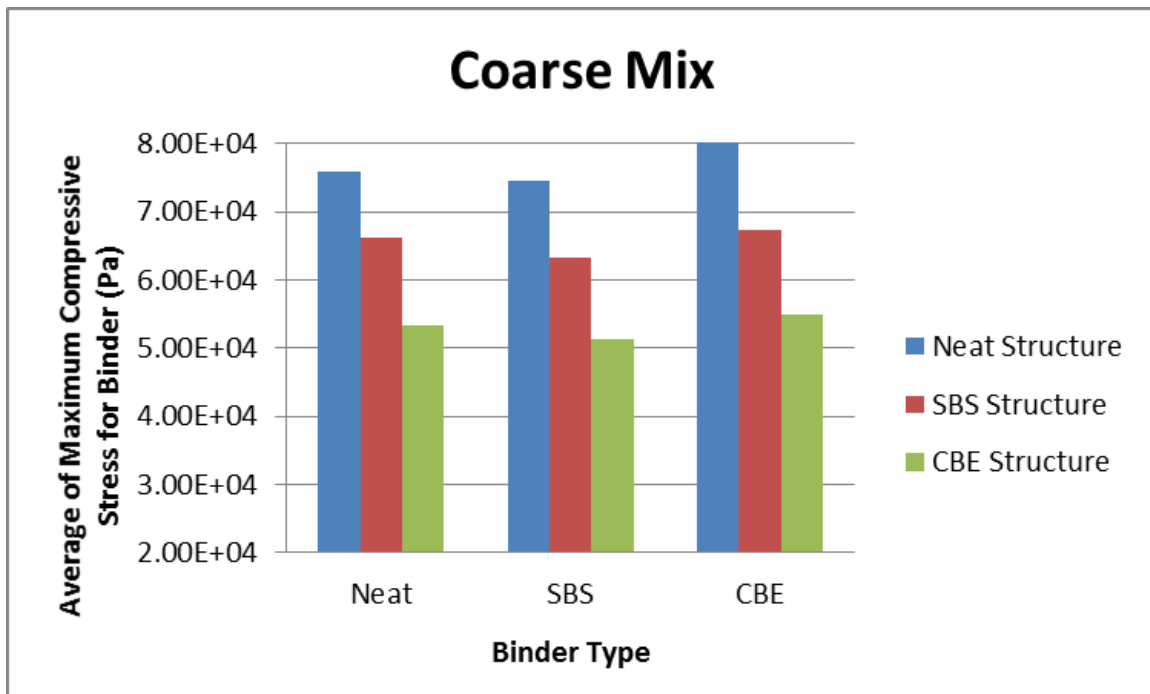


(b)

Figure V-9: Average of maximum compressive stress at 0.1s for mastic in (a) fine mix (b) coarse mix

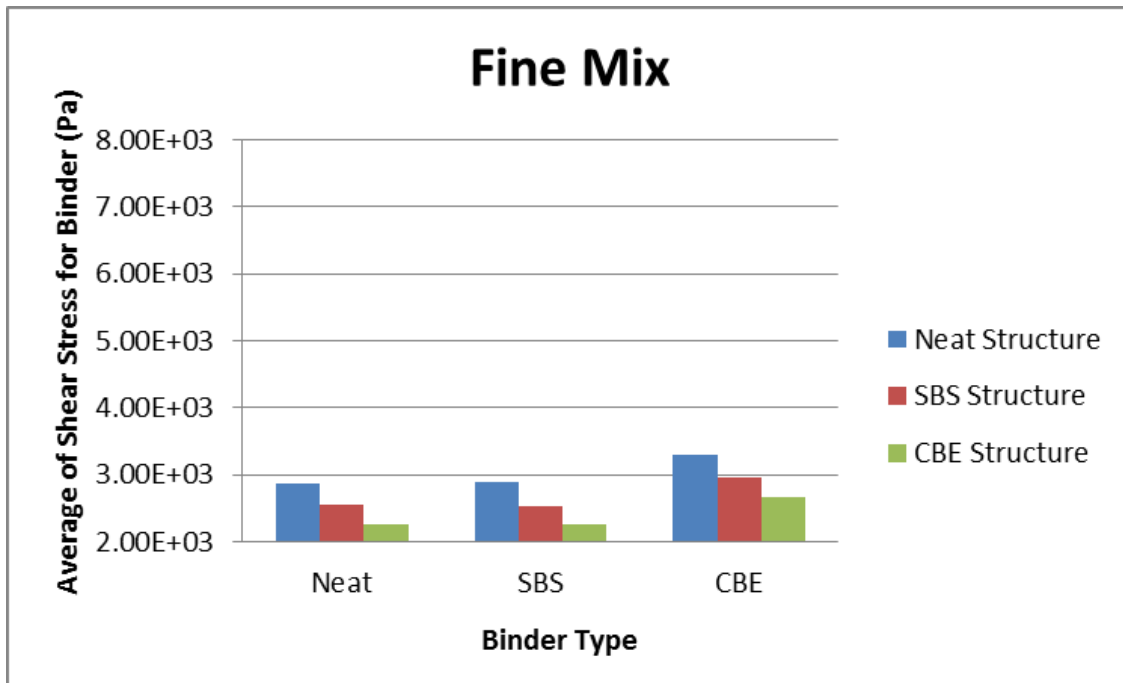


(a)

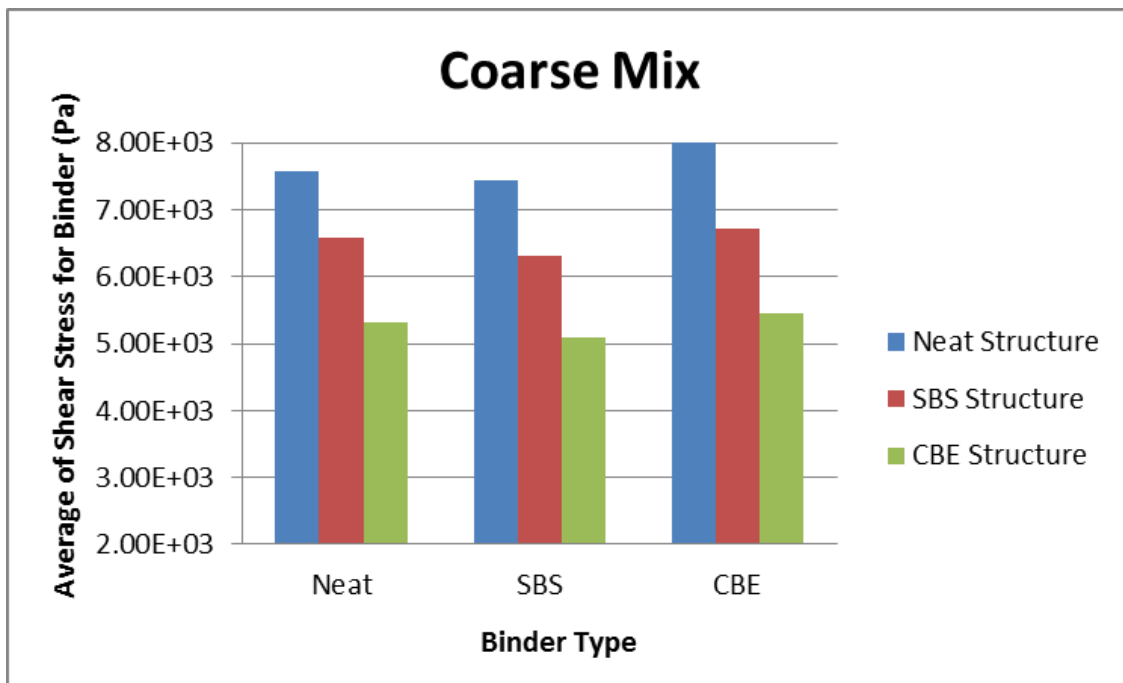


(b)

Figure V-10: Average of maximum compressive stress at 0.1s for asphalt binder in (a) fine mix (b) coarse mix



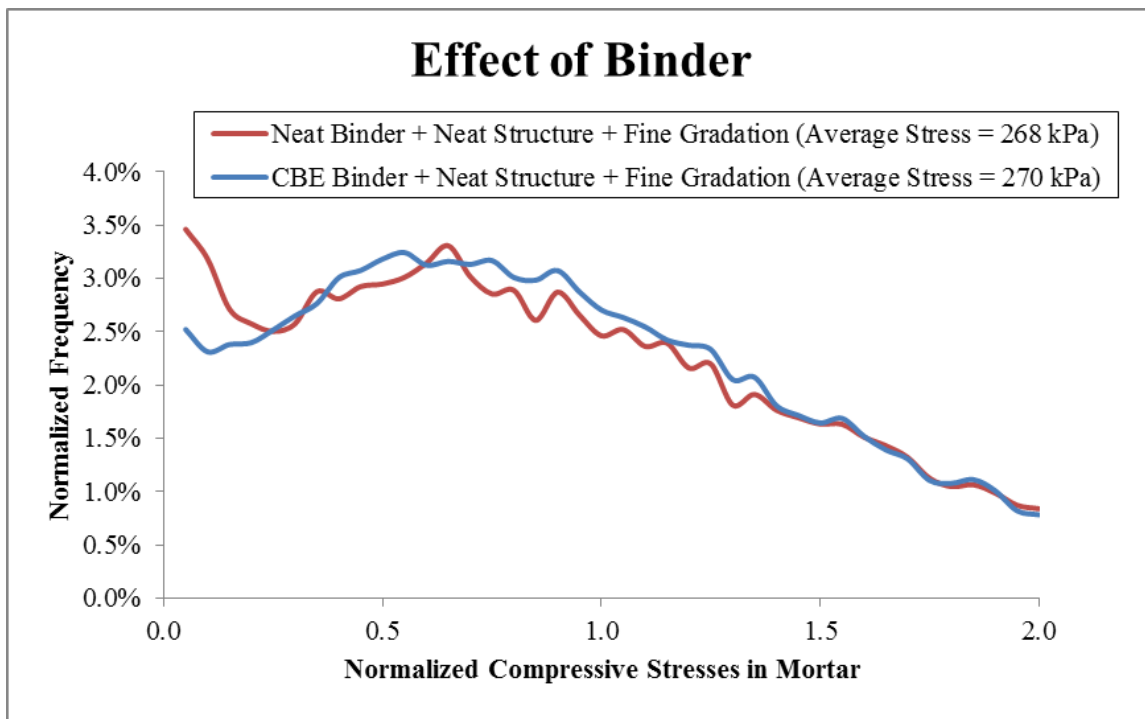
(a)



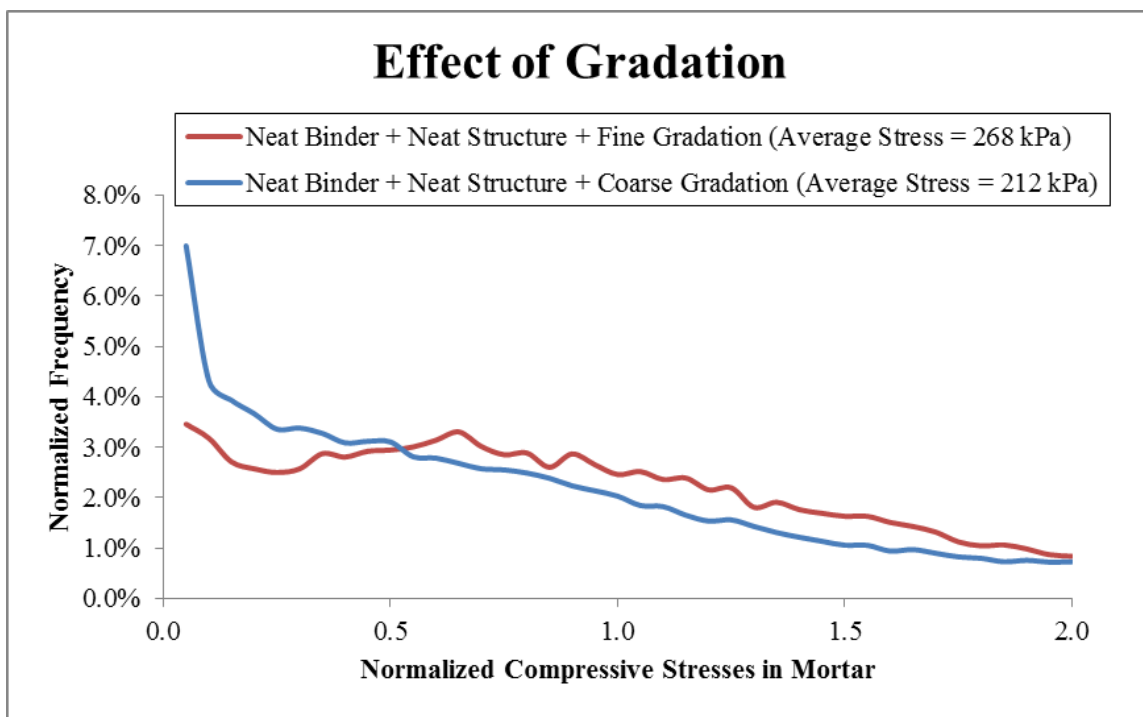
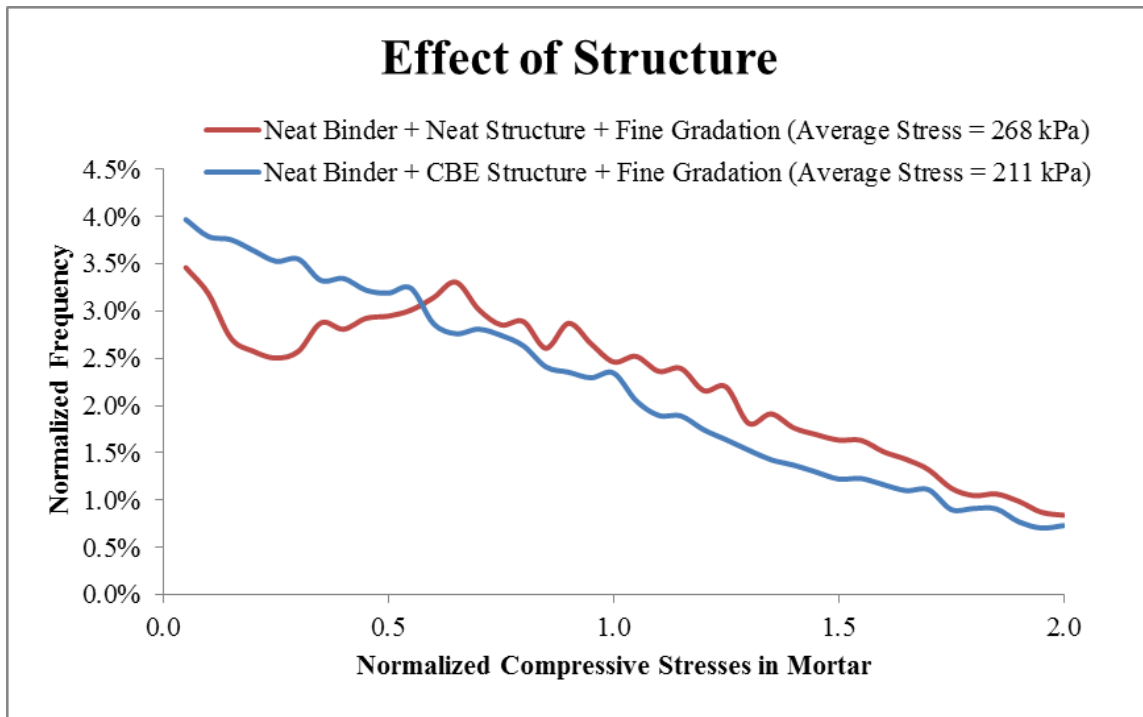
(b)

Figure V-11: Average of shear stress at 0.1s for asphalt binder in (a) fine mix (b) coarse mix

The distributions of the maximum compressive stresses in continuous phases at each length scale are also investigated through the stress-per-element histograms plotted against normalized element frequency, similarly as what Arshadi has conducted (56). The compressive stresses are normalized by the average compressive stresses in all matrix elements (as shown in Figure V-7 to Figure V-11) and the ratios are calculated and plotted. The effects of selected binder type, aggregate structure and aggregate gradation on the mortar stress distributions are illustrated in Figure V-12. As seen from the figures the distributions of stresses in mortar for different binders, structures and gradations are close to each other (with similar shapes) for higher stresses, but are significantly different at lower stresses.

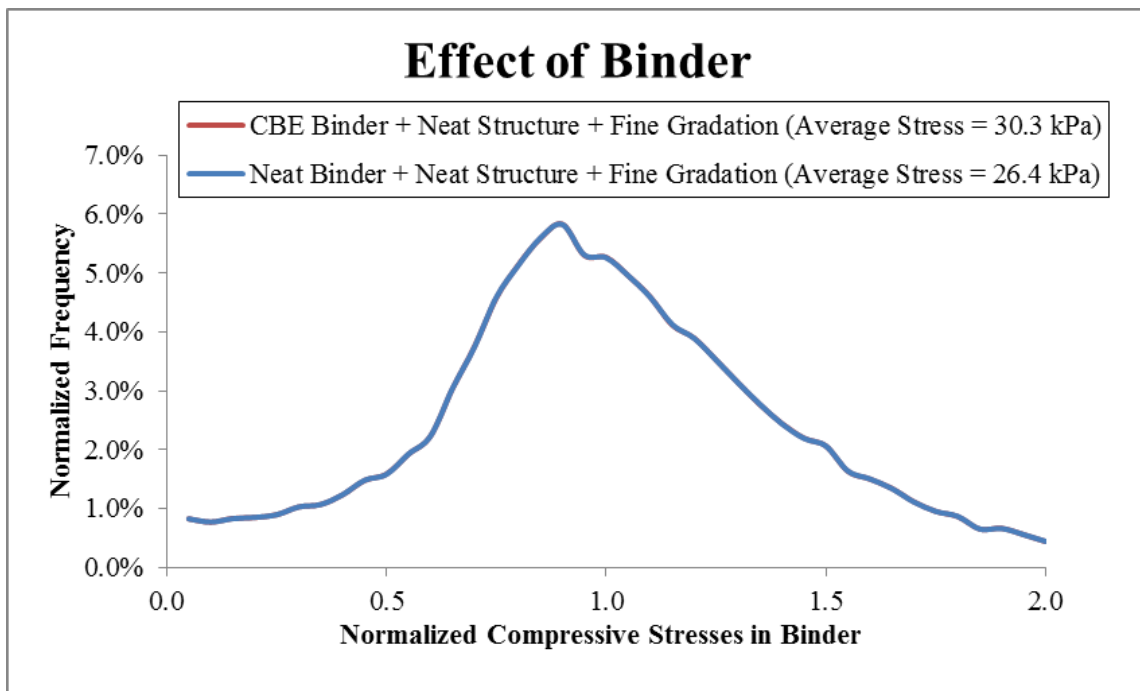


(a)

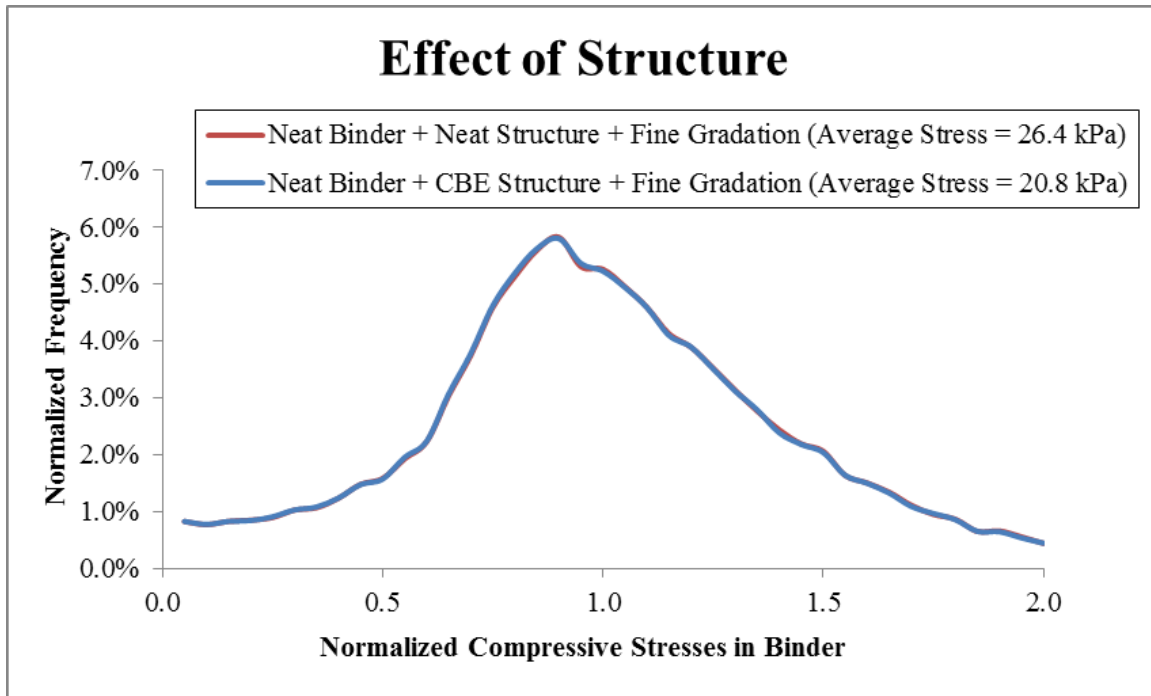


**Figure V-12: Distributions of maximum compressive stresses in mortar for (a) different binders (b) different structures (c) different gradations**

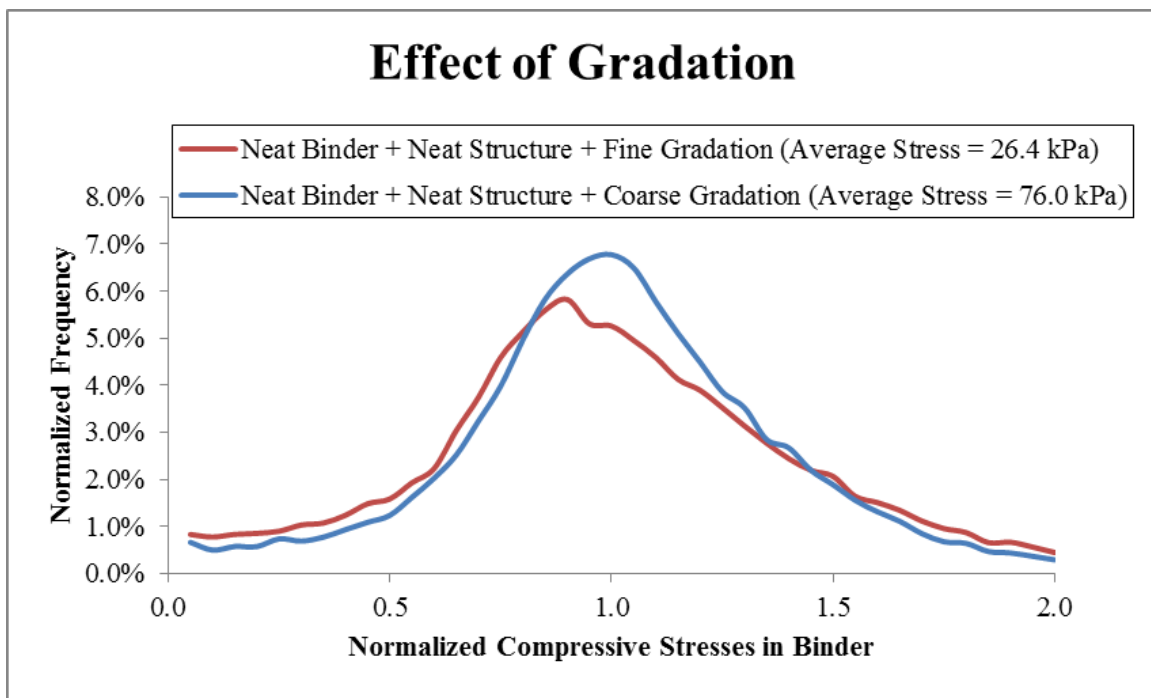
For the distributions of maximum compressive stresses in mastic and binder, it is expected that the binder type and aggregate structure would not have any significant effect as the same mortar and mastic images were shared in modeling for mixtures with different binders and aggregate structures. Due to the different gradations the volume fraction and particle distribution for different mixtures are also different, which can lead to the difference in stress distributions. The effects of binder, aggregate structure and gradation on the compressive stress distributions in binder shown in Figure V-13 further confirm these assumptions. It is also noticed that the distribution of compressive stresses in binder follows a normal distribution in general.



(a)



(b)



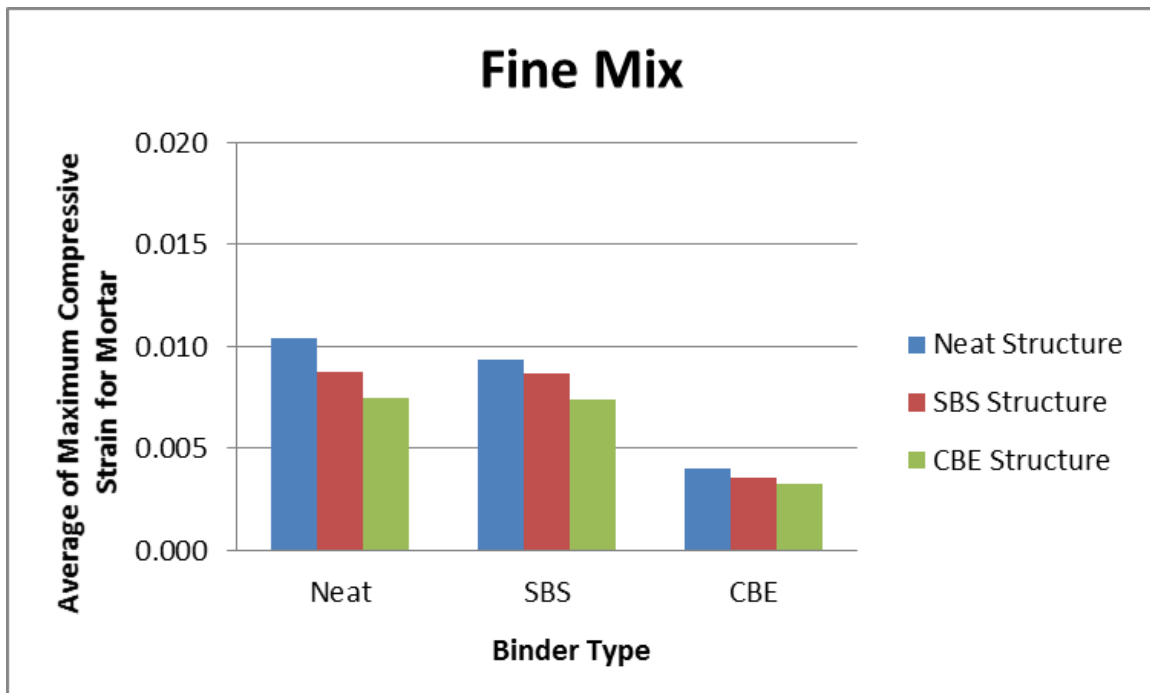
(c)

**Figure V-13: Distributions of maximum compressive stresses in binder for (a) different binders (b) different structures (c) different gradations**

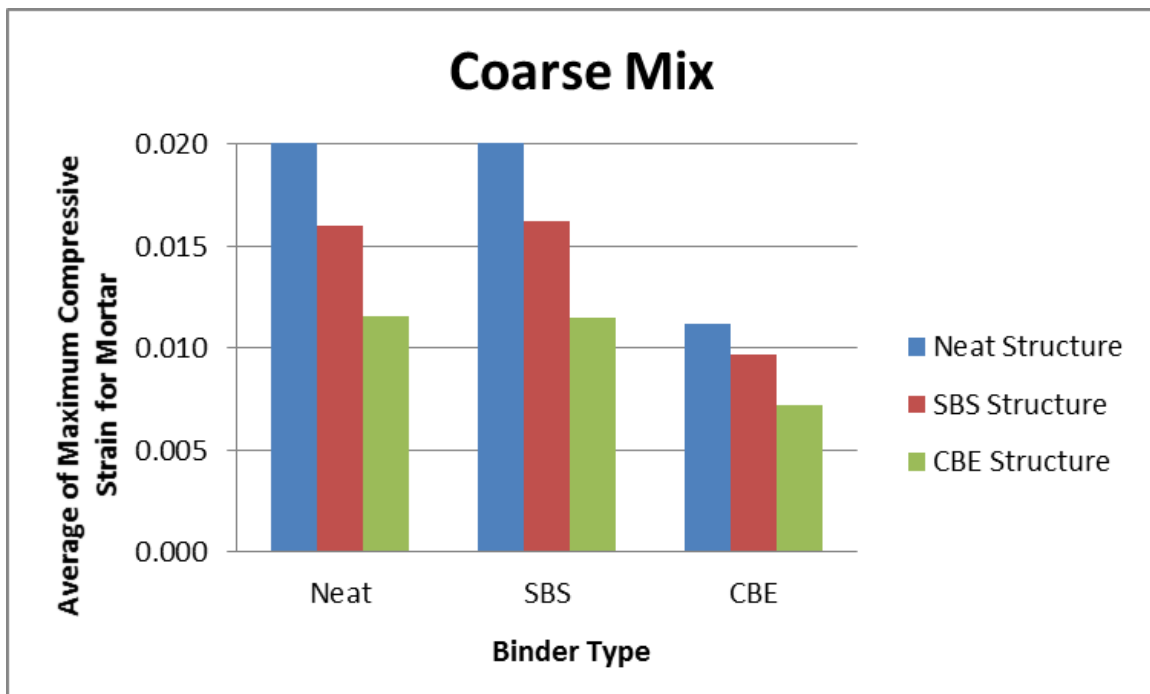
### 4.3 Strain Analysis

When the stresses are extracted from the modeling database file at each scale, the strains can also be obtained for further analysis. At mixture scale the maximum compressive strains for mortar in all mixtures by the end of all cycles (70s) were first extracted and averaged as shown in Figure V-14. It is clearly seen that the trends for strains in mortars are exactly the same as what was shown for mixtures in Figure V-6. When looking at the compressive strains after the loading for the first (0.1s) and last (69.1s) cycle as presented in Figure V-15 and Figure V-16, the similar trends are generally maintained; the SBS modified binder leads to slightly higher strains than the two other binders, which is different from what Figure V-14 shows by the end of all cycles. Considering SBS is a type of elastomeric modifier which typically has higher elastic recovery property, it is logical to see such change in trend from loading to unloading.

The average of maximum compressive strains of mastic and binder and the shear stress of asphalt binder at 0.1s are also presented in Figure V-17, Figure V-18 and Figure V-19. They all maintain the similar trends but the values are all of different magnitude.

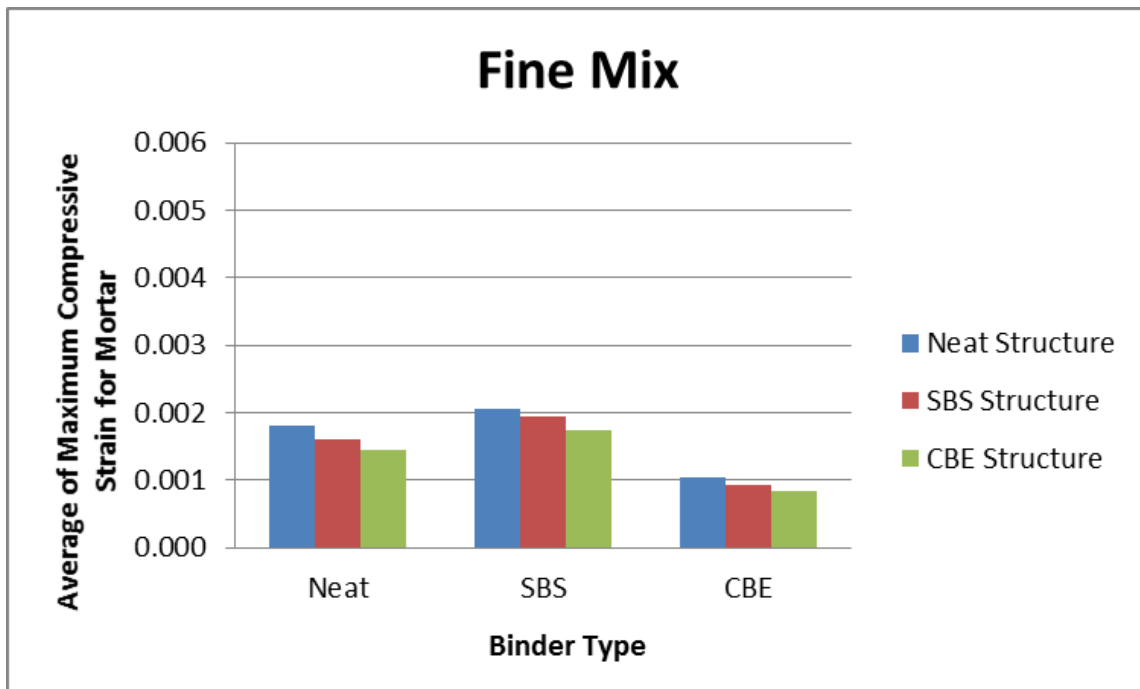


(a)

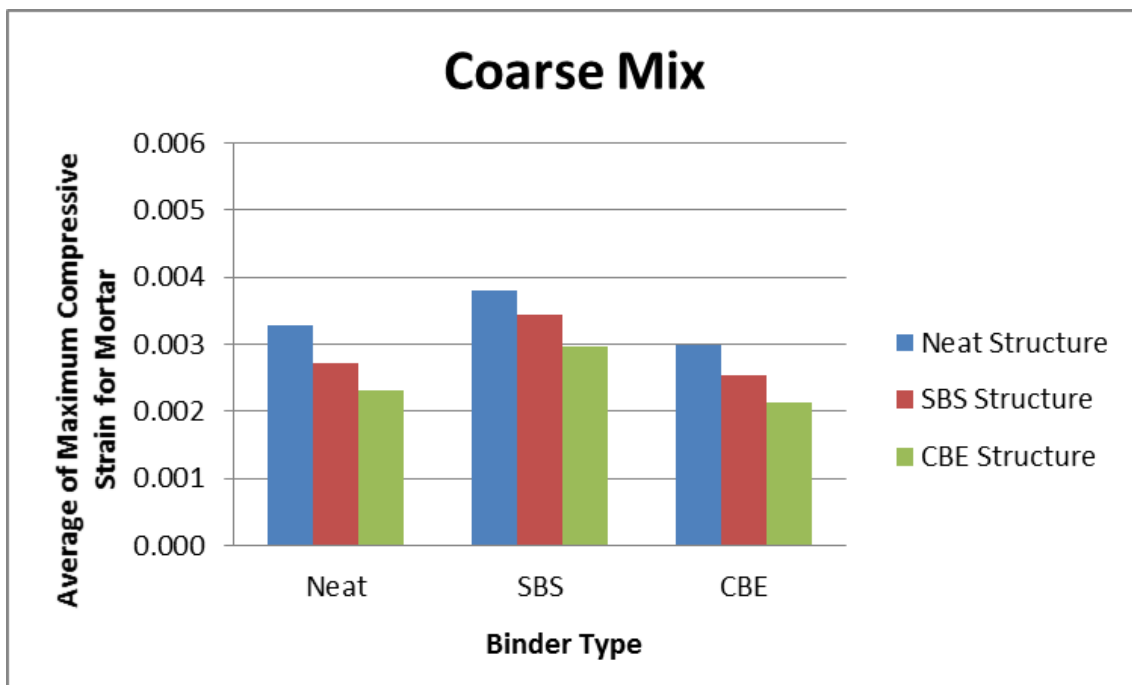


(b)

Figure V-14: Average of maximum compressive strain at 70s for mortar in (a) fine mix (b) coarse mix

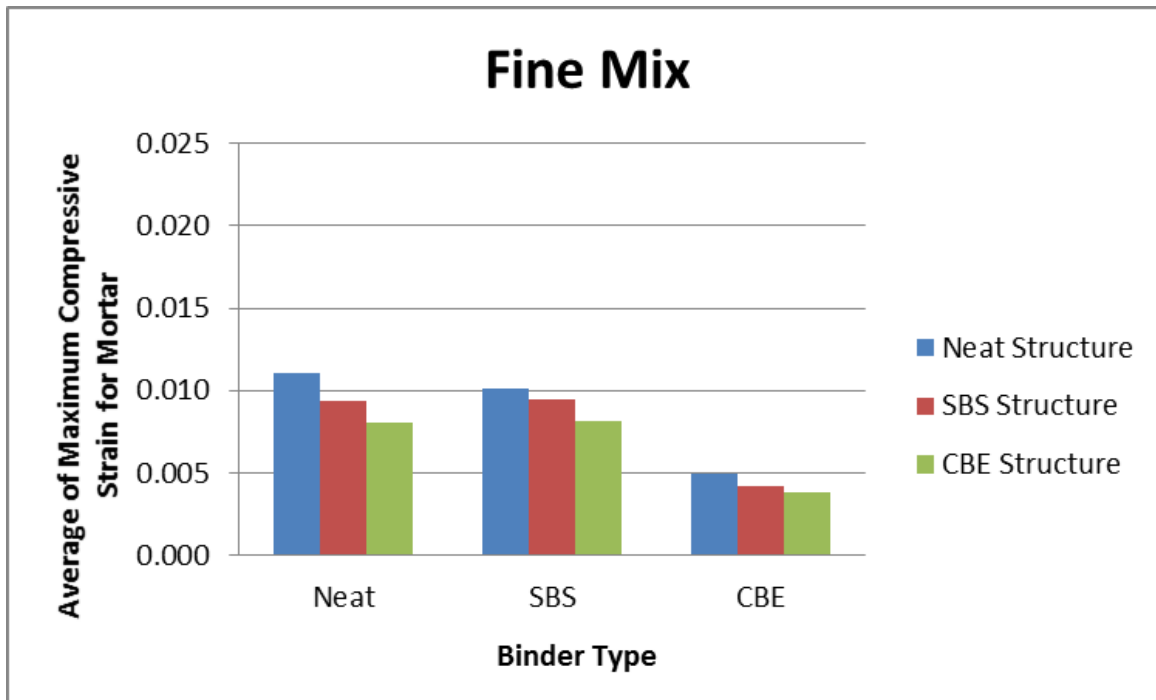


(a)

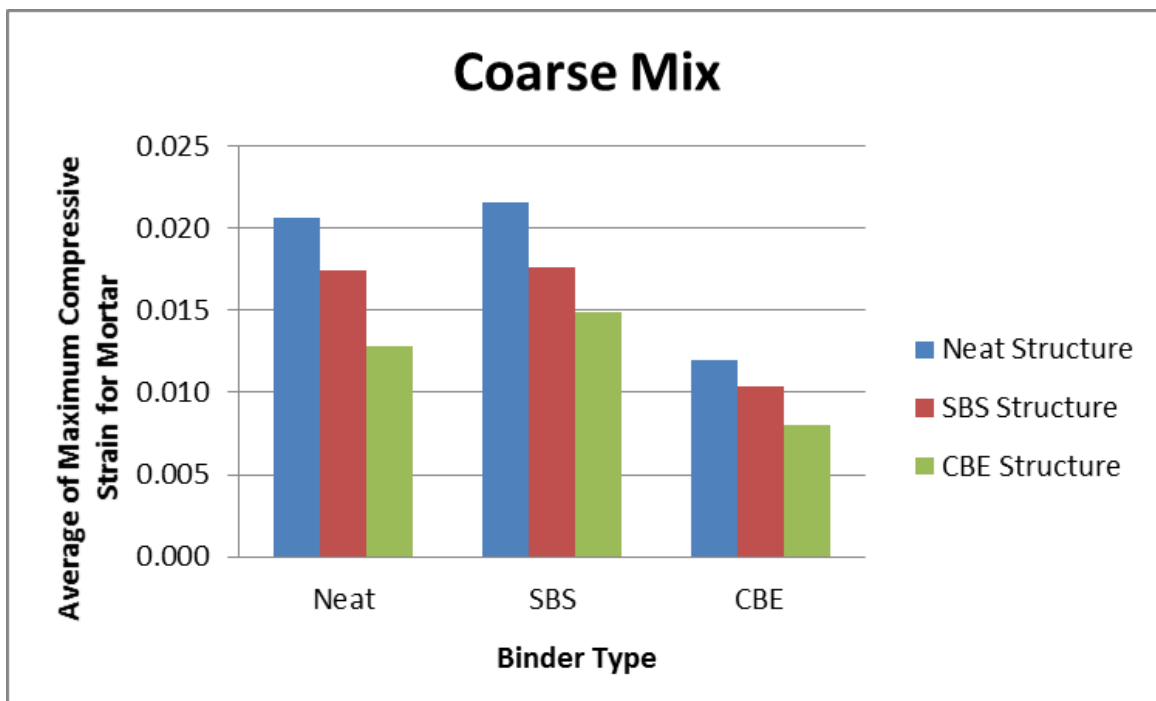


(b)

**Figure V-15: Average of maximum compressive strain at 0.1s for mortar in (a) fine mix (b) coarse mix**

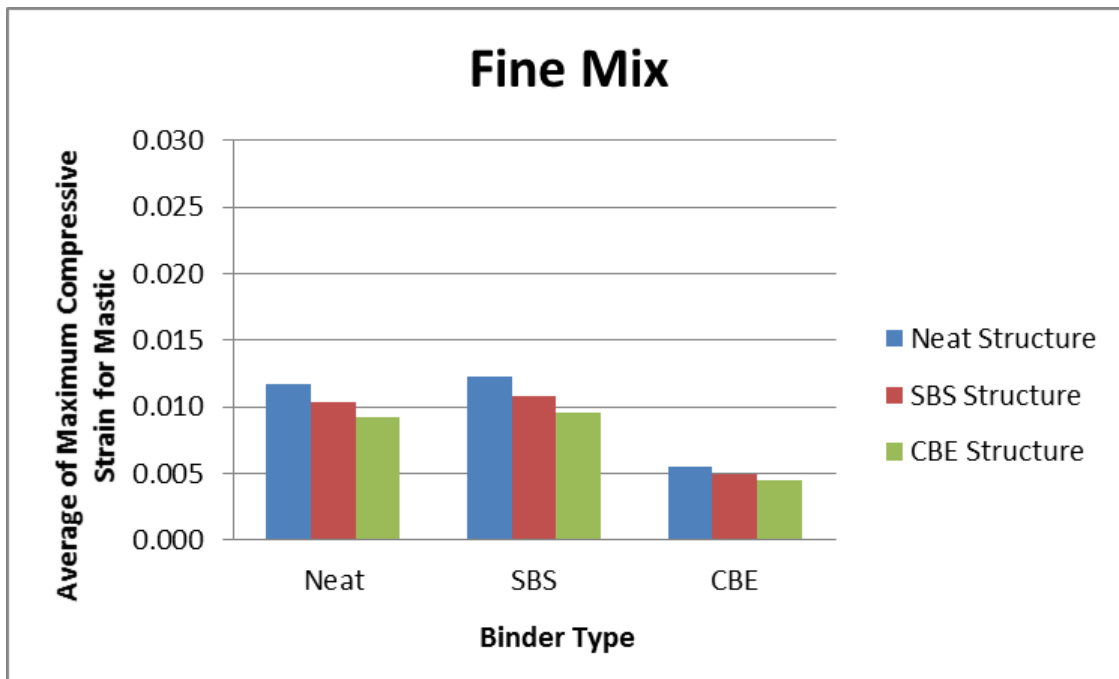


(a)

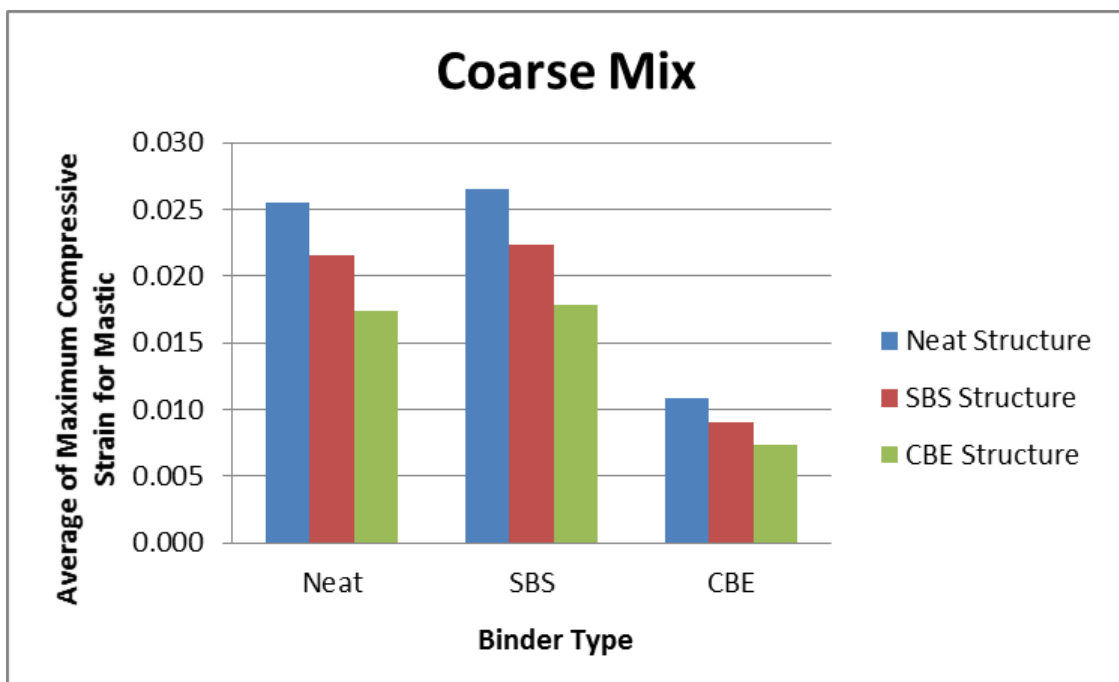


(b)

Figure V-16: Average of maximum compressive strain at 69.1s for mortar in (a) fine mix (b) coarse mix

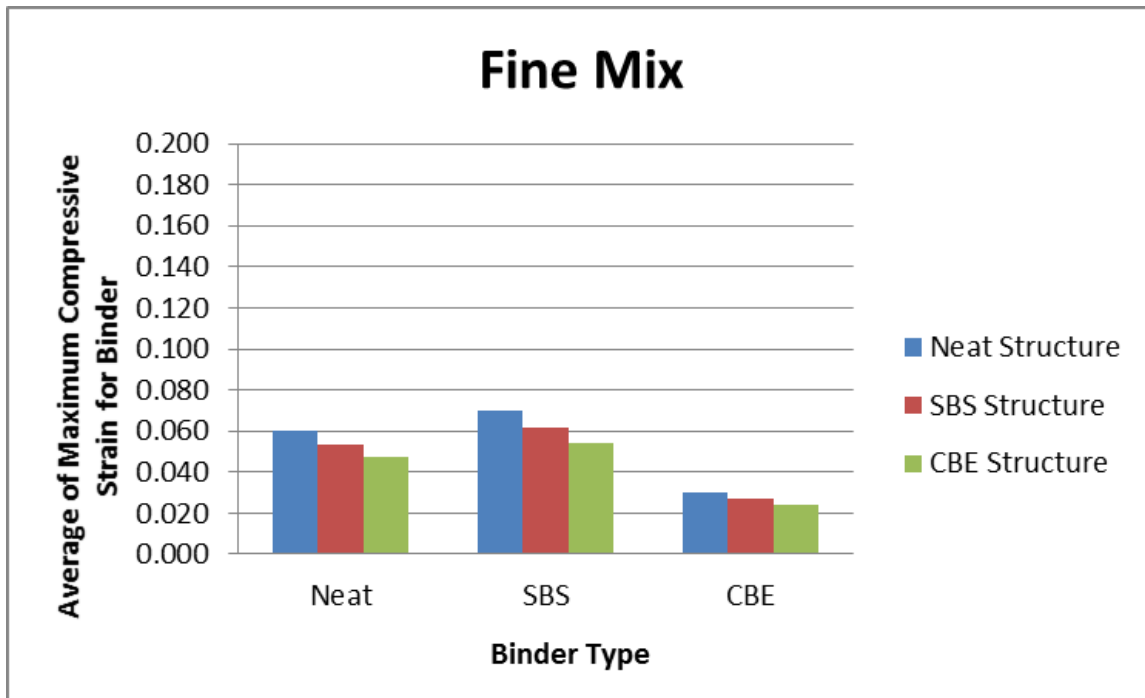


(a)

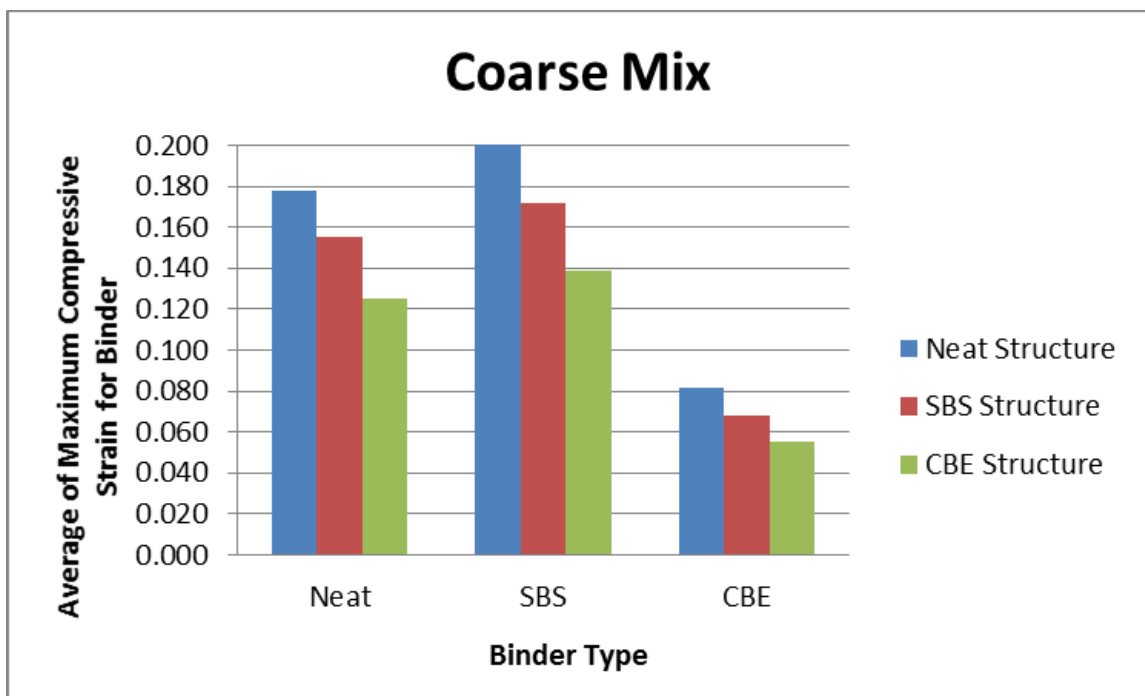


(b)

Figure V-17: Average of maximum compressive strain at 0.1s for mastic in (a) fine mix (b) coarse mix

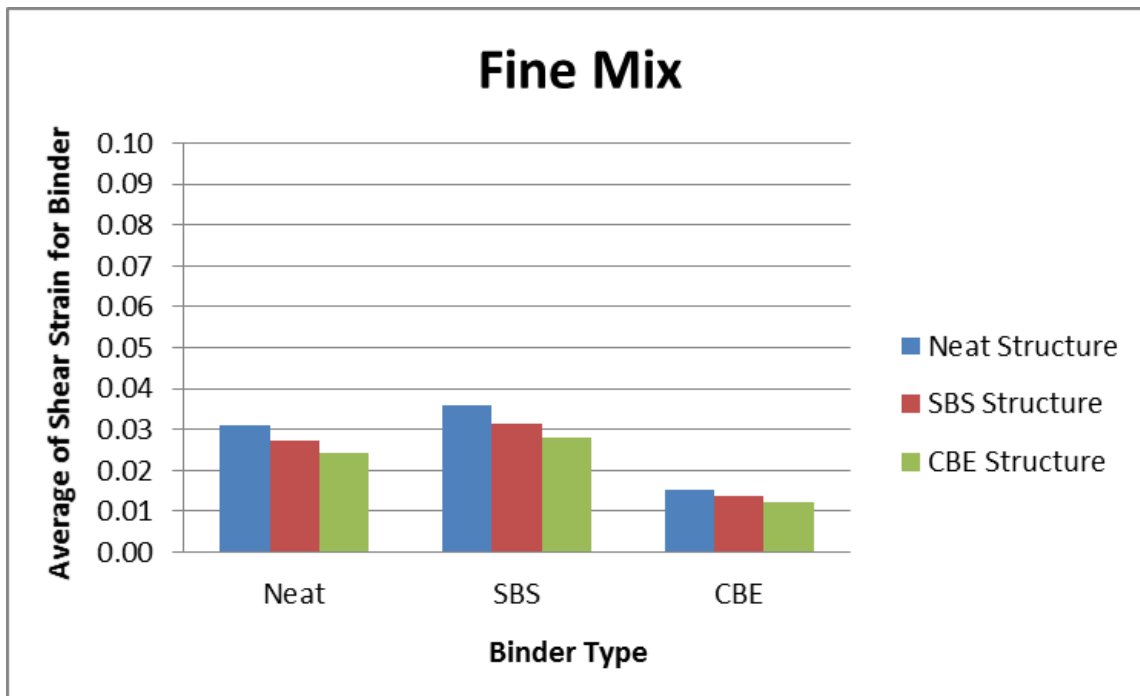


(a)

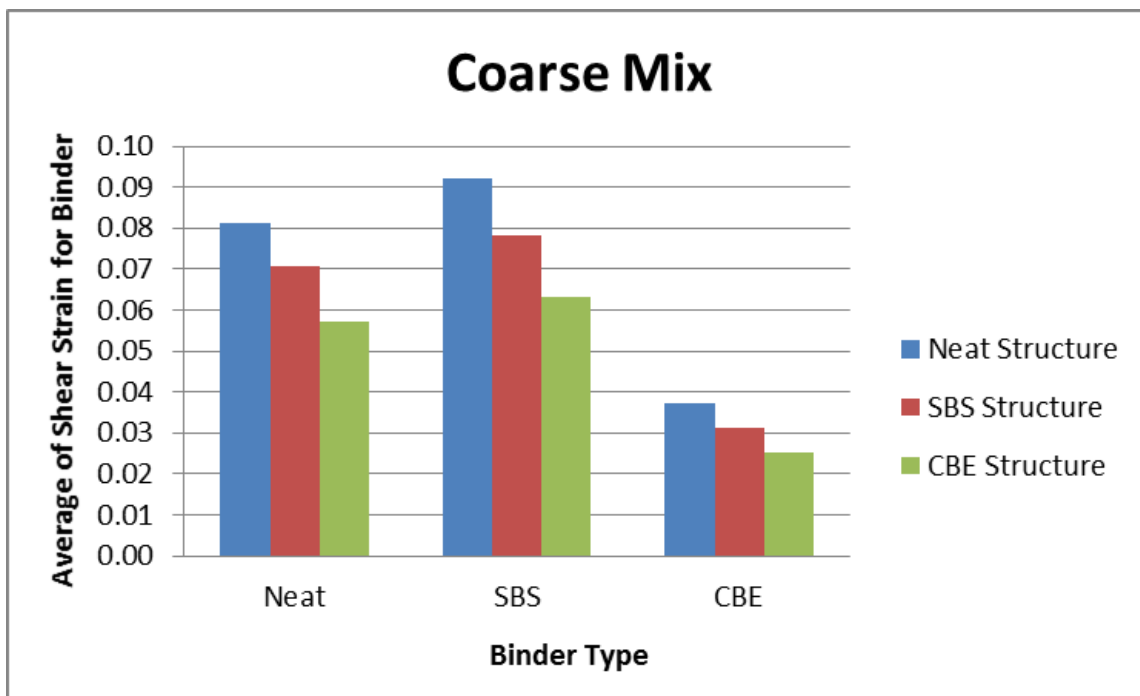


(b)

**Figure V-18: Average of maximum compressive strain at 0.1s for binder in (a) fine mix (b) coarse mix**



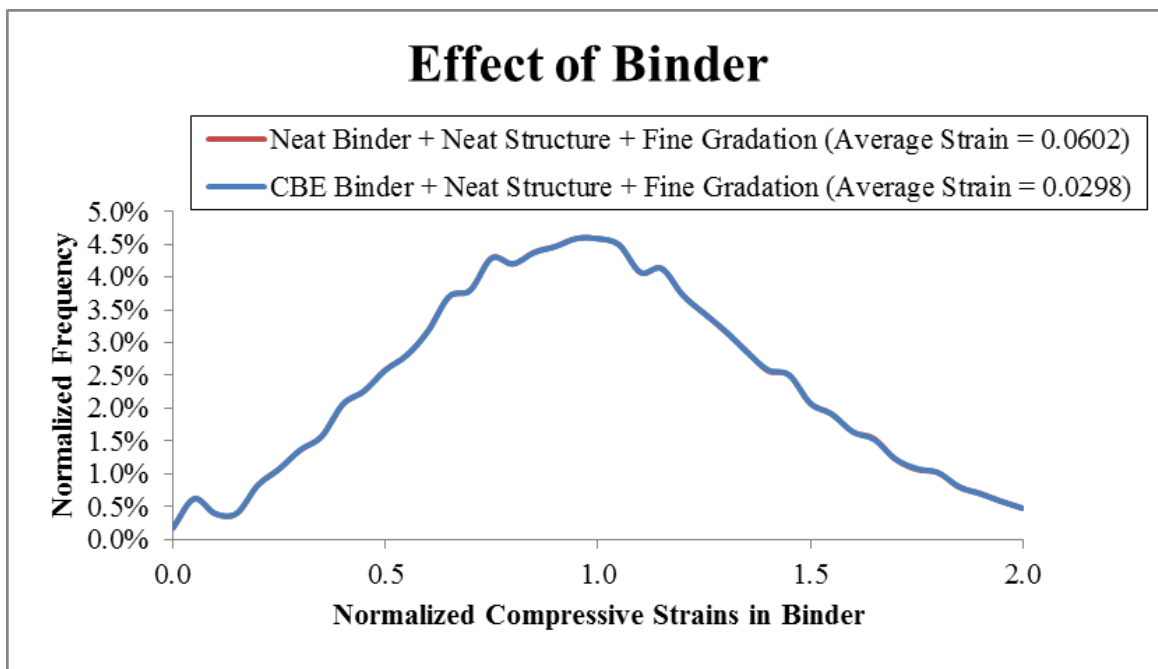
(a)



(b)

**Figure V-19: Average of shear strain at 0.1s for binder in (a) fine mix (b) coarse mix**

The distributions of maximum compressive strains in binder phase for mixtures with different binder types, aggregate structures and aggregate gradations are presented in Figure V-20. It is found that the effects of binder and structure are not significant at all as the same mastic and mortar images are shared in the multi-scale models of these mixtures; the gradation does affect the strain distributions, which is consistent with what have been seen in the binder stress distributions.



(a)

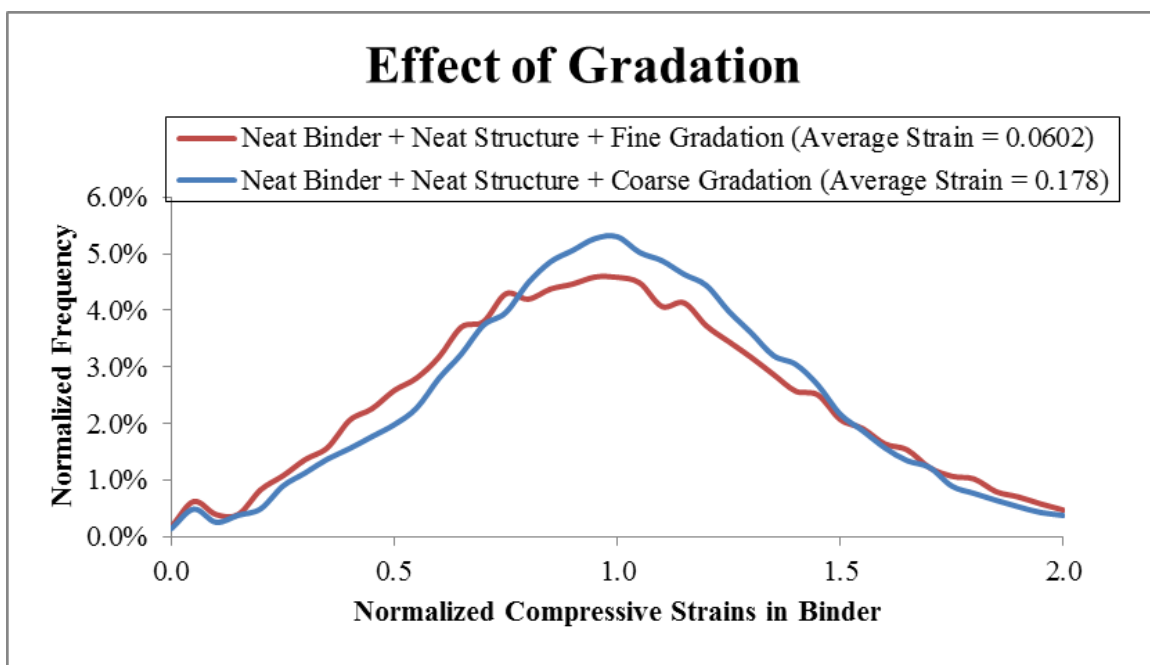
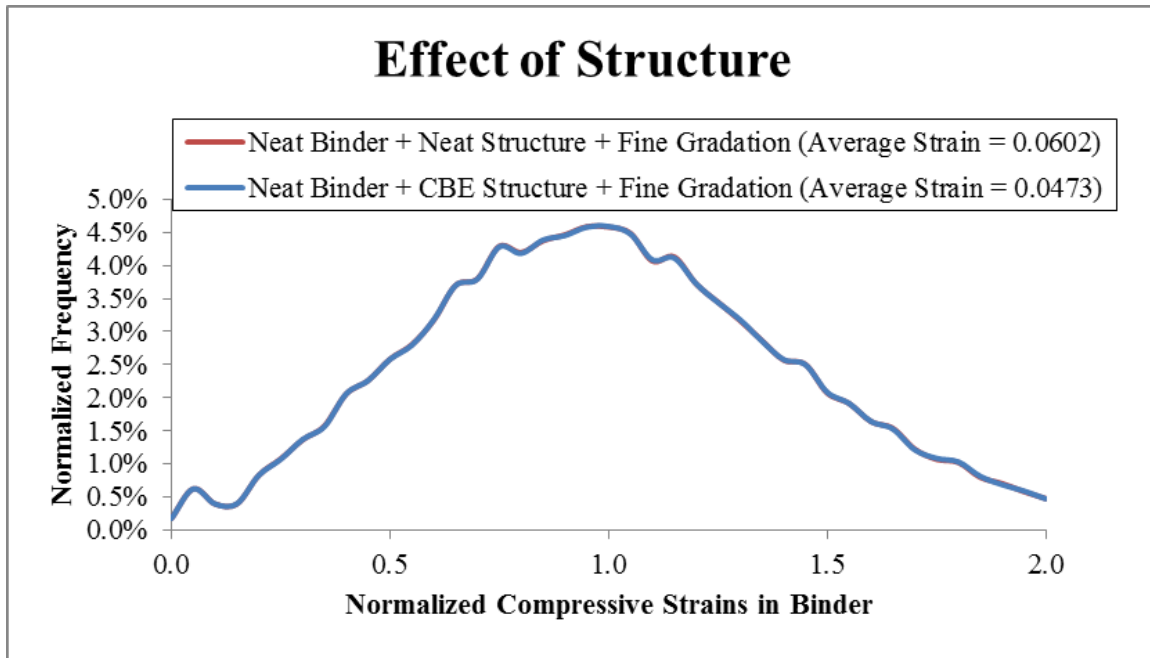


**Figure V-20: Distributions of maximum compressive strains in binder for (a) different binders (b) different structures (c) different gradations**

## **VI. Importance of Binder Non-recoverable Creep Compliance and Elasticity on Asphalt Mixture Rutting Resistance**

The contributions of the non-recoverable creep compliance ( $J_{nr}$ ) and elastic recovery ( $\%R$ ) of asphalt binder measured by MSCR test on the rutting resistance of the asphalt mixture are not clear and not possible to be studied through experimentation. Arshadi [56] tried to investigate the effects of  $J_{nr}$  and  $\%R$  on permanent deformation of asphalt mixtures when he first proposed the concept and framework of image-based multi-scale modeling (without any contact mechanics defined) in his Master's thesis. He concluded that lower  $J_{nr}$  and higher  $\%R$  lead to lower permanent deformation, and limiting  $J_{nr}$  of asphalt binder is more effective than increasing the  $\%R$ . However since no contact law or contact function were included in that model the simulation results may not be representative of what occurs in the asphalt mixture, especially considering the important role that contacts play in resisting permanent deformation of asphalt mixtures. In this chapter the similar research methodology was followed and the proposed MSCR-based multi-scale model with the improved contact mechanisms was used to investigate the effects of  $J_{nr}$  and  $\%R$  on the rutting behavior of asphalt mixtures.

### **1. Experimental Matrix**

Four asphalt binders s LJHR, HJHR, LJLR and HJLR (i.e. LJHR = Low  $J_{nr}$ , High  $\%R$ ) including one neat binder modified by Styrene Butadiene-Styrene (SBS) and three artificially created binders with 2 levels of  $J_{nr}$  and 2 levels of  $\%R$  were included in this study as shown in Table VI-1, similarly as Arshadi has used in his Master's thesis [56]. The  $J_{nr}$  and  $\%R$  values for all the binders were selected based on MSCR test under stress level of 0.1 kPa at 46°C since the asphalt mixture was tested at this temperature. The creep

and recovery curves of the four binders with different Jnr and %R were shown in Figure VI-1. The LJHR stands for the asphalt binder with low Jnr (0.018 kPa<sup>-1</sup>) and high recovery (74.4%), and similarly for HJHR, LJLR and HJLR binders. Among the four binders, LJHR binder is the only actual tested binder modified by 3.2% of SBS with a PG64-22 base binder. The two gradations introduced in Figure III-1 were again used.

**Table VI-1: Four binders with different levels of Jnr and %R included in this study**

Binder Type	MSCR Parameters (@46°C)	
	Jnr (kPa <sup>-1</sup> )	%R
LJHR (SBS Modified)	0.018	74.4
HJHR	0.036	74.4
LJLR	0.018	37.2
HJLR	0.036	37.2

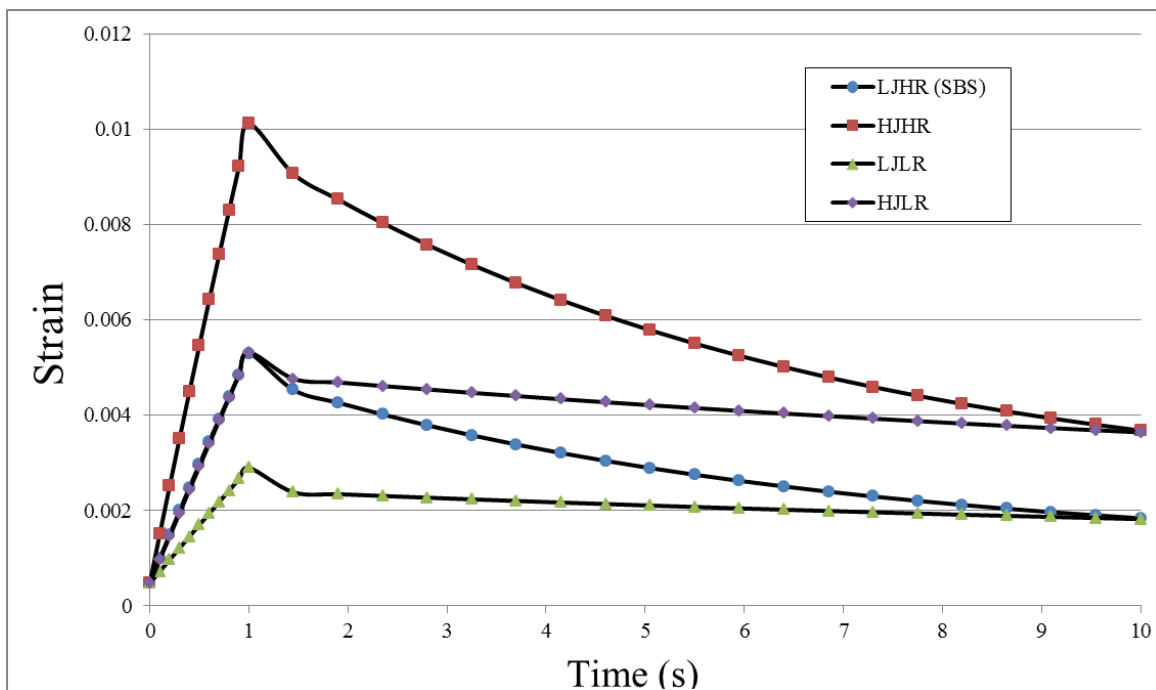
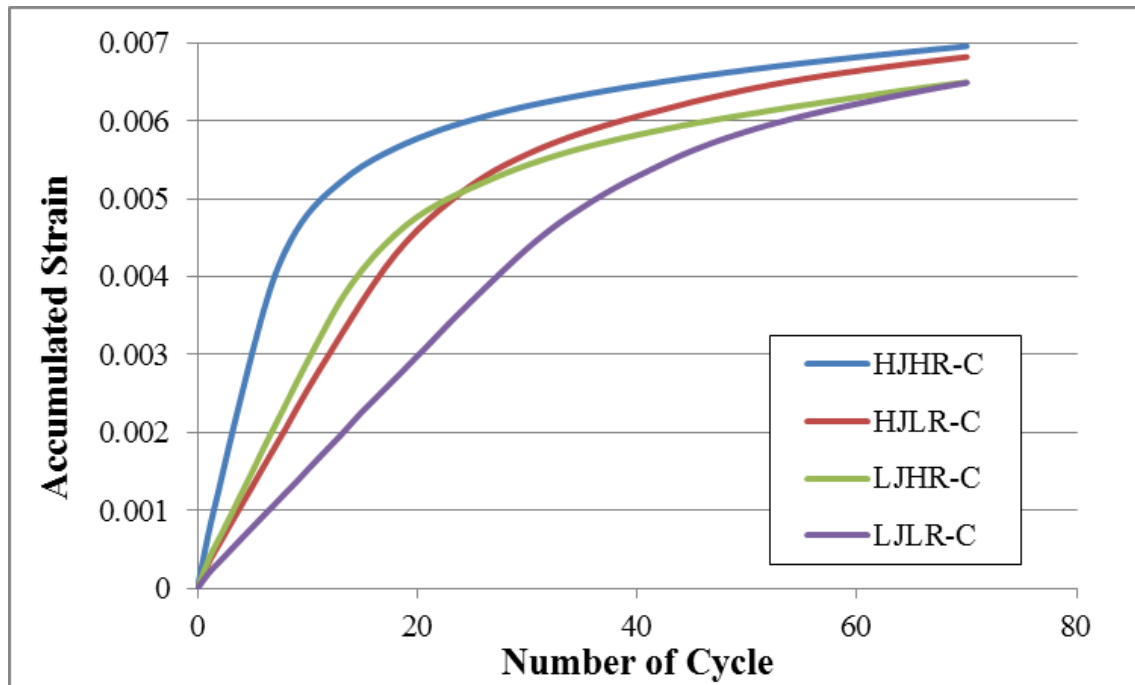


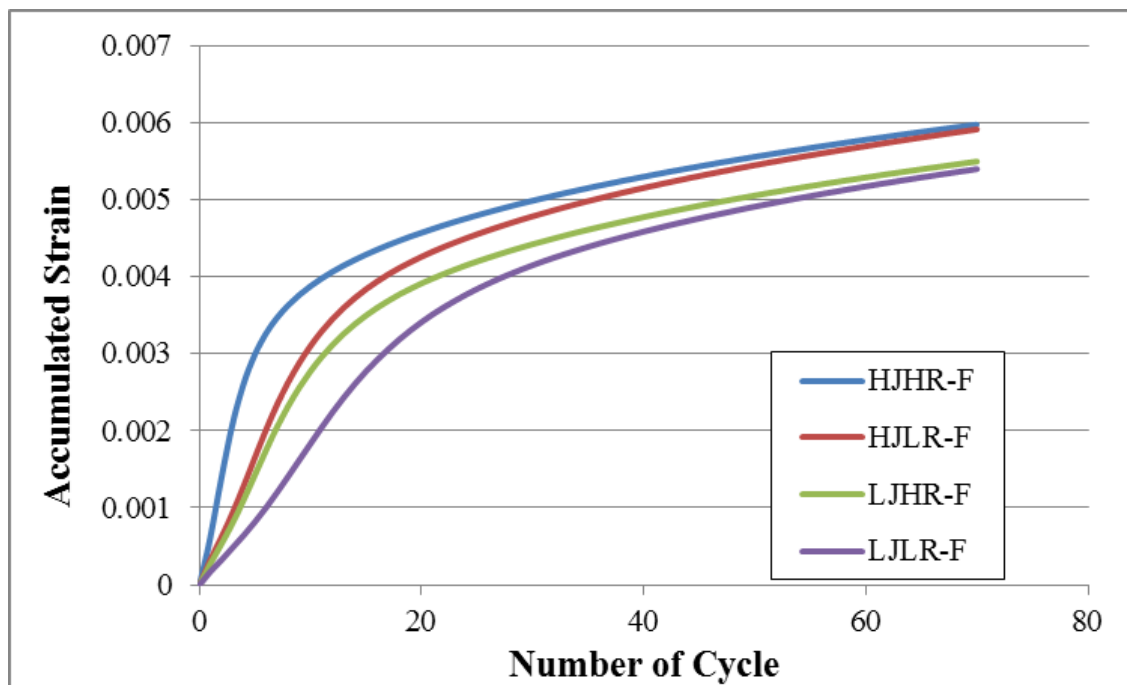
**Figure VI-1: Creep and recovery curves of the four binders with different Jnr and %R**

## 2. Permanent Strain Analysis

The permanent strain curves during the simulations of asphalt mixtures were obtained through the MSCR-based multi-scale model as presented in Figure VI-2. The final permanent strains after 70 cycles for all the mixtures are shown in Figure VI-3 and the ANOVA table is presented in Table VI-2 as well. From the ANOVA analysis it is seen that the aggregate gradation is the most significant factor relative to the asphalt binder properties as the fine mixtures perform much better than the coarse mixtures. By comparing  $J_{nr}$  and %R it is found that  $J_{nr}$  is much more critical in predicting permanent deformation resistance than %R with a higher F-value and lower p-value. The %R is not significant at the confidence level of 95% on the permanent strains of asphalt mixtures. This indicates that although the elasticity could be critical in cracking resistance of asphalt mixtures, it is not important in resisting permanent deformation at high temperatures for the mixtures tested in this study. Instead, the non-recoverable creep compliance of the asphalt binder is the major portion contributing to the rutting resistance of asphalt mixtures.



(a) Coarse mixtures



(b) Fine mixtures

Figure VI-2: Permanent strain curves for the mixtures with different binders

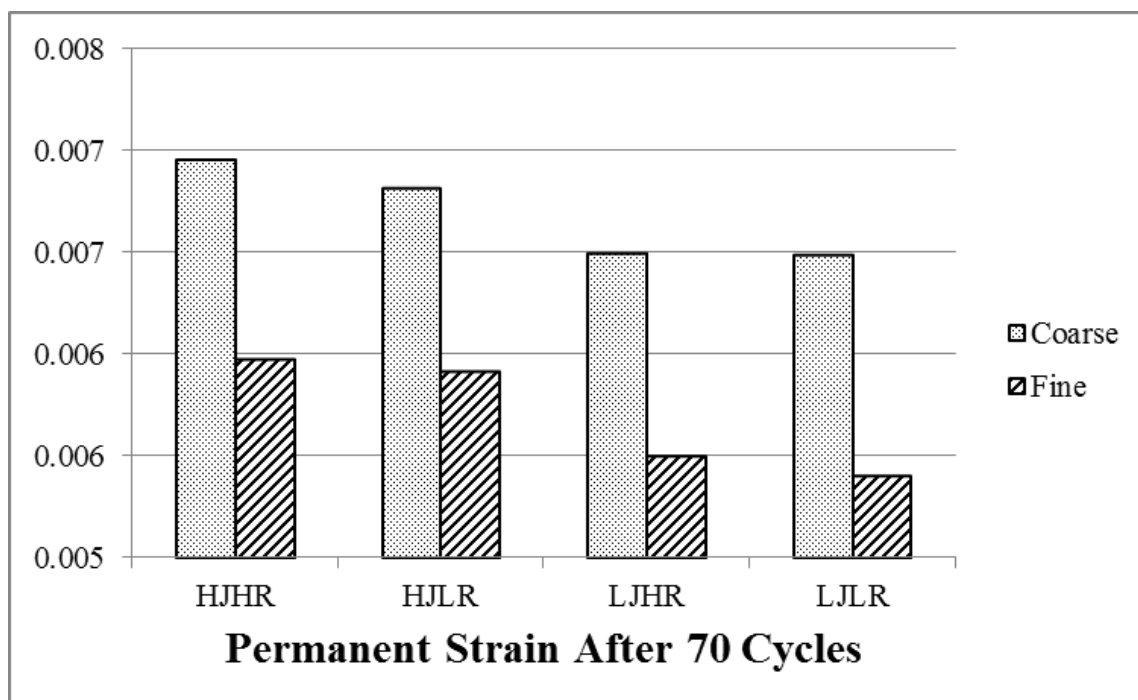


Figure VI-3: Permanent strains after 70 cycles for all mixtures

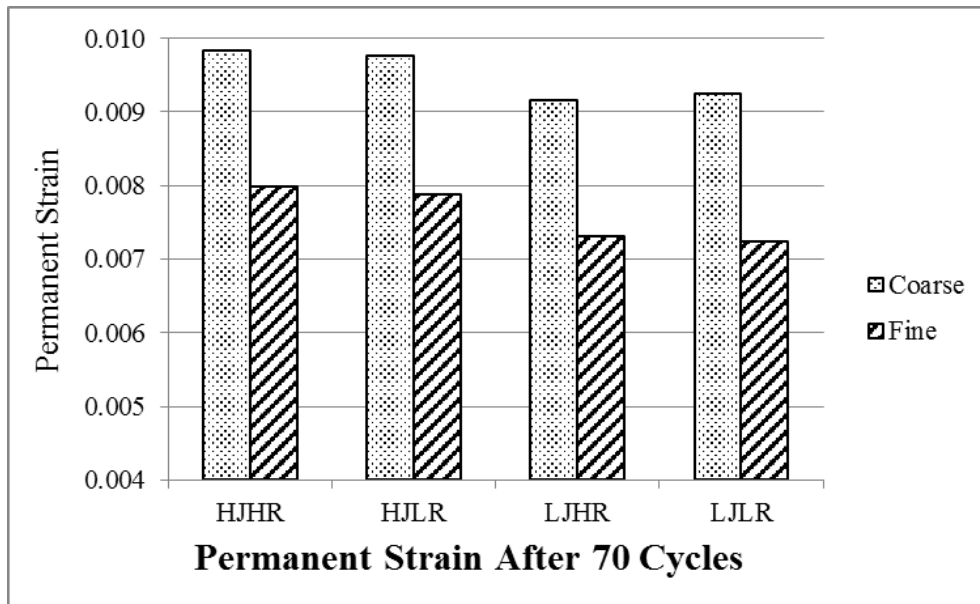
Table VI-2: ANOVA for all the mixtures analyzed using SBS structure

ANOVA - All Mixtures				
	DF	F-Value	Pr (>F)	Significance
Gradation	1	794.33	9.43E-06	***
Jnr	1	160.19	0.0002	***
%R	1	4.62	0.0979	.
Residuals	4			
$R^2_{adj}=99.27\%$				

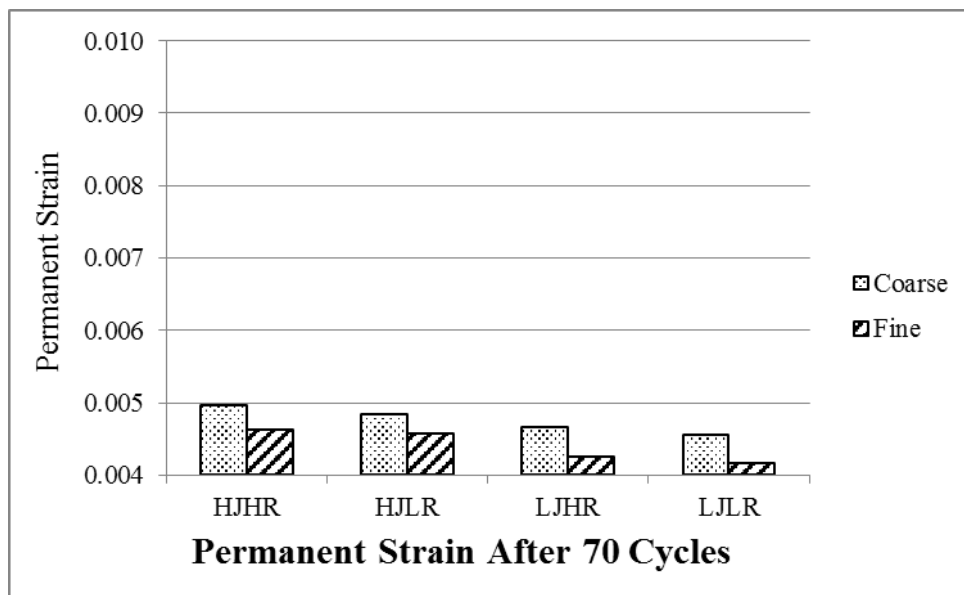
### 3. Effects of Jnr and %R in Mixes with Different Aggregate Structures

It should be noted that the above analysis was based on the SBS structure only as the SBS modified binder (LJHR) is the actual tested binder which was also used in the mixture test. In this section the analysis was expanded to include two other aggregate structures in the mixtures (neat structure and CBE structure) to evaluate the significance of binder

properties (Jnr and %R) and aggregate gradation. The results of permanent strains after 70 cycles and the ANOVA tables for the strains of mixes with these two structures are presented in Figure VI-4 and Table VI-3.



(a) Neat structure



(b) CBE structure

**Figure VI-4: Permanent strains after 70 cycles of repeated loading for (a) Neat structure and (b) CBE structure**

**Table VI-3: ANOVA of permanent strains for (a) Neat structure and (b) CBE structure**

(a) Neat structure

ANOVA - Neat Modified Structure				
	DF	F-Value	Pr (>F)	Significance
Gradation	1	2162.46	1.28E-06	***
Jnr	1	234.48	0.0001	***
%R	1	0.85	0.4099	
Residuals	4			
$R^2_{adj}=99.71\%$				

(b) CBE structure

ANOVA - CBE Modified Structure				
	DF	F-Value	Pr (>F)	Significance
Gradation	1	150.45	2.54E-04	***
Jnr	1	144.07	0.0003	***
%R	1	11.00	0.0295	*
Residuals	4			
$R^2_{adj}=97.74\%$				

From the figures and tables shown above it can be found that the conclusions drawn from previous section are still valid: aggregate gradation is still the most important factor in both structures; Jnr is also significantly affecting the permanent deformation of asphalt mixtures; %R shows little to no significance for these two structures. By comparing the F-values for Jnr in all three different structures from Table VI-2 and Table VI-3, it is also found that the importance of Jnr is more significant in a poorly-packed structure (neat structure) with a much higher F-value compared to that in relatively well-packed structures. This further verifies the conclusion in Chapter V regarding the effect of binder properties and different aggregate structures on the permanent deformation of asphalt mixtures.

The ANOVA analysis was also performed for all mixtures with three different aggregate structures. Similarly to Table V-3, aggregate structure is the most important factor among all factors rather than aggregate gradation. Binder Jnr is significant while %R is not at all. Therefore the non-recoverable creep compliance is the critical component of the asphalt binder contributing to the permanent deformation of asphalt mixture.

**Table VI-4: ANOVA for permanent strains of all mixtures with different structures**

ANOVA - All Mixtures				
	DF	F-Value	Pr (>F)	Significance
Structure	2	226.6468	1.73E-13	***
Gradation	1	49.79	1.40E-06	***
Jnr	1	9.47	0.0065	**
%R	1	0.20	0.6567	
Residuals	18			
$R^2_{adj}=95.67\%$				

## **VII. Prediction of Permanent Deformation for Asphalt Mixtures under Different Conditions**

### **1. Application of the Model to Asphalt Mixtures with/without Confining Pressure**

Both confined and unconfined flow number test results can correlate well with the rut depth in the field [57, 58]. However, research also indicates that the rate of deformation in the field is better simulated by the confined flow number test relative to unconfined test [57]. The debate between these two test conditions is beyond the scope of this research however it would be beneficial if the proposed image-based multi-scale model can be used to predict the permanent deformation of asphalt mixtures under both conditions. The model has already been validated to effectively predict the permanent deformation of asphalt mixtures without confining pressure through different mixtures in Chapter IV. In this section efforts are paid to investigate if the model is capable of predicting the permanent deformation of asphalt mixtures when confining pressure is applied.

Two types of asphalt mixtures (coded as “Waukesha-MT-S-28” and “Waukesha-MT-V-28”) from Wisconsin Highway Research Program Project 0092-15-04 “Analysis and Feasibility of Asphalt Pavement Performance-Based Specifications for WisDOT” were selected for simulation and testing [59]. A type of limestone aggregate (source from Waukesha County, WI) and two asphalt binders (with and without modification) were selected. The asphalt binders are graded as PG58-28S (unmodified) and PG58-28V (polymer modified) and test results for the two binders are presented in Table VII-1. The aggregate gradation is shown in Figure VII-1. It should be noted that the recycled asphalt

pavement (RAP) materials were also used in these mixtures with percent binder replacement (PBR) of 18%. The mixtures were designed to optimum asphalt content of 5.7% at target air voids content of 4.0% in order to meet the criteria for Median Traffic (MT) level which covers from 2 to 8 million ESALs. Then the performance samples with air voids of 7% were also prepared for image processing and Flow Number testing.

**Table VII-1: Binder Test Results**

Binder Grade	Original Binder		RTFO Binder				Softening Point (°C)
	G*/sin(δ) (kPa) @ 58°C	G*/sin(δ) (kPa) @ 64°C	G*/sin(δ) (kPa) @ 58 °C	G*/sin(δ) (kPa) @ 64 °C	Jnr, 3.2 kPa (kPa <sup>-1</sup> ) @ 58 °C	%R, 3.2 kPa (%) @ 58 °C	
PG 58-28 S	1.266	0.583	3.401	1.485	3.0	1.2	41.9
PG 58-28 V	1.627	0.873	8.096	4.223	0.42	47.9	51.1

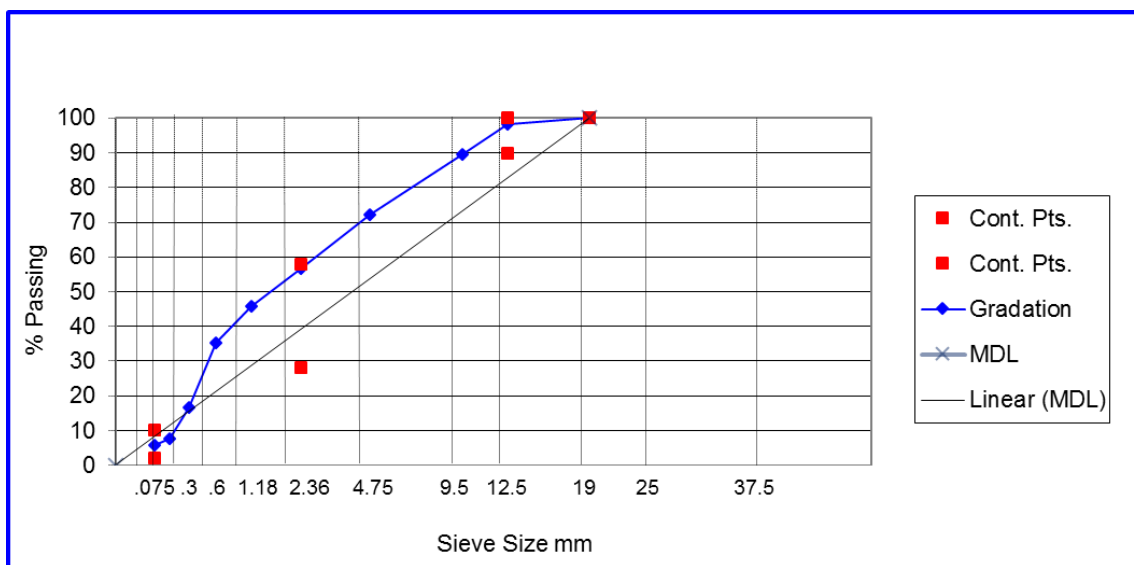


**Figure VII-1: Aggregate Gradation Used in This Study**

The improved multi-scale modeling procedure described in Chapter IV was followed to simulate the permanent deformation of the two types of mixtures. As the RAP binder is included in the mixtures, physically blended asphalt binders with fresh binders and 18% extracted RAP binder were prepared for frequency sweep test. RAP binders were extracted

from RAP mixtures using toluene and recovered with the Rota vapor method. The master curves for the two types of binders at 52°C are shown in Figure VII-2. The volume fractions for aggregate at mixture, mortar and mastic scales were calculated as 42.5%, 66.7% and 23.9% based on mix design information.

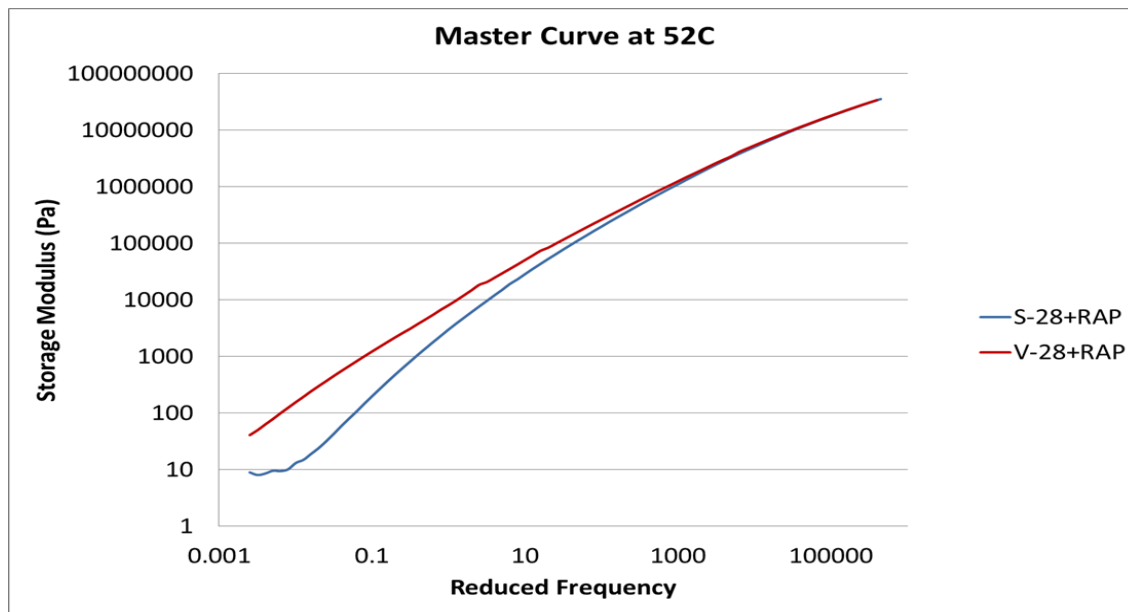


**Figure VII-2: Master curves for asphalt binders used in this study**

For the simulation of mixtures without confining pressure, the vertical stress applied was selected as 87 psi (600kPa) and the same modeling procedure used in previous chapters was followed. For the simulation of mixtures with confining pressure, a horizontal pressure of 10 psi (69 kPa) was applied to the asphalt mixture model and all other conditions were still maintained. Meanwhile, the Flow Number tests for the two type of mixtures under the same conditions as modeling (vertical stress of 87 psi and confining pressure of 10 psi) were performed to validate of the simulation results. Two replicates were tested for each type of mixture and the average values of the two replicates were plotted. It should be noted that the mixture FN data used in this study were obtained from the WHRP 0092-15-04 project (59) and Chaturabong's work (60).

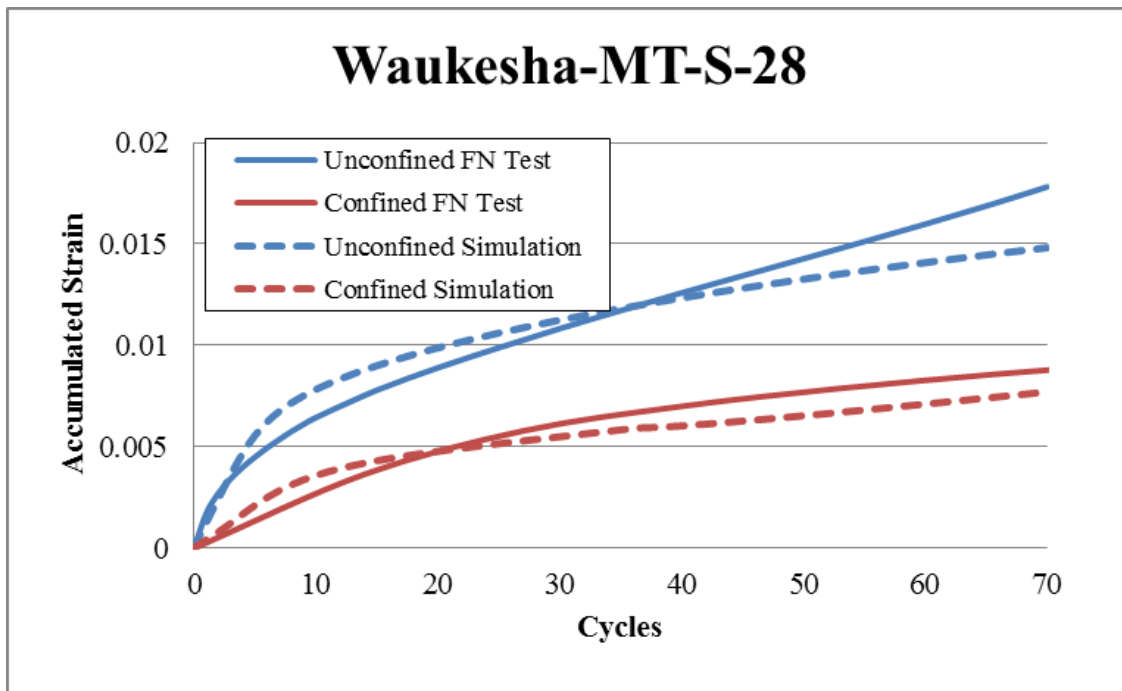


Figure VII-3: Simulation and FN test results for Waukesha-MT-S-28 mixtures with and without confining pressure

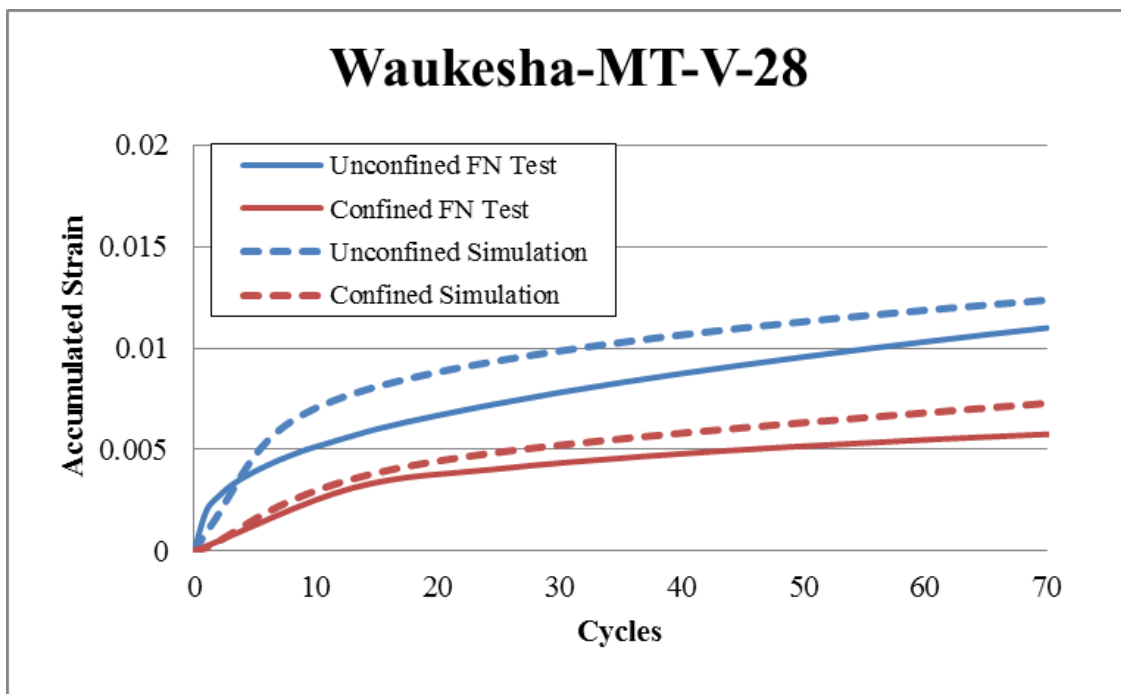


Figure VII-4: Simulation and FN test results for Waukesha-MT-V-28 mixtures with and without confining pressure

The unconfined flow number test results indicate that Waukesha-MT-V-28 mixture has better rutting resistance with a higher flow number of 220 relative to the Waukesha-MT-S-28 mixture which has a flow number of only 50. Both simulated and tested permanent deformation curves under unconfined and confined conditions for the two mixtures are plotted in Figure VII-3 and Figure VII-4. In general the simulation results are comparable with the test results under both confined and unconfined conditions after a number of cycles' loading indicating the effectiveness of the model in predicting the permanent deformation of asphalt mixture under both conditions. It is also noted that the simulated curve for Waukesha-MT-S-28 mixture under unconfined condition starts deviating from the tested curve after 40 cycles or so. Considering the flow number of this mixture is only 50 cycles, some of the initial contact points may get lost in the mixture during the test due to the large strain once the tertiary flow initiates at the flow number point, which causes the increase of the curve slope. Instead, the aggregate particles are connected in the model by these pre-defined contact points and maintained throughout the simulation therefore no significant change of the curve slope was observed. To better simulate the permanent deformation of asphalt mixtures during the tertiary flow, further improvements of the model and the contact mechanics are deemed necessary.

## **2. Investigate the Effect of Air Voids Content in Permanent Deformation of Asphalt Mixtures**

The permanent deformation of asphalt mixtures for the first few cycles (in primary and secondary zones) are typically considered as caused by densification; therefore it is hypothesized that by maintaining the same aggregate structure the decrease of air voids content would not significantly affect the permanent strains and the slope of the strain

curve. This hypothesis is difficult to be validated through experiment as maintaining the aggregate structure while compacting the mixture to different air voids is almost impossible. With the multi-scale model the aggregate structure can be maintained while the amount of air voids added into the mortar phase at mixture scale is changed. In this study the two WHRP mixtures involved in previous section were still used and the air voids content added was reduced from 7% to 4%. The procedure for adding the air voids was described in Chapter III and previous literature [9] and the multi-scale simulations were performed for these two mixtures with different air voids content. The simulation results are presented in Figure VII-5 and Figure VII-6.

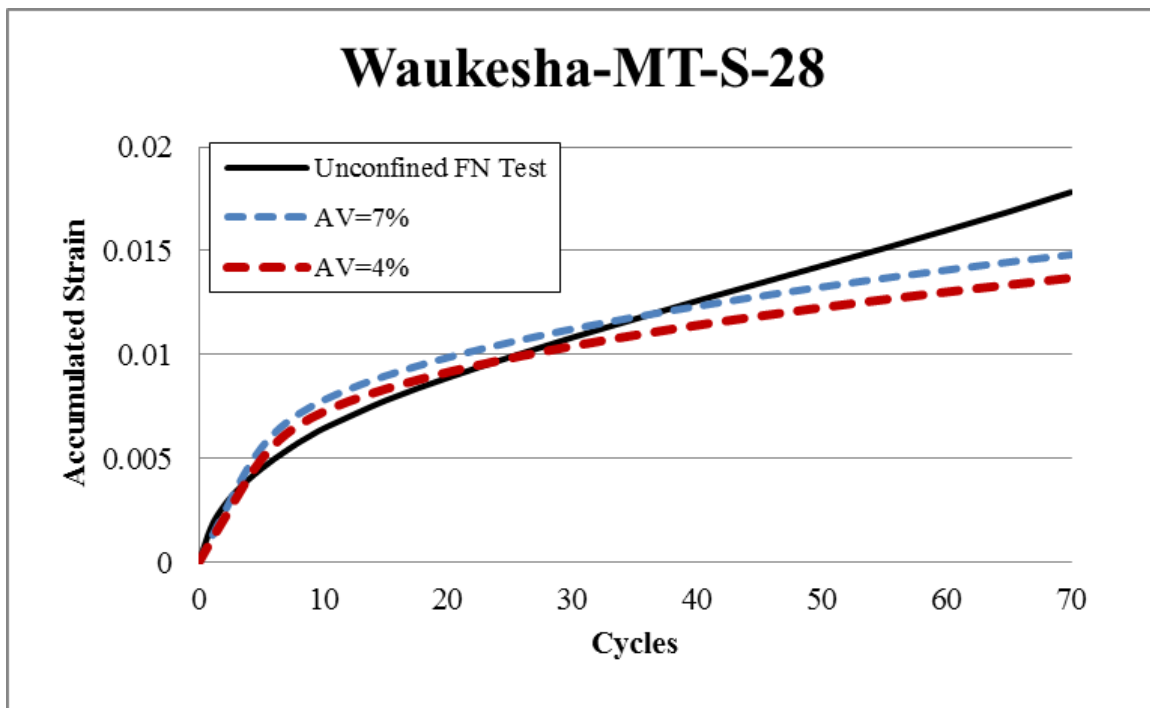


**Figure VII-5: Simulation results for Waukesha-MT-S-28 mixtures with air voids content of 4% and 7%**

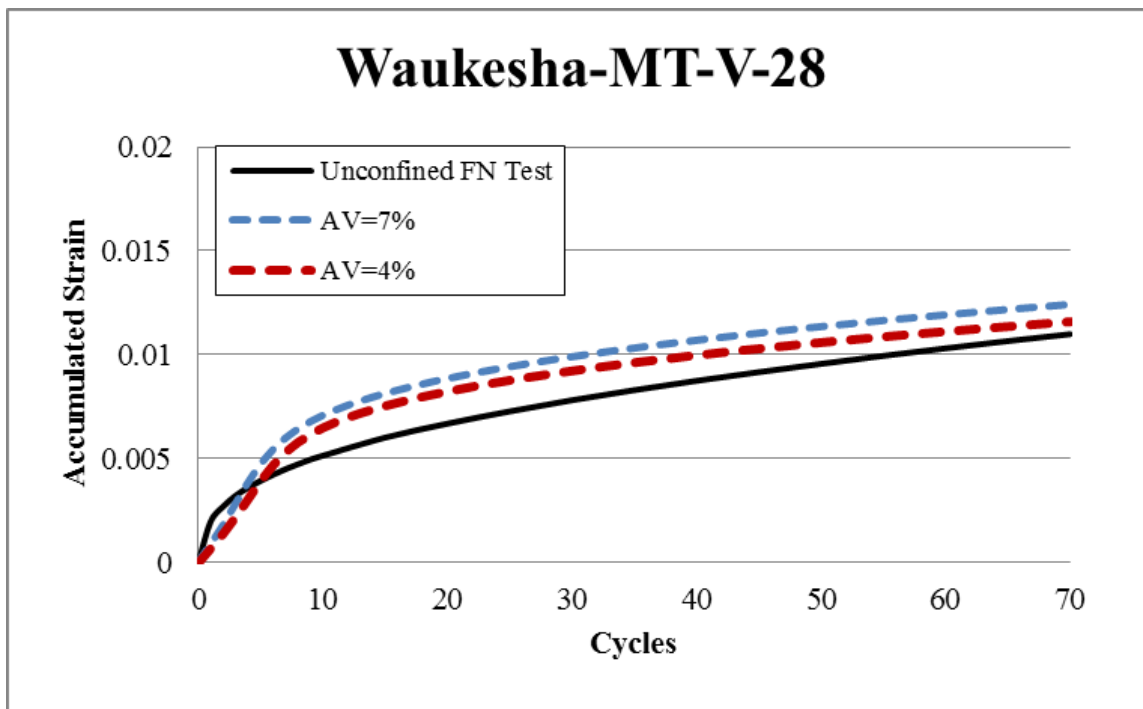


**Figure VII-6: Simulation results for Waukesha-MT-V-28 mixtures with air voids content of 4% and 7%**

As seen from figures shown above, the permanent deformation curves for both types of mixtures with two different air voids content are relatively close to each other, where the mixtures with 4% air voids have slightly lower permanent deformation than the mixtures with 7% air voids. To further validate the hypothesis, the permanent strain slopes of the last 10 cycles and permanent strains after 70 cycles for these mixtures were calculated and listed in Table VII-2 and Table VII-3. The permanent strain slopes and permanent strains after 70 cycles for mixtures with two levels of air voids content have only 6~8% differences, demonstrating that by reducing the air voids content from 7% to 4% no significant change has been observed for the permanent deformation curve of asphalt mixtures.

**Table VII-2: Comparison of permanent strain curve slope for mixtures with different air voids content**

	Permanent Strain Slope for Last 10 Cycles (per 1000 cycles)	
	Waukesha-MT-S-28	Waukesha-MT-V-28
AV=7%	0.074	0.050
AV=4%	0.067	0.047
Difference	8.4%	7.0%

**Table VII-3: Comparison of permanent strain after 70 cycles for mixtures with different air voids content**

	Permanent Strain After 70 Cycles	
	Waukesha-MT-S-28	Waukesha-MT-V-28
AV=7%	0.0148	0.0124
AV=4%	0.0137	0.0116
Difference	7.6%	6.6%

### 3. Simulate Asphalt Mixtures under Moisture Damage

Moisture damage are commonly considered either caused by the loss of adhesion between asphalt binder and aggregate or the weakening of cohesive strength within the asphalt binder/mastic film with the presence of moisture. Chaturabong [60] evaluated the effect of moisture in dry and wet Hamburg Wheel Tracking Test (HWTT) by comparing the slopes of permanent strain curves before and after the moisture damage occurs, and validated the cause of the moisture damage through the Binder Bond Strength test (AASHTO TP-91). This section explores the possibility of using the modeling tool to explain the mechanisms of moisture damage for asphalt mixtures under repeated loading. In this section it is

hypothesized that the decrease of the asphalt binder film stiffness caused by moisture significantly affects the permanent strain curve and the slope of the strain curve. To validate this hypothesis, the stiffness of the binder elements around aggregate elements (named as “asphalt binder film” in the following descriptions) at mastic scale was reduced to 1/10 of their original stiffness when moisture damage occurs. The value of 1/10 was taken arbitrarily as the purpose of this research is to investigate the effect of the moisture damage on the permanent strains through the reduction of binder stiffness. The binder film elements were searched based on the strategy as illustrated in Figure VII-7 and once they were found the new stiffness values were assigned to these film elements. MATLAB codes were written to process the mastic image (Appendix C) and generate the input file (Appendix D) to be imported into ABAQUS program. The asphalt mastic image presented in the ABAQUS with aggregate particle, asphalt binder and asphalt binder film elements is demonstrated in Figure VII-8.

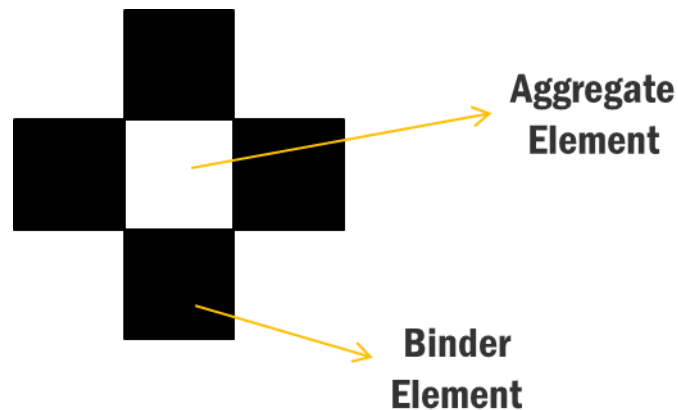


**Figure VII-7: Searching strategy for binder elements with reduced stiffness around aggregate element**

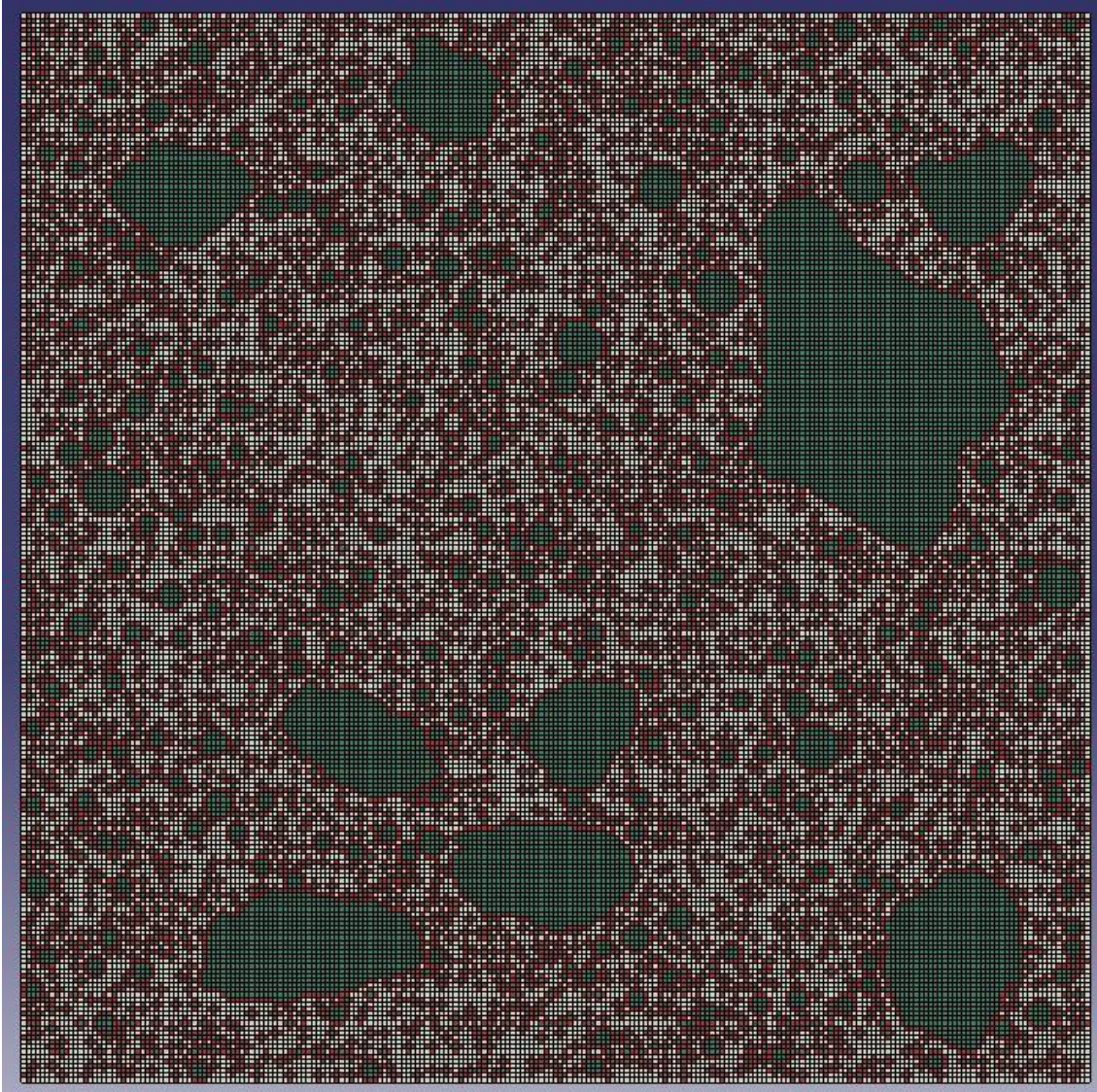


**Figure VII-8: Asphalt mastic image in ABAQUS with aggregate particle, asphalt binder and asphalt binder film elements**

The new mastic model was simulated and the outputs were extracted and analyzed for the simulation at mortar scale. The mortar and mixture images/models were maintained as the reduction of the stiffness was only assumed on binder film elements. Through the homogenization and upscaling the stiffness reduction effect can be transferred to mortar and mixture scale. The final simulation results for the permanent strain curves of the two WHRP mixtures used in previous sections with and without stiffness reduction on the

binder film elements representing the wet and dry conditions in the HWTT test are presented in Figure VII-9. It is found that the stiffness reduction of the binder film elements significantly increase the permanent strains for both types of mixtures through simulations.

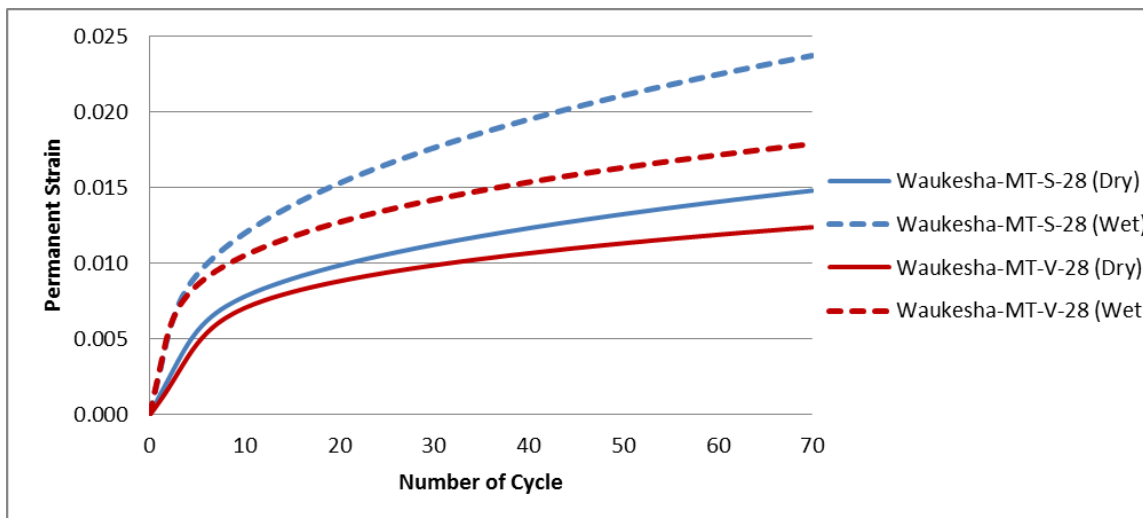


**Figure VII-9: Permanent strain curves for two types of mixtures simulated under dry and wet conditions**

The permanent strain curve slopes of these mixtures for the last 10 cycles were also calculated and presented in Table VII-4 to quantify the impact of moisture/stiffness reduction. The slope for the mixture without binder film stiffness reduction (or under dry condition) was named as ‘creep slope’ and the slope for the mixture with binder film stiffness reduction (or under wet condition) was named as ‘stripping slope’ to be maintained and comparable with the slopes from HWTT. The creep to stripping ratio which was found to be an indicator of moisture susceptibility of asphalt mixtures [60] was also listed in the table for comparison. As shown in the table, the stripping slopes for both type of mixtures are significantly higher than the creep slopes from simulations and HWTT tests, which clearly shows the effect of the moisture/binder film stiffness reduction. The Waukesha-MT-V-28 mixture shows better permanent deformation resistance at both dry

and wet conditions relative to the Waukesha-MT-S-28 mixture as the V-28 binder has much higher stiffness and also lower  $J_{nr}$  than S-28 binder based on Table VII-1. The simulated slope values are much lower than the HWTT tested slopes due to different sample geometries, test setup, load/stress applied etc., as the multi-scale model was established to simulate the FN test. The contact stress for FN test and simulation is 87 psi (600kPa) and this is lower than that for HWTT which is 105 psi (724 kPa) [60]. More discussions on differences between FN test and HWTT test can be found in the literature as well [60]. It is also noted that the ranking of the creep/stripping slope ratios for the two mixtures are not consistent from simulation and HWTT test. Considering the variation in the HWTT test (two replicates were tested) the range of the creep/stripping slope ratio may vary from 2.40 to 4.93 for Waukesha-MT-S-28 mixture, and from 1.91 to 7.32 for Waukesha-MT-V-28 mixture. Therefore it would be difficult to determine which mixture has higher slope ratio and verify the ranking obtained from simulation.

**Table VII-4: Comparison of creep slope, stripping slope and creep/stripping slope ratio between simulation and HWTT test results for two mixtures**

<b>Simulation</b>	Waukesha-MT-S-28	Waukesha-MT-V-28
Creep Slope (per 1000 cycles)	0.074	0.050
Stripping Slope (per 1000 cycles)	0.124	0.074
Creep/Stripping Slope Ratio	1.69	1.48

<b>HWTT</b>	Waukesha-MT-S-28	Waukesha-MT-V-28
Creep Slope (mm/1000 passes)	0.866	0.240
Stripping Slope (mm/1000 passes)	2.908	1.173
Creep/Stripping Slope Ratio	3.36	4.89

**2.40 ~ 4.93**

**1.91 ~ 7.32**

The slopes under both dry and wet conditions for the two mixtures from simulations were further correlated to the slopes from the HWTT test as shown in Figure VII-10. Results demonstrate that good correlation exists between the slopes obtained under either dry or wet conditions from the HWTT and the slopes from the simulations, indicating the effectiveness of the multi-scale model in predicting the permanent strain slopes under both dry and wet conditions.

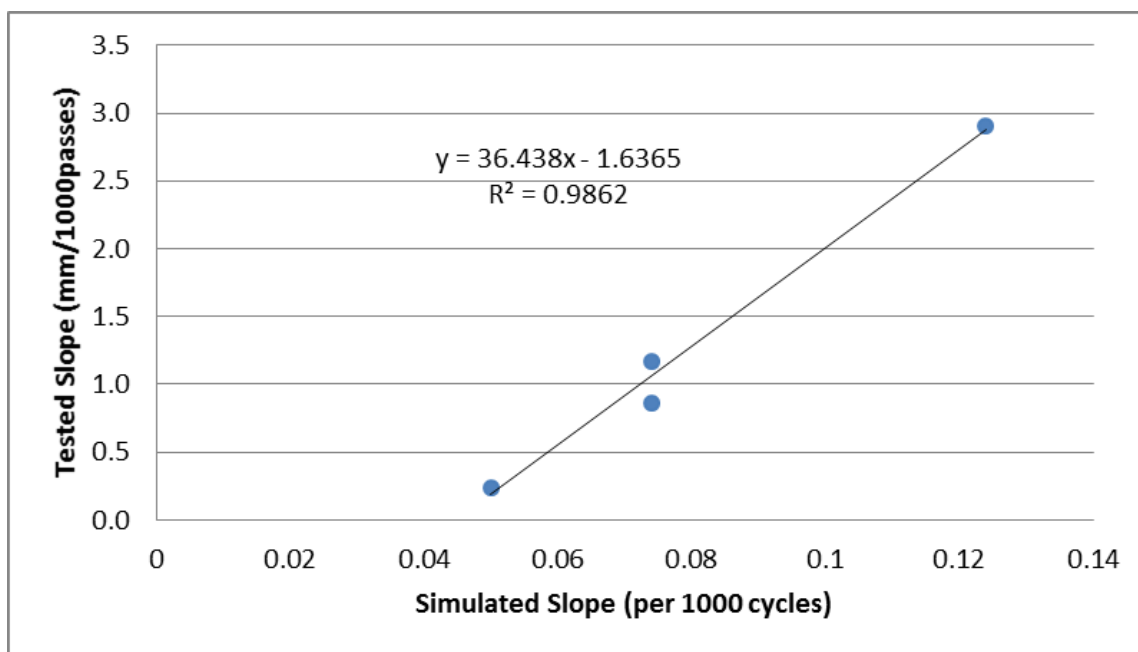


**Figure VII-10: Correlation between simulated slopes and test slopes**

#### **4. Effect of Loading Frequency on the Prediction of Permanent Deformation Using the Model**

The image-based multi-scale model developed in this study to simulate the permanent deformations for all asphalt mixtures were performed under the load of 345 kPa for 70 cycles, with each cycle consisting of 0.1s loading and 0.9s recovery period. This loading frequency was selected to be consistent with what has been used in mixture flow number test. However considering the complex loading conditions on the asphalt pavement in the

field, different loading frequencies may exist instead of a constant frequency. In this section three different loading frequencies were proposed to investigate the effect of the loading frequency on the prediction of permanent deformation of asphalt mixture using the multi-scale model with the proposed contact mechanisms, including:

- 0.01s loading + 0.09s recovery for each cycle
- 0.1s loading + 0.9s recovery for each cycle (this is the frequency used in previous sections throughout the dissertation)
- 1s loading + 9s recovery for each cycle

In total 70 cycles of loading/recovery simulations were performed for a fine mixture with SBS modified binder (same mixture used in Chapter IV) under each of the three frequencies and the simulation results are presented in Figure VII-11 below. Results show that the loading frequency significantly affects the permanent deformation of the asphalt mixtures. Further validations of the simulation results need to be performed using the flow number test under different loading frequencies in the future.

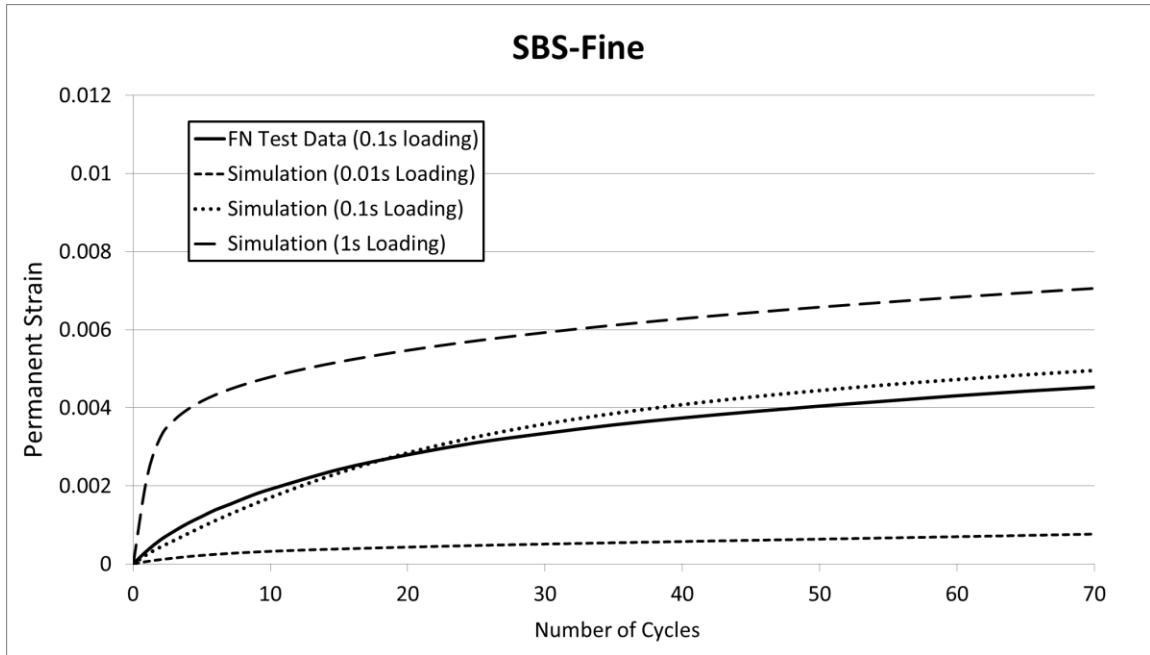


**Figure VII-11: Simulations of permanent deformation under different loading frequencies**

## **VIII. Summary of Findings and Conclusions**

### **1. Summary of Findings**

In this dissertation an image-based multi-scale finite element model was improved using a better aggregates' contact function and simulation approach. The improved model was validated through different types of asphalt mixtures and binders. The validated model was applied to predict the permanent deformation of asphalt mixtures at high temperatures and study the role of asphalt binder properties and aggregate internal structure in rutting resistance of asphalt mixtures. The main findings of this dissertation are summarized below:

1. Multi-scale modeling of asphalt mixtures is improved significantly with the addition of pre-defined aggregate-to-aggregate contact points in mortar and mixture images. The improved model is successfully validated by comparing predicted with measured permanent strain accumulation for different types of asphalt mixtures using the mixture flow number test. In addition, the model was extended to allow incorporating the repeated creep recovery (MSCR) binder test results directly without the need for other binder test. The MSCR is currently used as the standard test for grading of binders in practice.
2. The improved model was applied to simulate mixtures with different modified binders and aggregate structures. Results confirm earlier findings that better packing of the aggregates resulting from special binder modifiers can result in significantly improved resistance to rutting of mixtures. It is therefore confirmed that aggregate gradation is not necessarily a good predictor of packing as modified

- binder lubrication plays an important role in packing of aggregates during compaction.
3. Comparing simulated performance of mixtures with different aggregate structures indicates that asphalt binder properties affect rutting resistance of asphalt mixture more significantly in mixtures with a poorly-packed aggregate structure relative to the mixtures with a well-packed structure.
  4. The model is also applied to evaluate the contributions of the non-recoverable creep compliance and percent recovery of binders to the rutting resistance of the asphalt mixture. It is found that the elasticity is not necessarily required to improve resistance to permanent deformation at high temperatures. Instead, the non-recoverable creep compliance of the asphalt binder is the major contributor to the rutting resistance of asphalt mixtures.
  5. The improved model was used to evaluate the effects of mixture confinement, mixture air voids content, and the effects of moisture damage on permanent deformation of asphalt mixtures. Results show that in general the model is capable of simulating the effects of confinement. They also show that reducing the air voids content of asphalt mixtures from 7% to 4%, while maintaining the aggregate structure will not significantly change the permanent deformation rate of asphalt mixture. The model can also be used for simulating the mixture deformation under the effect of moisture by simulating weaker bond at the interface between aggregates and binder.

## **2. Conclusions**

It is concluded that introducing pre-defined contact points, and modifying the aggregates' contact function can significantly improve the image-based multi-scale finite element model to predict the permanent deformation of asphalt mixtures measured under controlled conditions in the lab. The model can successfully predict effects of voids content, confinement of mixture, and effect of moisture damage. This model is therefore expected to aid in more rational selection of aggregates and modification techniques to enhance the rutting resistance of asphalt pavements.

## **3. Future Work**

The current model was established on simulations of mixtures under a limited number of cycles of loading and unloading due to the constraints of computational resources. Therefore the tertiary zone in the permanent deformation curve from flow number test could not be captured. Limited data in the dissertation also demonstrates the need of improvement of contact mechanics for predicting the permanent deformation of asphalt mixtures once the tertiary flow initiates. It is recommended that future work be focused on the changes in contact points and packing of aggregates after increased number of cycles and for different geometries of mixture samples.

The assumption of linearity for asphalt binder was followed in this study through the multiple scales. However asphalt is a type of non-linear material in reality especially under high stress/strain conditions, therefore the non-linearity of the asphalt material needs to be considered in the future research.

The image-based multi-scale model could be further extended to predict the material behavior under the tensile stress/loading conditions, such as the conditions of Semi-Circular Bend Test. The effectiveness of this model to be applied to investigating both permanent deformation and cracking behavior of asphalt mixtures needs to be validated in the future.

## IX. References

- 1 Lu, Q. and Harvey, J.T. Evaluation of Hamburg Wheel Tracking Device Test with Laboratory and Field Performance Data. *Journal of Transportation Research Record*, Vol. 1970. pp. 25-44, 2006.
- 2 Sousa, J. B., Deacon, J. A., Weissman, S. L., Leahy, R. B., Harvey, J. T., Paulsen, G., Coplantz, J. S. and Monismith, C. L. Permanent Deformation Response of Asphalt Aggregate Mixes. Strategic Highway Research Program, National Research Council, Washington D. C., 1994.
- 3 Weissman, S. L., Harvey, J. T., Sackman, J. L. and Long, F. Selection of Laboratory Test Specimen Dimension for Permanent Deformation of Asphalt Concrete Pavements. *Transportation Research Record*, Vol. 1681, pp. 113-120, 1999.
- 4 Weissman, S. L. The Mechanics of Permanent Deformation in Asphalt Aggregate Mixtures: A Guide to Laboratory Test Selection. Symplistic Engineering Corp, pp. 55, 1997.
- 5 Sefidmazgi, N.R. Hot Mix Asphalt Design to Optimize Construction and Rutting Performance Properties. PhD thesis, University of Wisconsin-Madison, 2013.
- 6 Witczak, M. W., Kaloush, K., Peillinen, T., El-Basyouny, M., and Von Quintus, H. Simple Performance Test for Superpave Mix Design. NCHRP Report 465, National Research Council, Washington, D.C., 2002.
- 7 Sefidmazgi, N.R., Tashman, L. and Bahia, H. U. Internal Structure Characterization of Asphalt Mixtures for Rutting Performance Using Imaging Analysis. *Road Materials and Pavement Design*, Vol. 13, pp. 21-37, 2012.

- 8 Ying, H. X-ray Computed Tomography to Quantify Damage of Hot-Mix Asphalt in the Dynamic Complex Modulus and Flow Number Tests. MSc thesis, Louisiana State University, 2010.
- 9 Arshadi, A. Development of an Image-based Multi-Scale Finite Element Approach to Predict Fatigue Damage in Asphalt Mixtures. PhD thesis, University of Wisconsin-Madison, 2015.
- 10 D'Angelo, J., Reinke, G., Bahia, H and Marasteanu, M. Development in Asphalt Binder Specifications. Transportation Research Circular E-C147, Transportation Research Board, Washington, D.C., 2010.
- 11 Collins, J. H., Bouldin, M. G., Gelles, R. and Berker, A. Improved Performance of Paving Asphalts by Polymer Modification. Journal of the Association of Asphalt Paving Technologists, Vol. 60, pp. 43-79, 1991.
- 12 Khattak, M. J., and G. Y. Baladi. Engineering Properties of Polymer-Modified Asphalt Mixtures. Transportation Research Record: Journal of the Transportation Research Board, Transportation Research Board of the National Academies, Washington, D. C., 1998.
- 13 Kanitpong, K., and Bahia, H. U. Relating Adhesion and Cohesion of Asphalts to the Effect of Moisture on Laboratory Performance of Asphalt Mixtures. Transportation Research Record: Journal of the Transportation Research Board, Transportation Research Board of the National Academies, Washington, D. C., 2005.
- 14 Anderson, D. A., Christensen, D. W., Bahia, H. U., Dongre, R., Sharma, M. G., Antle, C. E. and Button, J. Binder Characterization and Evaluation. Volume 3: Physical Characterization. Strategic Highway Research Program, National Research Council, Washington, DC., 1994.

- 15 Delgadillo, R., Nam, K. and Bahia, H.U. Why do we need to change  $G^*/\sin\delta$  and How? Road Materials and Pavement Design, Vol.7, Issue 1, pp. 7-27, 2006.
- 16 Bahia, H.U., Hanson, D.I., Zeng, M., Zhai, H., Khatri, M.A. and Anderson, R.M. Characterization of Modified Asphalt Binders in Superpave Mix Design. NCHRP Report 459, National Academy Press, Washington, D.C., 2001.
- 17 Delgadillo, R., Cho, D. W. and Bahia, H. U. Nonlinearity of Repeated Creep and Recovery Binder Test and Relationship with Mixture Permanent Deformation. Transportation Research Records, Vol. 1962, Transportation Research Board, Washington, D.C., 2006.
- 18 Centeno, M., Sandoval, I., Cremades, I. and Alarcon, J. Assessing Rutting Susceptibility of Five Different Modified Asphalts in Bituminous Mixtures Using Rheology and Wheel Tracking Test. Transportation Research Board Annual Meeting Compendium of Papers, 2008.
- 19 D'Angelo, J., Kluttz, R., Dongre, R., Stephens, K. and Zanzotto, L. Revision of the Superpave High Temperature Binder Specification: The Multiple Stress Creep Recovery Test. Journal of Asphalt Paving Technologists, Vol.76, pp.123, 2007.
- 20 D'Angelo, J., Reinke, G., Bahia, H. and Marasteanu, M. Development in Asphalt Binder Specifications. Transportation Research Circular E-C147. Transportation Research Board, Washington, D.C., 2010.
- 21 Gierhart, D. Simple Talking Points for Sharing Why Your State Should Be Implementing MSCR. Presentation at SEAUPG MSCR Task Group Web Meeting, 2011.
- 22 Lethersich, W. The Mechanical Behavior of Bitumen. Journal of the Society of Chemical Industry, Vol. 61, No. 7, pp. 101-108, 1942.

- 23 Saal, R. and Labout, J. Rheological Properties of Asphalts. *Rheology: Theory and Applications*, Vol. 2, pp. 363-400, 1958.
- 24 Grabowski, W., Kuczma, M., and Slowik, M. Mathematical Modelling of Rheological Properties of Polymer Modified Bitumens. *Foundations of Civil and Environmental Engineering*, Vol. 2, pp. 27-42, 2002.
- 25 Papagiannakis, A. T., Abbas, A., and Masad E. Micromechanical Analysis of Viscoelastic Properties of Asphalt Concretes. *Transportation Research Record: Journal of the Transportation Research Board*, Vol. 1789, No. 1, pp. 113-120, 2002.
- 26 Dai, Q., and You, Z. Micromechanical Finite Element Framework for Predicting Viscoelastic Properties of Asphalt Mixtures. *Materials and Structures*, Vol. 41, No. 6, pp. 1025-1037, 2008.
- 27 Coenen, A.R. Image Analysis of Aggregate Structure Parameters as Performance Indicators of Rutting Resistance. PhD thesis, University of Wisconsin-Madison, 2011.
- 28 Masad, E., Jandhyala, V. K., Dasgupta, N., Somadevan, N., and Shashidhar, N. Characterization of Air Void Distribution in Asphalt Mixes Using X-ray Computed Tomography. *Journal of Materials in Civil Engineering*, Vol. 14, No. 2, pp. 122-129, 2002.
- 29 Adhikari, S., and You, Z. 3D Microstructural Models for Asphalt Mixtures Using X-ray Computed Tomography Images. *International Journal of Pavement Research and Technology*, Vol. 1, No. 3, pp. 94-99, 2008.
- 30 Yue, Z., Bekking, W. and Morin, I., Application of Digital Image Processing to Quantitative Study of Asphalt Concrete Microstructure. *Journal of Transportation Research Record*, Vol. 1492, pp. 53-60, 1995.
- 31 Masad, E., Muhunthan, B., Shashidhar, N. and Harman, T., Internal Structure

Characterization of Asphalt Concrete Using Image Analysis. *Journal of Computing in Civil Engineering*, Vol. 13, No. 2, pp. 88-95, 1999.

32 Marasteanu, M., Buttlar, W., Bahia, H. U. and Williams, C. Investigation of Low Temperature Cracking in Asphalt Pavements. National Pooled Fund Study-Phase II, 2012.

33 Teymourpour, P. Using Mastic Characterization to Predict Asphalt Mixture Low Temperature Cracking Behavior. PhD thesis, University of Wisconsin-Madison, 2015.

34 Kose, S, Guler M., Bahia. H. U. and Masad, E. Distribution of Strains within Hot-Mix Asphalt Binders: Applying Imaging and Finite-Element Techniques. *Transportation Research Record: Journal of the Transportation Research Board*, Vol. 1728, No. 1, pp. 21-27, 2000.

35 Sadd, M. H., Dai, Q., Parameswaran, V. and Shukla, A. Simulation of Asphalt Materials Using Finite Element Micromechanical Model with Damage Mechanics. *Transportation Research Record: Journal of the Transportation Research Board*, Vol. 1832, No. 1, pp. 86-95, 2003.

36 Turner, M. J., Clough, R. W., Martin, H. C. and Topp, L. J. Stiffness and Deflection Analysis of Complex Structures. *Journal of the Aeronautical Sciences*, Vol. 23, No. 9, pp. 805-823, 1956.

37 Chen, H., Marshek, K., and Saraf, C. L. Effects of Truck Tire Contact Pressure Distribution on the Design of Flexible Pavements: A Three-dimensional Finite Element Approach. *Transportation Research Record*, Vol. 1095, pp. 72-78, 1986.

38 Helwany, S., Dyer, J. and Leidy, J. Finite-element Analyses of Flexible Pavements. *Journal of Transportation Engineering*, Vol. 124, No. 5, pp. 491-499, 1998.

- 39 Hua, J. Finite Element Modeling and Analysis of Accelerated Pavement Testing Devices and Rutting Phenomenon. PhD thesis, Purdue University, 2000.
- 40 Dai, Q., and You, Z. Prediction of Creep Stiffness of Asphalt Mixture with Micromechanical Finite-element and Discrete-element Models. *Journal of Engineering Mechanics*, Vol. 133, No. 2, pp. 163-173, 2007.
- 41 Darabi, M. K., Abu Al-Rub, R. K. Masad, E. A., Huang, C. and Little, D. N. A Thermo-viscoelastic–viscoplastic–viscodamage Constitutive Model for Asphaltic Materials. *International Journal of Solids and Structures*, Vol. 48, No. 1, pp. 191-207, 2001.
- 42 Lutif, J., Souza, F., Kim, Y., Soares, J. and Allen, D. Multiscale Modeling to Predict Mechanical Behavior of Asphalt Mixtures. *Transportation Research Record: Journal of the Transportation Research Board*, Vol. 2181, No. 1, pp. 28-35, 2010.
- 43 Aigner, E., Lackner, R. and Pichler, C. Multiscale Prediction of Viscoelastic Properties of Asphalt Concrete. *Journal of Materials in Civil Engineering*, Vol. 21, No. 12, pp. 771-780, 2009.
- 44 Valenta, R., Sejnoha, M. and Zeman, J. Macroscopic Constitutive Law for Mastic Asphalt Mixtures from Multiscale Modeling. *International Journal for Multiscale Computational Engineering*, Vol. 8, No. 1, 2010.
- 45 Yin, A., Yang, X., Yang, S. and Jiang, W. Multiscale Fracture Simulation of Three-point Bending Asphalt Mixture Beam Considering Material Heterogeneity. *Engineering Fracture Mechanics*, Vol. 78, No. 12, pp. 2414-2428, 2011.
- 46 Underwood, S. Multiscale Constitutive Modeling of Asphalt Concrete. PhD thesis, North Carolina State University, 2011.

- 47 Zocher, M. A., S. E. Groves, and D. H. Allen. A Three-dimensional Finite Element Formulation for Thermo-viscoelastic Orthotropic Media. *International Journal for Numerical Methods in Engineering*, Vol. 40, No. 12, pp. 2267-2288, 1997.
- 48 Lakes, R. S. *Viscoelastic Materials*, Cambridge University Press, 2009.
- 49 Nowick, A. S. and Berry, B. S. *Anelastic Relaxation in Crystalline Solids*, New York: Academic, 1972.
- 50 Ferry, J. D. *Viscoelastic Properties of Polymers*, 2nd ed., New York: J. Wiley, 1970.
- 51 Bahia, H. et al. Characterization of Binder Damage Resistance to Rutting. Report O, Asphalt Research Consortium, Federal Highway Administration, 2013.
- 52 Kong, J. and Yuan, J. Application of Linear Viscoelasticity Differential Constitutive Equations in ABAQUS. *Proceedings of 2010 International Conference on Computer Design and Applications*, Vol.5, pp. 152-156, 2010.
- 53 NCHRP Report 673: A Manual for Design of Hot Mix Asphalt with Commentary. Transportation Research Board, 2011,
- 54 2002 Design Guide, developed for NCHRP Project 1-37a by ERES Division, Applied Research Associates and Arizona State University, July 2004.
- 55 Christensen, D., McQueen and Bahia, H. Selection of High-Temperature Binder PG Grades for Airfield Pavements. 2007 FAA Worldwide Airport Technology Transfer Conference. Atlantic City, New Jersey, USA, 2007.
- 56 Arshadi, A. Importance of Asphalt Binder Properties on Rut Resistance of Asphalt Mixture. MS Thesis, University of Wisconsin-Madison, 2013.

57 Witzak, M.W., K. Kaloush, T. Pellinen, M. El-Basyouny, and H. Von Quintus. 2002. Simple Performance Test for Superpave Mix Design. Washington D.C.: NCHRP Report 465, National Cooperative Highway Research Program.

58 Ulloa, C.A. Development of a Mechanistic-Based Approach to Evaluate Critical Conditions of Hot Mix Asphalt Mixtures. PhD Thesis. 2013.

59 Bahia, H.U. et al. Analysis and Feasibility of Asphalt Pavement Performance-Based Specifications for WisDOT. Wisconsin Highway Research Program Project 0092-15-04 Final Report, 2016.

60 Chaturabong, P. Mechanisms of Asphalt Mixture Rutting Failure in the Hamburg Wheel Tracking Test and the Potential for Replacing the Flow Number Test. PhD Thesis, University of Wisconsin-Madison, 2016.

## Appendix A: Pre-defined Contact Points Generation Codes for Mixture Image (1 pixel)

```

function ContactPointsColor(filename)
MaterialIdentifier = imread(filename);
imshow = size(MaterialIdentifier);
xsize = imshow(1);
ysize = imshow(2);
K= repmat(MaterialIdentifier, [1,1,3]);
CP=0;
for i=1:xsize
    for j=1:ysize
        if MaterialIdentifier(i,j)==255
            M(i,j)=255;

            if j+2<=ysize && MaterialIdentifier(i,j+1)==0
                if MaterialIdentifier(i,j+2)==255
                    M(i,j+1)=235;
                    CP=CP+1;
                end;
            end;

            if i+2<=xsize && MaterialIdentifier(i+1,j)==0
                if MaterialIdentifier(i+2,j)==255
                    M(i+1,j)=235;
                    CP=CP+1;
                end;
            end;

            if j>=3 && MaterialIdentifier(i,j-1)==0
                if MaterialIdentifier(i,j-2)==255
                    M(i,j-1)=235;
                    CP=CP+1;
                end;
            end;

            if i>=3 && MaterialIdentifier(i-1,j)==0
                if MaterialIdentifier(i-2,j)==255
                    M(i-1,j)=235;
                    CP=CP+1;
                end;
            end;

        else
            M(i,j)=MaterialIdentifier(i,j);
        end;
    end;
end;

for i=1:xsize
    for j=1:ysize
        if M(i,j)==235
            K(i,j,1)=255;

```

```
        K(i,j,2)=0;
        K(i,j,3)=0;
    end;
end;
end;

NUMBER=CP/2

% for i=1:xsize
%     for j=1:ysize
%         if M(i,j)>=235
%             M(i,j)=255;
%         else
%             M(i,j)=0;
%         end;
%     end;
% end;

imwrite(K,'mixc-2.tif');
```

## Appendix B: Pre-defined Contact Points Generation Codes for Mortar Image (2 Pixels)

```

function ContactPoints2(filename)
MaterialIdentifier = imread(filename);
imshow = size(MaterialIdentifier);
xsize = imshow(1);
ysize = imshow(2);
K= repmat(MaterialIdentifier, [1,1,3]);
aggregate=0;
binder=0;
CPA=0;
CPB=0;
for i=1:xsize
    for j=1:ysize
        if MaterialIdentifier(i,j)==255
            M(i,j)=255;

            if j+2<=ysize && MaterialIdentifier(i,j+1)==0
                if MaterialIdentifier(i,j+2)==255
                    M(i,j+1)=235;
                    CPA=CPA+1;
                end;
            end;

            if i+2<=xsize && MaterialIdentifier(i+1,j)==0
                if MaterialIdentifier(i+2,j)==255
                    M(i+1,j)=235;
                    CPA=CPA+1;
                end;
            end;

            if j>=3 && MaterialIdentifier(i,j-1)==0
                if MaterialIdentifier(i,j-2)==255
                    M(i,j-1)=235;
                    CPA=CPA+1;
                end;
            end;

            if i>=3 && MaterialIdentifier(i-1,j)==0
                if MaterialIdentifier(i-2,j)==255
                    M(i-1,j)=235;
                    CPA=CPA+1;
                end;
            end;

            if j+3<=ysize && MaterialIdentifier(i,j+1)==0 &&
MaterialIdentifier(i,j+2)==0
                if MaterialIdentifier(i,j+3)==255
                    M(i,j+1)=235;
                    M(i,j+2)=235;
                    CPB=CPB+1;
                end;
            end;
        end;
    end;
end;

```

```

        if i+3<=xsize && MaterialIdentifier(i+1,j)==0 &&
MaterialIdentifier(i+2,j)==0
            if MaterialIdentifier(i+3,j)==255
                M(i+1,j)=235;
                M(i+2,j)=235;
                CPB=CPB+1;
            end;
        end;

        if j>=4 && MaterialIdentifier(i,j-1)==0 &&
MaterialIdentifier(i,j-2)==0
            if MaterialIdentifier(i,j-3)==255
                M(i,j-1)=235;
                M(i,j-2)=235;
                CPB=CPB+1;
            end;
        end;

        if i>=4 && MaterialIdentifier(i-1,j)==0 &&
MaterialIdentifier(i-2,j)==0
            if MaterialIdentifier(i-3,j)==255
                M(i-1,j)=235;
                M(i-2,j)=235;
                CPB=CPB+1;
            end;
        end;

    else
        M(i,j)=MaterialIdentifier(i,j);
    end;
end;
end;

for i=1:xsize
    for j=1:ysize
        if M(i,j)==235
            K(i,j,1)=255;
            K(i,j,2)=0;
            K(i,j,3)=0;
        end;
    end;
end;

NUMBERA=CPA/2
NUMBERB=CPB/2

% for i=1:xsize
%     for j=1:ysize
%         if M(i,j)>=235
%             M(i,j)=255;
%             aggregate=aggregate+1;
%         else
%             M(i,j)=0;
%             binder=binder+1;
%
```

```
%         end;
%     end;
% end;
%
% BP=100*binder/xsize/ysize
% AP=100*aggregate/xsize/ysize

imwrite(K, 'mortarc-2.tif');
```

## Appendix C: Definition of Asphalt Binder Film Pixels in Asphalt Mastic for Moisture Damage Analysis

```

function Film(filename)
MaterialIdentifier = imread(filename);
imshow = size(MaterialIdentifier);
xsize = imshow(1);
ysize = imshow(2);
M=zeros(xsize,ysize);
K= repmat(MaterialIdentifier,[1,1,3]);
CP=0;
for i=1:xsize
    for j=1:ysize
        if MaterialIdentifier(i,j)==255
            M(i,j)=255;

            if j<=(ysize-1) && MaterialIdentifier(i,j+1)==0
                M(i,j+1)=235;
                CP=CP+1;
            end;

            if i<=(xsize-1) && MaterialIdentifier(i+1,j)==0
                M(i+1,j)=235;
                CP=CP+1;
            end;

            if j>=2 && MaterialIdentifier(i,j-1)==0
                M(i,j-1)=235;
                CP=CP+1;
            end;

            if i>=2 && MaterialIdentifier(i-1,j)==0
                M(i-1,j)=235;
                CP=CP+1;
            end;

        else
            end;
        end;
    end;

for i=1:xsize
    for j=1:ysize
        if M(i,j)==235
            K(i,j,1)=255;
            K(i,j,2)=0;
            K(i,j,3)=0;
        end;
    end;
end;

NUMBER=CP

imwrite(K,'Mastic-2.tif');

```

## Appendix D: Matlab Codes for Generating Abaqus Input Files for Moisture Damage Analysis

```

function Input(filename)
MaterialIdentifier = imread(filename);
imshow = size(MaterialIdentifier);
xsize = imshow(1);
ysize = imshow(2);
aggregate=0;
binder=0;
film=0;
%%%%%%%%%%%%%%%%%%%%%%%%%%%%%%%%%%%%%%%%%%%%%%%%%%%%%%%%%%%%%%%%%%%%%%%%
M=zeros(xsize,ysize);
for i=1:xsize
    for j=1:ysize
        if MaterialIdentifier(i,j)==255
            M(i,j)=255;

            if j<=(ysize-1) && MaterialIdentifier(i,j+1)==0
                M(i,j+1)=100;
            end;

            if i<=(xsize-1) && MaterialIdentifier(i+1,j)==0
                M(i+1,j)=100;
            end;

            if j>=2 && MaterialIdentifier(i,j-1)==0
                M(i,j-1)=100;
            end;

            if i>=2 && MaterialIdentifier(i-1,j)==0
                M(i-1,j)=100;
            end;
        end;
    end;
end;
%%%%%%%%%%%%%%%%%%%%%%%%%%%%%%%%%%%%%%%%%%%%%%%%%%%%%%%%%%%%%%%%%%%%%%%%
for i=1:xsize
    for j=1:ysize
        if M(i,j)==0
            binder=binder+1;
        end;

        if M(i,j)==100
            film=film+1;
        end;

        if M(i,j)==255
            aggregate=aggregate+1;
        end;
    end;
end;

BP=100*binder/xsize/ysize

```

```

FP=100*film/xsize/ysize
AP=100*aggregate/xsize/ysize
imshow(M)

%-----
---
pixel=1;

Tfilename=strrep(filename, '.tif', '');
newfilename=[Tfilename, '', '.inp'];
file = fopen(newfilename, 'w');
fprintf(file, '*Heading\n');
fprintf(file, '** Job name: MultiScale Model name: Student\n');
fprintf(file, '** Generated by: Abaqus/CAE Student Edition 6.8-2\n');
fprintf(file, '*Preprint, echo=NO, model=NO, history=NO, contact=NO\n');
fprintf(file, '**\n');
fprintf(file, '** PARTS\n');
fprintf(file, '**\n');
fprintf(file, '*Part, name=PART-1\n');
fprintf(file, '*Node\n');
NuNode=0;
for i=1:xsize+1
    for j=1:ysize+1
        NuNode=NuNode+1;
        fprintf(file, '%8.0f, %8.3f, %8.3f\n', NuNode, (j-1)*pixel, (1-
i)*pixel);
    end;
end;

fprintf(file, '*Element, type=CPE4\n');
NuElement=0;
for i=1:xsize
    for j=1:ysize
        NuElement=NuElement+1;
        n1=i*(ysize+1)+j;
        n2=i*(ysize+1)+j+1;
        n3=(i-1)*(ysize+1)+j+1;
        n4=(i-1)*(ysize+1)+j;
        fprintf(file, '%8.0f, %8.0f, %8.0f, %8.0f,
%8.0f\n', NuElement, n1, n2, n3, n4);
    end;
end;

fprintf(file, '*Elset, elset=Bin, internal\n');
NuElement=0;
for i=1:xsize
    for j=1:ysize
        NuElement=NuElement+1;
        if M(i,j)==0
            fprintf(file, '%8.0f\n', NuElement);
        end;
    end;
end;

```

```

end;
fprintf(file, '\n');
fprintf(file, '*Elset, elset=Agg, internal\n');
NuElement=0;
for i=1:xsize
    for j=1:ysize
        NuElement=NuElement+1;
        if M(i,j)==255
            fprintf(file, '%8.0f\n', NuElement);
        end;
    end;
end;
fprintf(file, '\n');
fprintf(file, '*Elset, elset=Film, internal\n');
NuElement=0;
for i=1:xsize
    for j=1:ysize
        NuElement=NuElement+1;
        if M(i,j)==100
            fprintf(file, '%8.0f\n', NuElement);
        end;
    end;
end;
end;
%-----
fprintf(file, '\n');
fprintf(file, '** Section: AggSec\n');
fprintf(file, '*Solid Section, elset=Agg, material=AGGREGATE\n');
fprintf(file, '');
fprintf(file, '** Section: BinSec\n');
fprintf(file, '*Solid Section, elset=Bin, material=BINDER\n');
fprintf(file, '');
fprintf(file, '** Section: FilmSec\n');
fprintf(file, '*Solid Section, elset=Film, material=FILM\n');
fprintf(file, '');
fprintf(file, '*End Part\n');
%-----
fprintf(file, '**\n');
fprintf(file, '**\n');
fprintf(file, '** ASSEMBLY\n');
fprintf(file, '**\n');
fprintf(file, '*Assembly, name=Assembly\n');
fprintf(file, '**\n');
fprintf(file, '*Instance, name=PART-1-1, part=PART-1\n');
fprintf(file, '*End Instance\n');

fprintf(file, '**\n');
fprintf(file, '*Nset, nset=U2, internal, instance=PART-1-1,
generate\n');
fprintf(file, '%8.0f, %8.0f,
%8.0f\n', xsize*(ysize+1)+1, (xsize+1)*(ysize+1), 1);
fprintf(file, '*Nset, nset=U1, internal, instance=PART-1-1,
generate\n');
fprintf(file, '%8.0f, %8.0f, %8.0f\n', 1, xsize*(ysize+1)+1, ysize+1);
fprintf(file, '*Elset, elset=Pressure, internal, instance=PART-1-1,
generate\n');
fprintf(file, '%8.0f, %8.0f, %8.0f\n', 1, ysize, 1);
fprintf(file, '*Surface, type=ELEMENT, name=Load, internal\n');

```

```

fprintf(file, 'Pressure, S3\n');

fprintf(file, '*End Assembly\n');
%-----
fprintf(file, '**\n');
fprintf(file, '** MATERIALS\n');
fprintf(file, '**\n');
fprintf(file, '*Material, name=AGGREGATE\n');
fprintf(file, '*Elastic\n');
fprintf(file, '2.5e+10, 0.25\n');
fprintf(file, '*Material, name=FILM\n');
fprintf(file, '*Elastic\n');
fprintf(file, '1e6, 0.3\n');
fprintf(file, '*Material, name=BINDER\n');
fprintf(file, '*Elastic, moduli=INSTANTANEOUS\n');
fprintf(file, '71591267.132473, 0.5\n');
fprintf(file, '*Viscoelastic, time=PRONY\n');
fprintf(file, ' 0.9975, 0.9975, 0.0094\n');
fprintf(file, ' 0.0024, 0.0024, 1.5164\n');

fprintf(file, '**\n');
fprintf(file, '** BOUNDARY CONDITIONS\n');
fprintf(file, '**\n');
fprintf(file, '** Name: Disp-BC-1 Type: Displacement/Rotation\n');
fprintf(file, '*Boundary\n');
fprintf(file, 'U2, 2, 2\n');
fprintf(file, '** Name: Disp-BC-2 Type: Displacement/Rotation\n');
fprintf(file, '*Boundary\n');
fprintf(file, 'U1, 1, 1\n');
fprintf(file, '*Boundary\n');
fprintf(file, 'U1-1, 1, 1\n');
%-----
NC=1;
for i=1:NC
    fprintf(file, '** -----
    -----\n');
    fprintf(file, '**\n');
    fprintf(file, '** STEP: L%0.0f\n', i);
    fprintf(file, '**\n');
    fprintf(file, '*Step, name=L%0.0f, inc=1000\n', i);
    fprintf(file, '*Visco, cetol=1e-05\n');
    fprintf(file, '0.1, 1, 0.001, 0.4\n');
    fprintf(file, '**\n');
    fprintf(file, '** LOADS\n');
    fprintf(file, '**\n');
    fprintf(file, '** Name: SURFFORCE-%0.0f Type: Pressure\n', i);
    fprintf(file, '*Dsload, op=NEW\n');
    fprintf(file, 'Load, P, 100\n');
    fprintf(file, '**\n');
    fprintf(file, '** OUTPUT REQUESTS\n');
    fprintf(file, '**\n');
    fprintf(file, '*Restart, write, frequency=0\n');
    fprintf(file, '**\n');
    fprintf(file, '** FIELD OUTPUT: F-Output-%0.0f\n', 2*(i-1)+1);
    fprintf(file, '**\n');

```

```

fprintf(file, '*Output, field, variable=PRESELECT\n');
fprintf(file, '**\n');
fprintf(file, '** HISTORY OUTPUT: H-Output-%0.0f\n', 2*(i-1)+1);
fprintf(file, '**\n');
fprintf(file, '*Output, history, variable=PRESELECT\n');
fprintf(file, '*End Step\n');
fprintf(file, '** -----\n');
-----\n');
fprintf(file, '**\n');
fprintf(file, '** STEP: U%0.0f\n', i);
fprintf(file, '**\n');
fprintf(file, '*Step, name=U%0.0f, inc=1000\n', i);
fprintf(file, '*Visco, cetol=1e-05\n');
fprintf(file, '0.9, 9, 0.001, 3\n');
fprintf(file, '**\n');
fprintf(file, '** LOADS\n');
fprintf(file, '**\n');
fprintf(file, '** Name: SURFFORCE-%0.0f   Type: Pressure\n', i);
fprintf(file, '*Dsload, op=NEW\n');
fprintf(file, '**\n');
fprintf(file, '** OUTPUT REQUESTS\n');
fprintf(file, '**\n');
fprintf(file, '*Restart, write, frequency=0\n');
fprintf(file, '**\n');
fprintf(file, '** FIELD OUTPUT: F-Output-%0.0f\n', 2*i);
fprintf(file, '**\n');
fprintf(file, '*Output, field, variable=PRESELECT\n');
fprintf(file, '**\n');
fprintf(file, '** HISTORY OUTPUT: H-Output-%0.0f\n', 2*i);
fprintf(file, '**\n');
fprintf(file, '*Output, history, variable=PRESELECT\n');
fprintf(file, '*End Step\n');
end;

fclose(file);

```